NASA
Technical
Paper
2439

July 1985

Nacelle/Pylon/Wing Integration on a Transport Model With a Natural Laminar Flow Nacelle

Milton Lamb,
William K. Abeyounis,
and James C. Patterson, Jr.

NASA

NASA Technical Paper 2439

1985

Nacelle/Pylon/Wing Integration on a Transport Model With a Natural Laminar Flow Nacelle

Milton Lamb,
William K. Abeyounis,
and James C. Patterson, Jr.

Langley Research Center
Hampton, Virginia

National Aeronautics and Space Administration

Scientific and Technical Information Branch

Introduction

Extensive efforts are underway to develop efficient transport aircraft with reduced direct operating costs (ref. 1). Much of this effort is focused on providing extensive laminar boundary layers on the various aerodynamic surfaces of the aircraft (ref. 2). Laminar boundary layers can be maintained naturally by favorable pressure gradients. Pressure gradients favorable for laminar boundary layers are not favorable for lifting surfaces because of the rearward position of minimum pressure coupled with the trailing-edge pressure recovery. In addition, many of the lifting surfaces on transport aircraft have significant leading-edge sweep angles that generate spanwise flows which are unfavorable to maintaining laminar boundary layers. Since nacelles are not required to carry lift and have negligible leading-edge sweep, they may be designed to have favorable pressure gradients for maintaining laminar boundary layers on a large portion of their surface. Nacelles could, therefore, be a candidate for natural laminar flow. As shown in reference 3, a reduction on the order of 1½ to 2 percent of total aircraft drag at cruise may be achieved with little or no weight penalty by maintaining laminar flow on the nacelle.

An earlier study (ref. 3) was conducted in the Langley 16-Foot Transonic Tunnel to determine the extent of laminar flow obtainable on an isolated nacelle designed to have a favorable pressure distribution over approximately 70 percent of the fan cowl length. Integration tests conducted on a full-span model would involve nacelle sizes considerably smaller than the isolated nacelle previously tested. The smaller nacelle with its lower Reynolds number is expected to have natural laminar flow over a larger portion of the nacelle length.

The main purposes of this study were twofold: First, to determine if the philosophy used in the design of this smaller nacelle, as well as the isolated nacelle, would result in laminar flow over that portion of the nacelle for which it was designed; and second, to determine if integration concepts had any adverse effect on the extent of laminar flow on the nacelle. In addition, this study determined the level of nacelle drag reductions that may be obtained with flow-through laminar flow nacelles installed on a high-wing transonic transport configuration. The effects of fixed and free transition as well as longitudinal position and pylon contouring were also investigated. Extensive static-pressure measurements were taken on the nacelle and wing. The investigation was conducted in the Langley 16-Foot Transonic Tunnel at free-stream Mach numbers from 0.70 to 0.82 and angles of attack from -2.5° to 4.0°.

Symbols and Abbreviations

A	area, in^2
A_{ref}	wing reference area, 529.590 in^2
BL	butt line of model (lateral dimension), in.
b	wing span, 63.121 in.
C_D	drag coefficient, $\frac{\text{Drag}}{q_\infty A_{\text{ref}}}$
ΔC_D	installed drag, $C_{D,\text{WBNP}} - C_{D,\text{WB}}$
C_L	lift coefficient, $\frac{\text{Lift}}{q_\infty A_{\text{ref}}}$
C_m	pitching-moment coefficient, $\frac{\text{Pitching moment}}{q_\infty \bar{c} A_{\text{ref}}}$
C_p	pressure coefficient, $(p - p_\infty)/q_\infty$
c	chord measure in wing reference plane, in.
c_W	chord of wing at intersection with pylon, 9.972 in.
$\bar{c}$	mean geometric chord, 9.107 in.
F_{in}	nacelle internal drag, lb
FS	fuselage station (axial dimension measured from model nose), in.
k	constant in figure 1(c)
l	nacelle length, 12.770 in.
M	Mach number
m	mass, slugs
NBL	nacelle butt line, in. (fig. 3)
NWL	nacelle water line, in. (fig. 3)
NS	nacelle station (axial dimension measured from nacelle lip), in.
p	local static pressure, lb/in^2
p_∞	free-stream static pressure, lb/in^2
q_∞	free-stream dynamic pressure, lb/in^2
r	nacelle radius, in.
V	velocity, ft/sec
WL	fuselage water line, in.
WRP	wing reference plane (fig. 1(a))
x	local axial dimension, in.
x_{LE}	axial distance from pylon leading edge for defining cap leading-edge section shape, in. (fig. 4(a))
$x_{\text{LE,N}}$	leading edge of nacelle, in.

x_{TE} axial distance from pylon trailing edge for defining strut trailing-edge section shape, in.

y local lateral dimension, in.

z local vertical dimension, in.

α angle of attack, deg

η $y/(b/2)$ for wing pressure locations (fig. 1(c))

ϕ circumferential angular measurements for nacelle orifice locations, deg (fig. 2)

Subscripts:

exit nacelle exit

o nacelle inlet

Model components:

B body

N nacelle

P pylon

W wing

Experimental Apparatus and Procedure

Wind Tunnel

The experimental investigation was conducted in the Langley 16-Foot Transonic Tunnel. This tunnel is an atmospheric, single-return wind tunnel with continuous air exchange and is capable of operating at Mach numbers from 0.20 to 1.30. A detailed description of the tunnel is presented in references 4 and 5.

Model and Support System

The 1/24-scale model, representative of a wide-body transport, is shown in figure 1(a), and a photograph of the model with laminar flow nacelles in the forward position is shown in figure 1(b). The model, which had a high wing with supercritical airfoil sections, was mounted on a sting-supported six-component strain-gage balance. Details of the fuselage, wing, and wing pressure orifice locations can be found in references 6 and 7. For these tests, the wing of reference 6 was modified to reduce the curvature of the wing lower surface in the region around the nacelle pylon (see fig. 1(c)) to reduce the flow velocities in that region.

A low-order panel method (ref. 8) in conjunction with a specific compressibility correction technique (ref. 9) was used in designing the long-duct flow-through laminar flow nacelle to solve for the basic installed flow field, with no consideration for laminar boundary-layer stability theory. The desired nacelle shape was analytically modeled into the wing-body flow field, and the resulting pressure gradient of the nacelle was checked for separation as well as for peak surface Mach number. If either the pressure gradient or peak Mach number proved unsatisfactory, the nacelle contour was modified and the entire process was repeated until a satisfactory shape was obtained. The final nacelle contour, shown in figure 2, had a highly polished surface and a favorable pressure gradient over a significant portion (60 percent) of its length. As shown in figure 3, the nacelle was installed in a forward position (top sketch) or a rearward position (bottom sketch) on the symmetrical pylon and in a forward position (middle sketch) on a contoured pylon.

Details of the symmetrical pylons are shown in figure 4(a) and details of the contoured pylon are shown in figure 4(b). Because flow acceleration around pylons is a major contributor to the high velocity peaks on the wing lower surface, the pylon was contoured in an attempt to reduce these high velocities. The low-order panel method discussed earlier was used to design the contoured pylon using the wing/body/nacelle flow field obtained for the laminar flow nacelle in the forward position.

Instrumentation and Data Reduction

The model aerodynamic force and moment data were obtained by an internally mounted six-component strain-gage balance. The model surface static pressures were measured by scanning electrical strain-gage transducers located in the model nose to reduce the lag time required between data points. Sting cavity pressures, measured by remotely located strain-gage transducers, were used to correct the cavity pressure to the free-stream static pressure. Based on repeated runs, the accuracy was equivalent to 1 count of drag (C_D of 0.0001).

All wind-tunnel parameters and model data were recorded simultaneously on magnetic tape. Except for scanning valve pressures, averaged values were used to compute all parameters. The model angle of attack was computed by correcting the support strut angle, both for sting deflections based on balance loads and for tunnel upflow determined from inverted model runs in a previous tunnel entry (ref. 6). Sting-cavity pressures were used to correct the longitudinal balance components for pressure forces in the sting cavity. Nacelle internal drag corrections were made by using internal static pressures to determine the mass flow for a one-dimensional flow calculation; that is,

$$F_{\text{in}} = mV_{\text{exit}} - mV_o + (p_{\text{exit}} - p_o)A_{\text{exit}}$$

Forces and moments were transferred to the model moment center, the quarter-chord point of the mean geometric chord on the model water line.

The turbulent skin-friction drag for the nacelles was calculated by the method of Frankl and Voishel for compressible turbulent flow over a flat plate. Laminar skin-friction drag for the nacelles was calculated by the method of Blasius. No corrections were made for grit drag.

Tests

This experimental wind-tunnel investigation was conducted in the Langley 16-Foot Transonic Tunnel at free-stream Mach numbers from 0.70 to 0.82 and Reynolds number from approximately 2.5×10^6 to 3.0×10^6 based on the mean geometric chord of the wing. The model angle of attack was varied from $-2.5°$ to $4.0°$. Boundary-layer transition on the model was fixed using a grit-transition-strip procedure (ref. 10). A 0.1-in-wide strip of No. 100 carborundum grit was attached 1.0-in. behind the nose of the fuselage. Strips of No. 90 and No. 80 grit were applied on the upper and lower wing surfaces (see fig. 11 of ref. 7) in a rearward position in order to match the boundary-layer thickness at the trailing edge of the wing (ref. 11). In those cases where it was desirable to fix transition on the nacelles, a 0.10-in. strip of No. 120 grit was placed 1.05 in. ($x/l = 0.08$) and 0.375 in. ($x/l = 0.03$) aft of the nacelle lip on the external and internal surfaces, respectively. The text matrix is shown in the table below.

Mach number	Angle of attack, deg	Nacelle position	Pylon	Nacelle transition
0.70 to 0.82	−2.5 to 4.0	Forward	Symmetrical	Free & fixed
0.70 to 0.82	−2.5 to 4.0	Forward	Contoured	Free & fixed
0.70 to 0.82	−2.5 to 4.0	Rearward	Symmetrical	Free & fixed

Results and Discussion

The basic aerodynamic characteristics of the different nacelle configurations are presented in figures 5 to 7. The wing-body configuration with original wing leading edge is presented to show the effect of nacelle installation with wing leading-edge modification and the effect of free and fixed nacelle transition. The addition of the nacelles reduced the lift coefficient and increased the drag coefficient. Fixing the nacelle transition caused a significant increase in drag coefficient while lift and pitching-moment coefficients were affected only slightly, if at all.

Laminar Flow Design

The purpose of this study, as discussed earlier, was aimed at determining if a nacelle designed to achieve laminar flow over a large portion of the nacelle length could be integrated into a transport (nacelle/pylon/wing integration) configuration and preserve the extent of laminar flow achieved on the isolated nacelle. For the configuration with the nacelle in the forward position (position which should produce the least interference), the drag reduction due to laminar flow (increment between fixed and free transition) is approximately 9 counts. (See fig. 5(e).) Calculations of the skin-friction drag for the nacelle with fixed and free transition (indication of the extent of laminar flow achieved on the nacelle) indicate that the drag reduction expected for a nacelle of this size with 60-percent laminar flow (observed in sublimation runs) is approximately 9 counts. Thus, it would seem that the ability to design a nacelle to achieve laminar flow has not been significantly altered by integration.

Effect of Nacelle Position

The effect of longitudinal position of the nacelles on the longitudinal aerodynamic characteristics is shown in figure 8. The nacelles were installed on symmetrical pylons such that the ratio $x_{\text{LE,N}}/c_W$ was -1.20 or -0.90. (See fig. 3.) A large reduction in lift and increase in drag is associated with installing the nacelle in the rearward position ($x_{\text{LE,N}}/c_W = -0.90$). This increase in drag and the associated loss in lift are revealed by the wing pressure distributions presented in figure 9. While there is some decrease in upper surface pressure coefficients near the wing leading edge (see fig. 9), there is a large decrease in the lower surface pressure coefficients. This large decrease is possibly due to flow acceleration between the nacelle/pylon/wing and fuselage as the nacelle is moved rearward, thus resulting in shock-induced boundary-layer separation and the increase in drag shown in figure 8.

Pylon Contouring

The effect of pylon contouring on the longitudinal aerodynamic characteristics is shown in figure 10. This contoured-pylon configuration exhibits less drag than the configuration with symmetrical pylons. The increment in drag between the symmetrical and contoured pylons increases with increasing Mach number, not unusual since the contoured pylon was designed for $M = 0.80$. The wing pressure data inboard of the pylon (fig. 11) show that the contoured pylon allows a better pressure recovery on the upper surface and reduces the lower surface velocities, thereby producing lift and reducing drag as noted in figure 10.

Installed Drag

In figure 12, the installed drag coefficients ($\Delta C_D = C_{D,\text{WBNP}} - C_{D,\text{WB}}$) are presented across the Mach number range for the configuration cruise condition ($C_L = 0.45$). The curves were obtained from interpolated values of C_D at $C_L = 0.45$. Configurations with the nacelles installed in the forward position (figs. 12(a) and (b)) show only slight changes in installed drag over the Mach number range. The contoured-pylon configuration with free transition (fig. 12(b)) exhibits less drag than the symmetrical-pylon configuration with free transition (figs. 12(a) and (c)). The installed drag for the nacelle-forward symmetrical-pylon configuration with fixed transition remains essentially constant over the Mach number range, whereas the installed drag for the contoured-pylon configuration with fixed transition decreases as Mach number increases. For the configuration with rearward-installed nacelles (fig. 12(c)), installed drag increases rapidly with Mach number and the increment between free and fixed transition decreases rapidly with Mach number.

Nacelle Pressures

Figures 13 to 15 show the nacelle pressure-coefficient distributions at $C_L \approx 0.45$ over the Mach number range. These pressure distributions will probably explain the extreme differences noted for the installed drags. For the configurations with the nacelles in the forward position (figs. 13 and 14), the pressure-coefficient distribution over the Mach number range is similar, with only a slight increase in peak pressure coefficient with increase in Mach number. However, for the configuration with the nacelles in the rearward position (fig. 15), peak pressure coefficient increases rapidly with Mach number, particularly on the inboard side in the region close to the nacelle-pylon juncture. This high peak pressure is essentially the same for free and fixed transition and tends to override the pressure differences (i.e., a local disturbance due to transition strip) resulting from fixed transition at low values of x/l. This probably explains why the free and fixed transition installed drag approaches the same value at the higher Mach numbers.

Comparison of Installed Drag at $M = 0.80$

The installed drag coefficients at $M = 0.80$ and $C_L = 0.45$ are compared in figure 16, with the drag broken down into skin-friction drag and interference drag. For free transition, laminar flow was assumed to exist over 60 percent of the nacelle length (based on design and on sublimation pictures). Since only the nacelles were allowed to have free transition, the differences between the same nacelle-pylon configurations with free and fixed transition should be essentially equal to the skin-friction differences between turbulent and laminar flow. Such is the case except for the contoured-pylon configuration of about 4 counts higher. This increase in drag is attributed to interference drag.

Conclusions

An experimental investigation has been conducted in the Langley 16-Foot Transonic Tunnel to determine the effects of installing flow-through laminar flow nacelles on a high-wing transonic transport configuration. The effects of fixed and free transition as well as longitudinal position and pylon contouring were obtained. The results of this investigation indicate the following:

1. The ability to achieve laminar flow on the nacelle was not significantly altered by nacelle/pylon/wing integration for the nacelles on symmetrical pylons.
2. The increment of drag between free and fixed transition was essentially the calculated differences between turbulent and laminar flow on the nacelles.
3. With the nacelles in a forward position, the installed drag for the contoured pylon was less than that for the symmetrical pylons.
4. The contoured pylon had increased interference drag with fixed nacelle transition.
5. The installed drag for the nacelles in a rearward position was greater than that for the nacelles in a forward position.
6. The increment between free and fixed transition for the rearward nacelle decreased with an increase in Mach number, probably due to the high peak pressures which overrode the pressure differences resulting from fixed transition.

NASA Langley Research Center
Hampton, VA 23665
April 1, 1985

References

1. James, Robert L., Jr.; and Maddalon, Dal V.: *Airframe Technology for Aircraft Energy Efficiency*. NASA TM-85749, 1984.
2. Wagner, Richard D.; Maddalon, Dal V.; and Fischer, Michael C.: TechnologyDevelopments for Laminar Boundary Layer Control on Subsonic Transport Air-

the Fluid Dynamics Panel Symposium on Improvement of Aerodynamic Performance Through Boundary Layer Control and High Lift Systems (Brussels, Belgium), May 1984.

3. Younghans, J. L.; and Lahti, D. J.: Analytical and Experimental Studies on Natural Laminar Flow Nacelles. AIAA-84-0034, Jan. 1984.
4. Corson, Blake W., Jr.; Runckel, Jack F.; and Igoe, William B.: *Calibration of the Langley 16-Foot Transonic Tunnel With Test Section Air Removal.* NASA TR R-423, 1974.
5. Peddrew, Kathryn H., compiler: *A User's Guide to the Langley 16-Foot Transonic Tunnel.* NASA TM-83186, 1981.
6. Lee, Edwin E., Jr.; and Pendergraft, Odis C., Jr.: *Installation Effects of Long-Duct, Pylon-Mounted Nacelles on a Twin-Jet Transport Model With a Swept, Supercritical Wing.* NASA TP-2457, 1985.
7. Abeyounis, William K.; and Patterson, James C., Jr.: *Effect of Underwing Aft-Mounted Nacelles on the Longitudinal Aerodynamic Characteristics of a High-Wing Transport Airplane.* NASA TP-2447, 1985.
8. Maskew, Brian: Prediction of Subsonic Aerodynamic Characteristics—A Case for Low-Order Panel Methods. AIAA-81-0252, Jan. 1981.
9. Dietrich, D. A.; Oehler, S. L.; and Stockman, N. O.: Compressible Flow Analysis About Three-Dimensional Wing Surfaces Using a Combination Technique. AIAA-83-0183, Jan. 1983.
10. Braslow, Albert L.; Hicks, Raymond M.; and Harris, Roy V., Jr.: *Use of Grit-Type Boundary-Layer-Transition Trips on Wind-Tunnel Models.* NASA TN D-3579, 1966.
11. Blackwell, James A., Jr.: *Preliminary Study Effects of Reynolds Number and Boundary-Layer Transition Location on Shock-Induced Separation.* NASA TN D-5003, 1969.

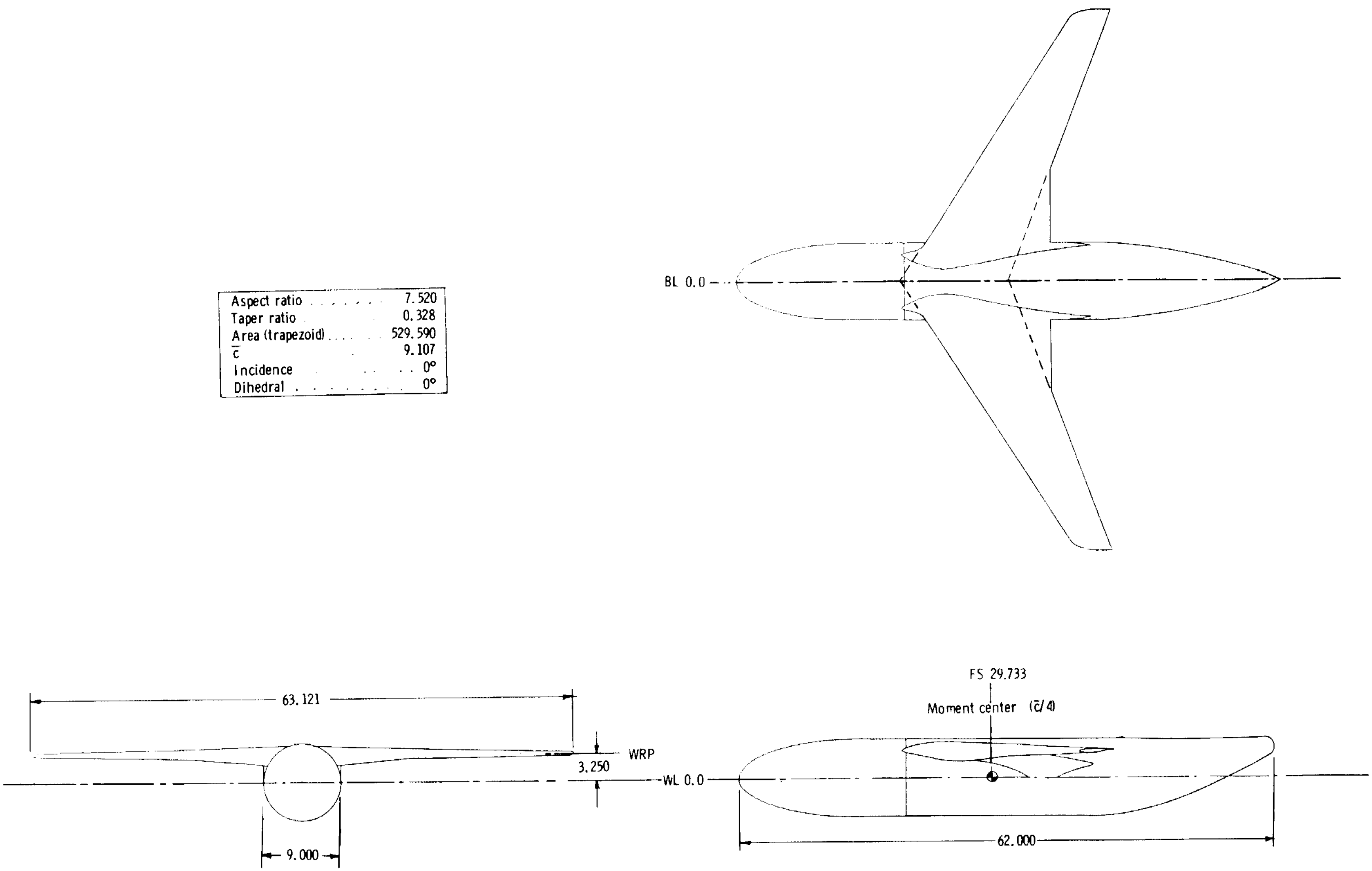

(a) General layout.

Figure 1. Details of model. Linear dimensions are in inches.

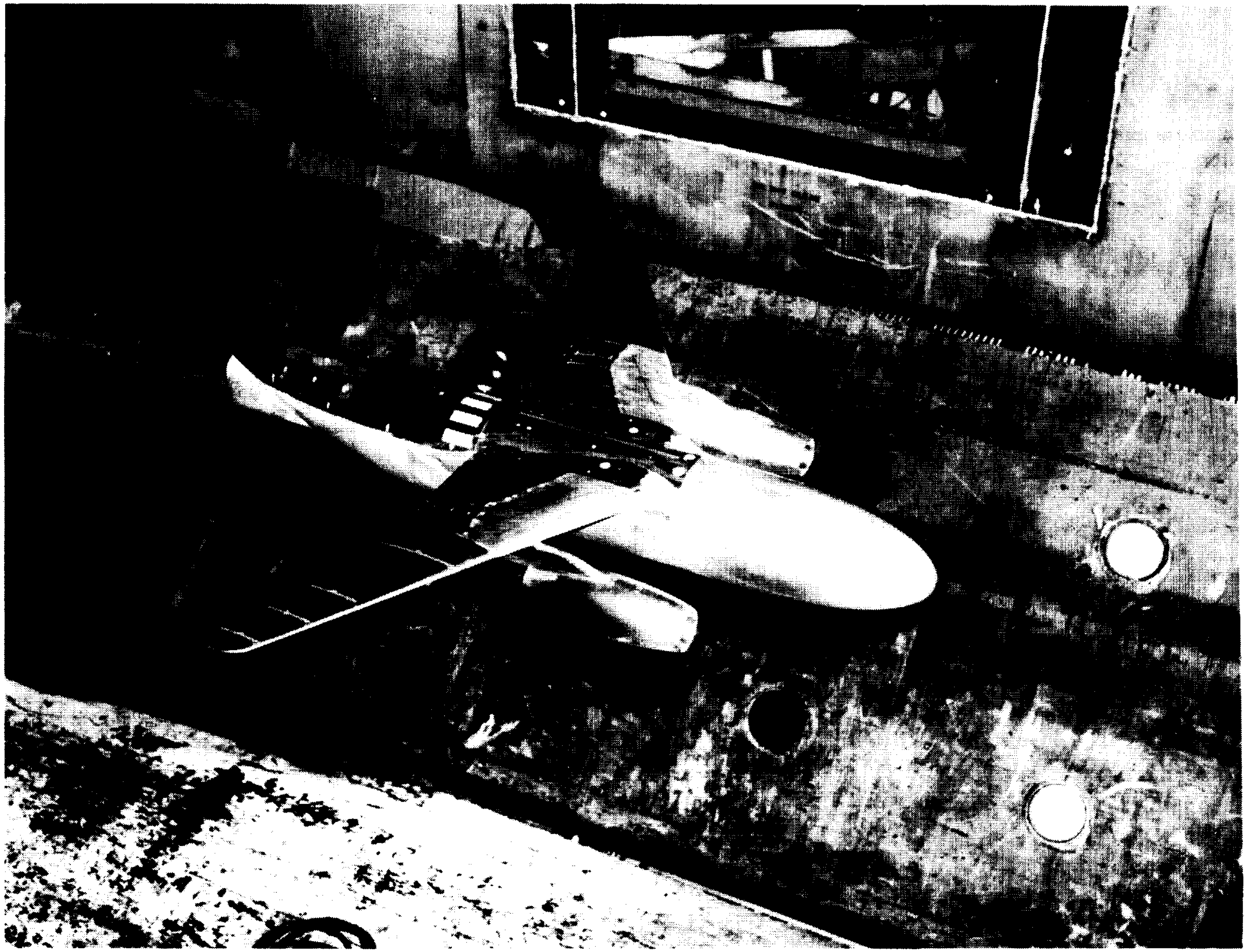

L-83-7290

(b) Model with laminar flow nacelles installed in forward position.

Figure 1. Continued.

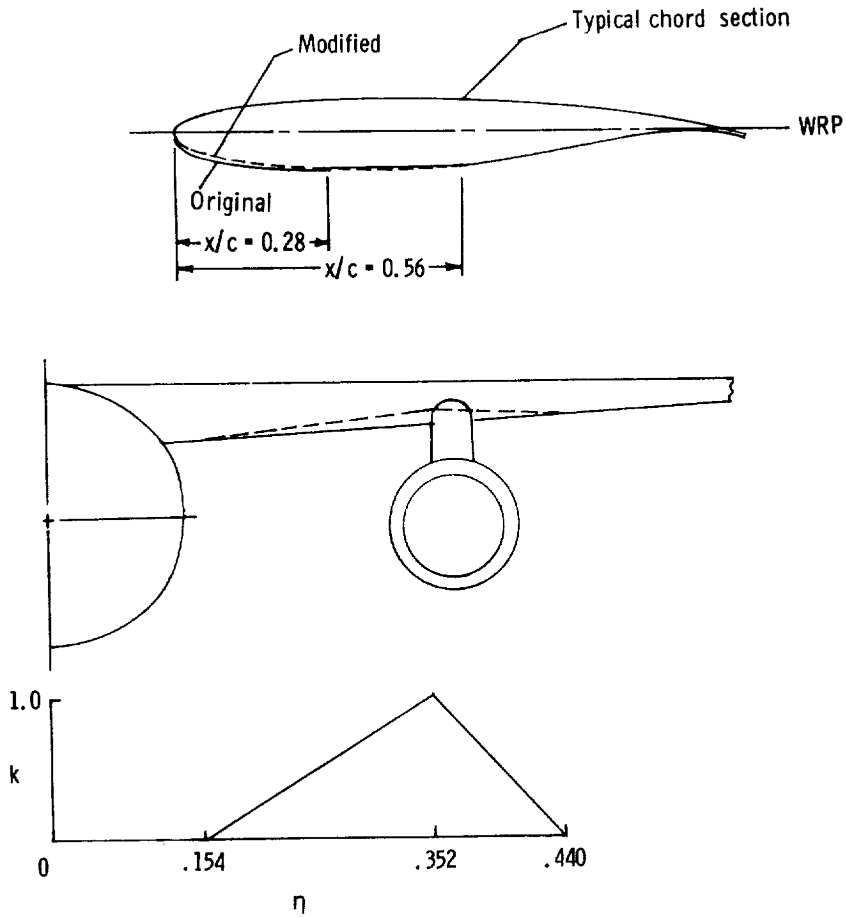

At any local station: $(z/c)_{\text{modified}} = (z/c)_{\text{original}} - (\Delta z/c)\,(k)$

Negative sign on $\Delta z/c$ values indicate undercut
Positive sign on $\Delta z/c$ values indicate material added

x/c	Δz/c	x/c	Δz/c	x/c	Δz/c
0.000	0.0000	0.120	-0.0064	0.360	0.0013
0.002	-0.0044	0.140	-0.0055	0.380	0.0013
0.005	-0.0064	0.160	-0.0045	0.400	0.0013
0.010	-0.0079	0.180	-0.0035	0.420	0.0012
0.020	-0.0092	0.200	-0.0027	0.440	0.0011
0.030	-0.0095	0.220	-0.0019	0.460	0.0008
0.040	-0.0094	0.240	-0.0012	0.480	0.0006
0.050	-0.0092	0.260	-0.0005	0.500	0.0004
0.060	-0.0089	0.280	0.0000	0.520	0.0003
0.070	-0.0085	0.300	0.0004	0.540	0.0001
0.080	-0.0081	0.320	0.0007	0.560	0.0000
0.100	-0.0072	0.340	0.0011		

(c) Wing leading-edge modifications.

Figure 1. Concluded.

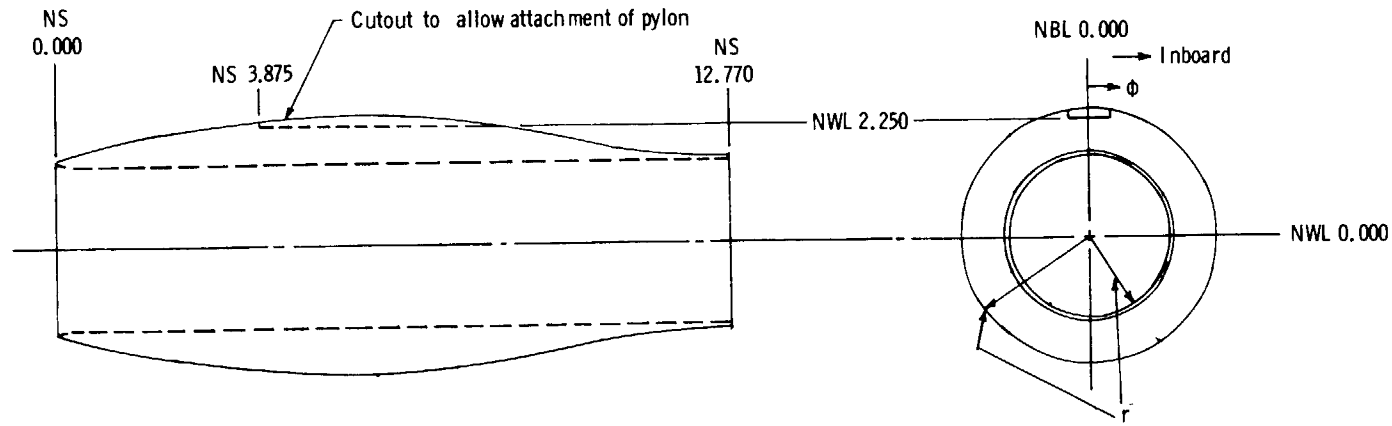

Internal contour[a]	
NS	r
0.	1.62860
0.00374	1.61909
0.01237	1.61026
0.02490	1.60181
0.04149	1.59349
0.06276	1.58519
0.08970	1.57688
0.12328	1.56873
0.16518	1.56096
0.21701	1.55406
0.28852	1.54841
0.36000	1.54660
12.77000	1.54660

[a]Dimensions are given to an accuracy to insure laminar flow of nacelle.

External contour[a]					
NS	r	NS	r	NS	r
0.	1.62860	0.20547	1.71286	7.25273	2.35259
0.00070	1.62950	0.24316	1.72478	7.67800	2.30450
0.00155	1.63031	0.28764	1.73830	7.93260	2.26944
0.00261	1.63119	0.34002	1.75359	8.18720	2.23030
0.00389	1.63217	0.40167	1.77084	8.44180	2.18778
0.00544	1.63327	0.47413	1.79026	8.69640	2.14260
0.00730	1.63451	0.55951	1.81214	8.95100	2.09543
0.00951	1.63590	0.65999	1.83668	9.20560	2.04695
0.01215	1.63748	1.04999	1.92214	9.46020	1.99783
0.01528	1.63926	1.43999	1.99544	9.71480	1.94871
0.01899	1.64128	1.83000	2.06020	9.96940	1.90022
0.02339	1.64358	2.22000	2.11907	10.22400	1.85299
0.02860	1.64619	2.61000	2.17363	10.47860	1.80762
0.03475	1.64915	3.00000	2.22451	10.73320	1.76471
0.04203	1.65252	3.42527	2.27534	10.98780	1.72483
0.05062	1.65634	3.85055	2.32025	11.24240	1.68856
0.06077	1.66069	4.27582	2.35817	11.49700	1.65644
0.07274	1.66562	4.70109	2.38809	11.75160	1.62902
0.08686	1.67123	5.12636	2.40909	12.00620	1.62902
0.10352	1.67760	5.55164	2.42029	12.26080	1.60682
0.12303	1.68479	5.97691	2.42093	12.51540	1.58012
0.14615	1.69300	6.40218	2.41027	12.77000	1.57660
0.17338	1.70230	6.82745	2.38768		

[a]Dimensions are given to an accuracy to insure laminar flow of nacelle.

External pressure orifices[a] located at Φ of –						
NS	0°	30°	90°	180°	270°	330°
0.20	↓	↓	↓	↓	↓	↓
0.50	↓	↓	↓	↓	↓	↓
1.00	↓	↓	↓	↓	↓	↓
2.00	↓	↓	↓	↓	↓	↓
3.75	↓	↓	↓	↓	↓	↓
5.00		↓	↓	↓	↓	↓
6.00		↓	↓	↓	↓	↓
7.00		↓	↓	↓	↓	↓
8.00		↓	↓	↓	↓	↓
9.00		↓	↓	↓	↓	↓
10.00		↓	↓	↓	↓	↓
11.75		↓	↓	↓	↓	↓

[a]Internal pressure orifices located at NS 2.50 for Φ of 0°, 90°, 180°, and 270°.

Figure 2. Details of nacelles. Linear dimensions are in inches.

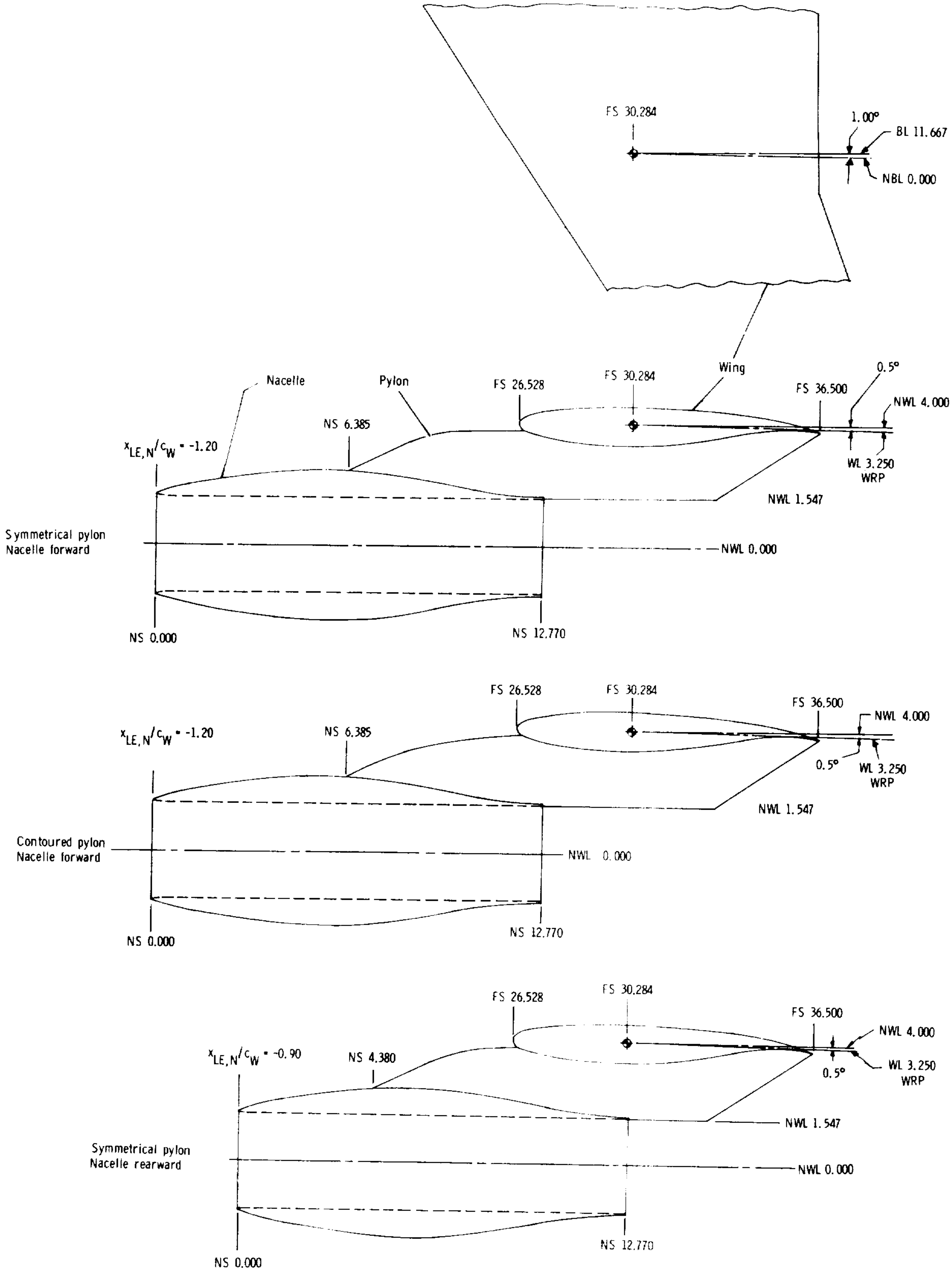

Figure 3. Nacelle test matrix. Linear dimensions are in inches.

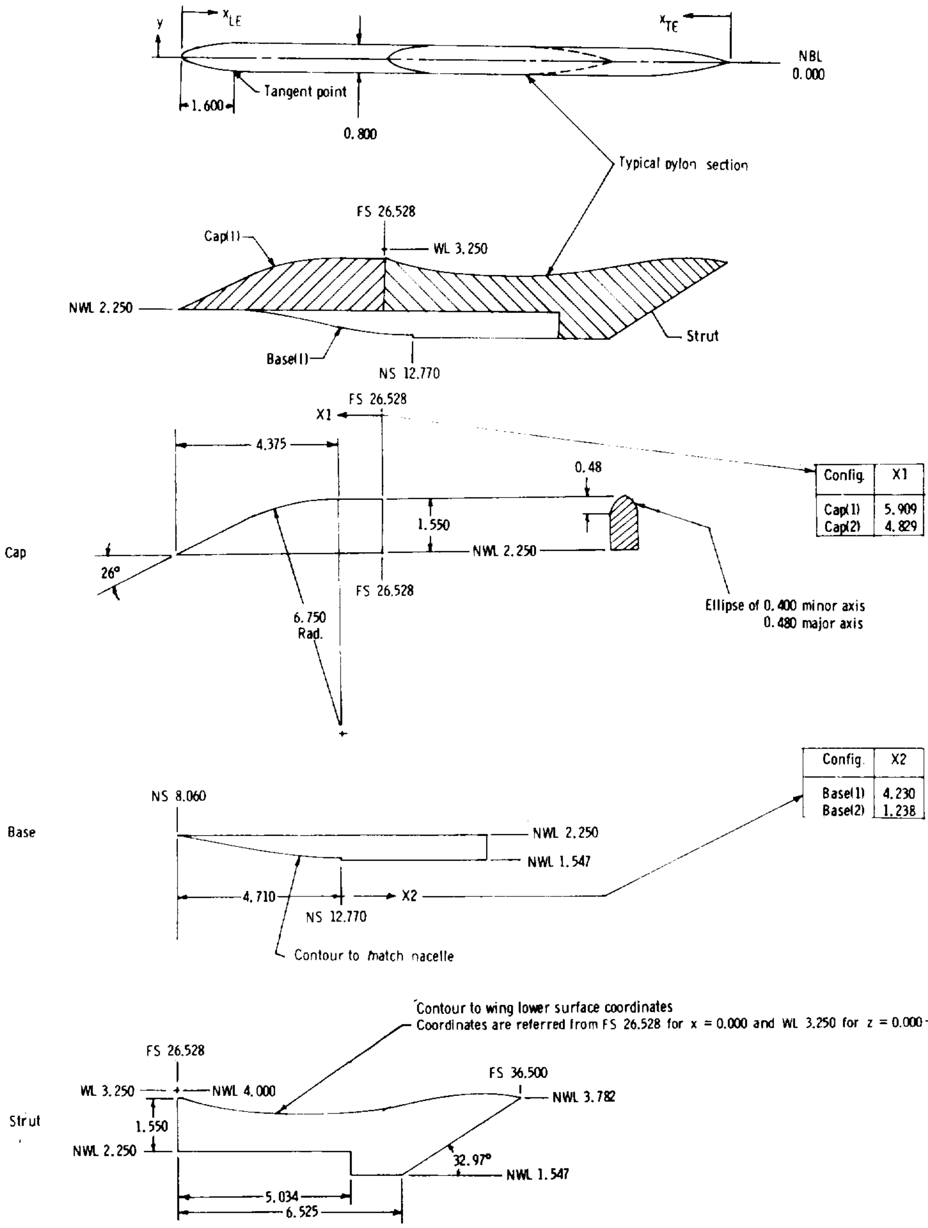

Config.	X1
Cap(1)	5.909
Cap(2)	4.829

Config.	X2
Base(1)	4.230
Base(2)	1.238

Pylon leading-edge section	
x_{LE}	y
0.000	0.000
0.020	0.060
0.030	0.073
0.050	0.091
0.100	0.124
0.200	0.173
0.300	0.211
0.400	0.243
0.600	0.294
0.800	0.332
1.000	0.361
1.200	0.382
1.400	0.395
1.600	0.400

Pylon trailing-edge section	
x_{TE}	y
0.000	0.008
0.501	0.072
1.003	0.129
1.504	0.200
2.005	0.282
2.507	0.334
2.841	0.375
3.108	0.393
3.342	0.400

Lower wing coordinates			
x	z	x	z
0.000	-0.038	3.490	-0.672
0.020	-0.099	3.989	-0.668
0.050	-0.137	4.488	-0.649
0.100	-0.179	4.986	-0.613
0.199	-0.234	5.485	-0.559
0.399	-0.308	5.983	-0.489
0.598	-0.365	6.482	-0.404
0.798	-0.412	6.981	-0.312
0.997	-0.453	7.479	-0.221
1.396	-0.519	7.978	-0.139
1.795	-0.573	8.477	-0.081
2.194	-0.613	8.975	-0.063
2.593	-0.642	9.972	-0.164
2.992	-0.661		

Pylon configuration	Components
Nacelle forward	Cap(1) + Base(1) + Strut
Nacelle rearward	Cap(2) + Base(2) + Strut

(a) Symmetrical pylon.

Figure 4. Details of pylons. Linear dimensions are in inches.

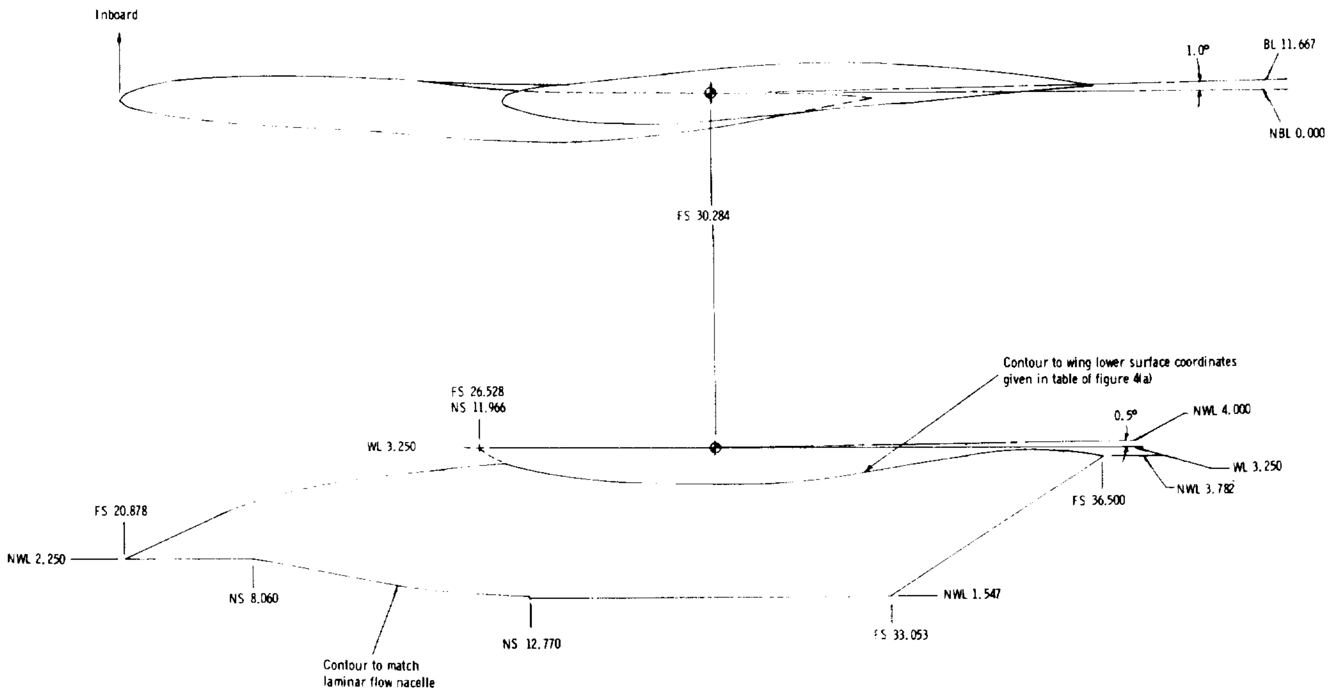

Coordinates in aircraft reference system at WL of -											
1.000				1.800				2.600			
x_{in}	y_{in}	x_{out}	y_{out}	x_{in}	y_{in}	x_{out}	y_{out}	x_{in}	y_{in}	x_{out}	y_{out}
19.967	11.569	19.967	11.569	21.614	11.497	21.614	11.497	23.839	11.494	23.839	11.494
20.634	11.328	20.633	11.806	22.287	11.273	22.274	11.751	24.427	11.305	24.446	11.759
21.317	11.236	21.309	11.908	22.927	11.202	22.902	11.863	25.025	11.249	25.026	11.887
22.002	11.201	21.984	11.967	23.567	11.181	23.576	11.942	25.621	11.239	25.609	11.981
22.640	11.204	22.659	12.002	24.206	11.196	24.206	11.992	26.215	11.264	26.238	12.057
23.281	11.226	23.295	12.027	24.844	11.232	24.837	12.033	26.812	11.314	26.822	12.119
23.959	11.258	23.964	12.068	25.498	11.278	25.481	12.079	27.428	11.363	27.414	12.164
24.636	11.298	24.634	12.100	26.149	11.330	26.125	12.131	28.015	11.387	28.031	12.187
25.314	11.344	25.304	12.145	26.805	11.392	26.766	12.192	28.605	11.389	28.614	12.189
25.991	11.396	25.973	12.197	27.434	11.443	27.432	12.244	29.197	11.375	29.194	12.175
26.631	11.452	26.636	12.258	28.066	11.467	28.096	12.267	29.791	11.346	29.805	12.147
27.331	11.516	27.328	12.317	28.706	11.467	28.719	12.267	30.395	11.315	30.389	12.108
27.998	11.549	27.980	12.340	29.382	11.454	29.367	12.241	30.985	11.297	30.977	12.063
28.670	11.568	28.681	12.325	30.017	11.437	30.011	12.188	31.577	11.290	31.562	12.011
29.347	11.578	29.327	12.280	30.655	11.431	30.693	12.119	32.170	11.296	32.194	11.951
30.032	11.579	30.020	12.204	31.296	11.435	31.327	12.047	32.765	11.317	32.777	11.896
30.672	11.589	30.652	12.124	31.938	11.451	31.960	11.972	33.359	11.354	33.359	11.845
31.313	11.607	31.334	12.032	32.630	11.485	32.592	11.898	33.951	11.409	33.993	11.796
32.004	11.638	32.016	11.938	33.273	11.534	33.273	11.824	34.590	11.485	34.581	11.756
32.645	11.681	32.650	11.854	33.912	11.601	33.909	11.765	35.177	11.567	35.170	11.721
33.334	11.756	33.334	11.756	34.548	11.698	34.548	11.698	35.762	11.659	35.762	11.659

(b) Contoured pylon.

Figure 4. Concluded.

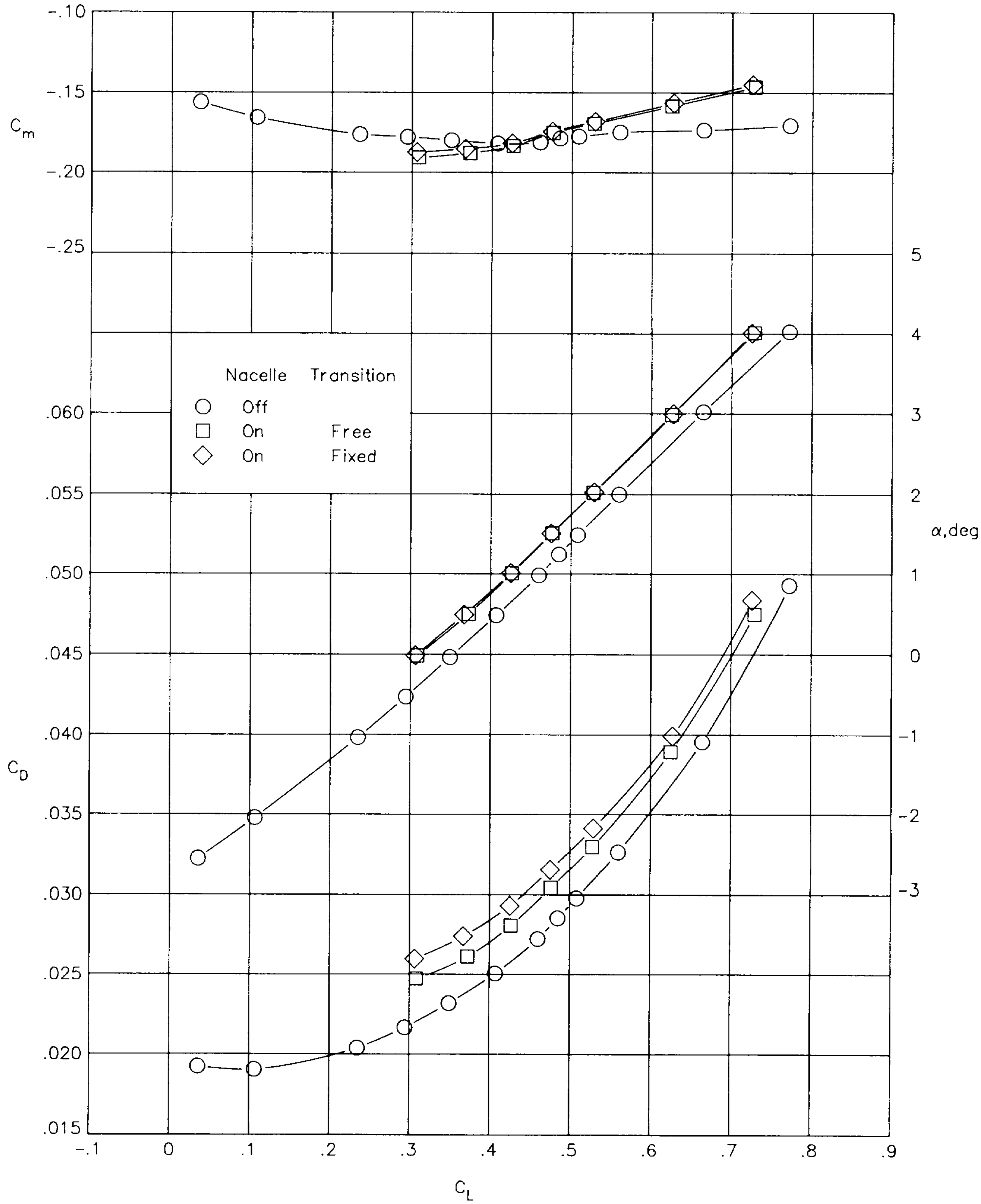

(a) $M = 0.70$.

Figure 5. Longitudinal aerodynamic characteristics with nacelles in forward position on symmetrical pylons.

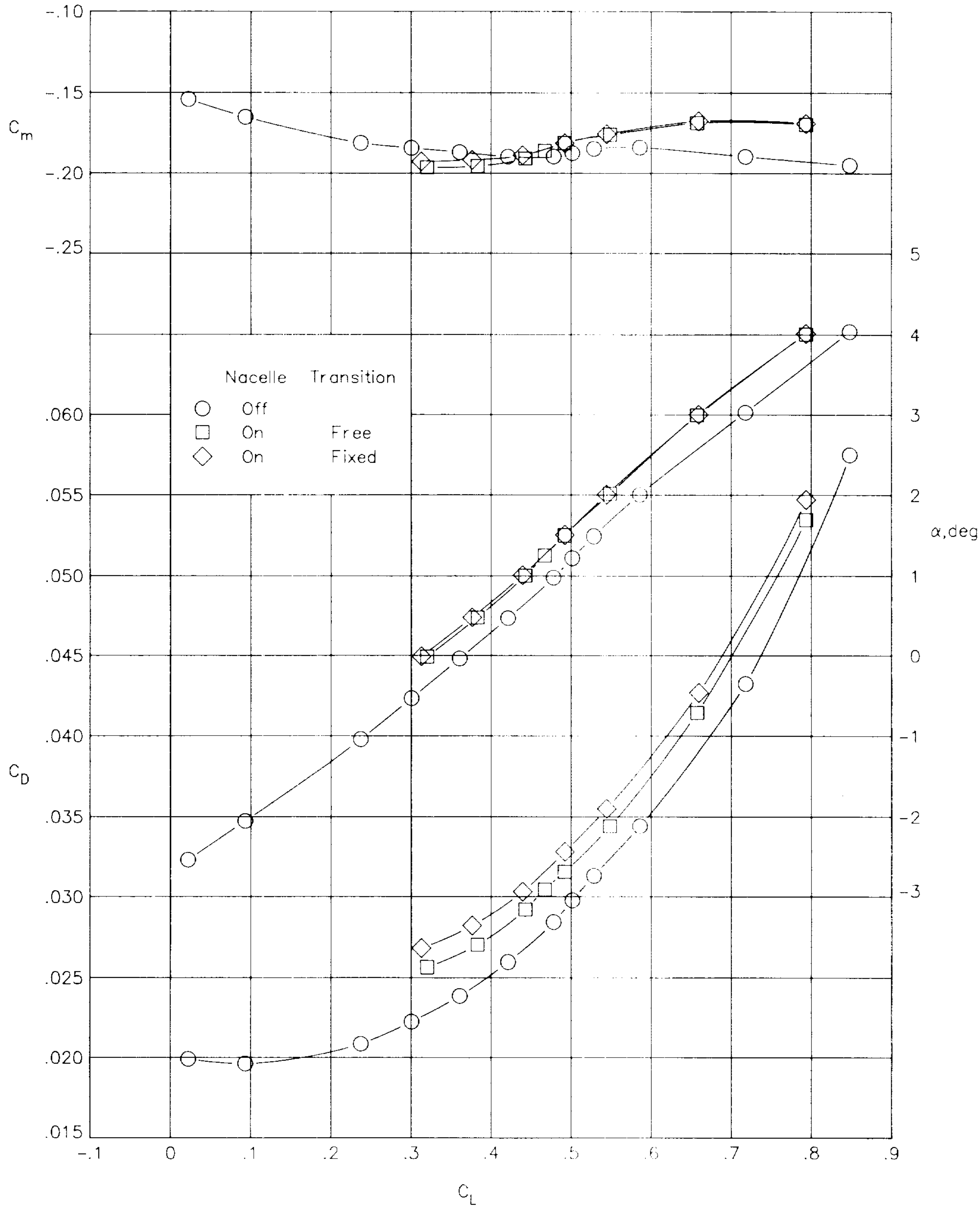

(b) $M = 0.75$.

Figure 5. Continued.

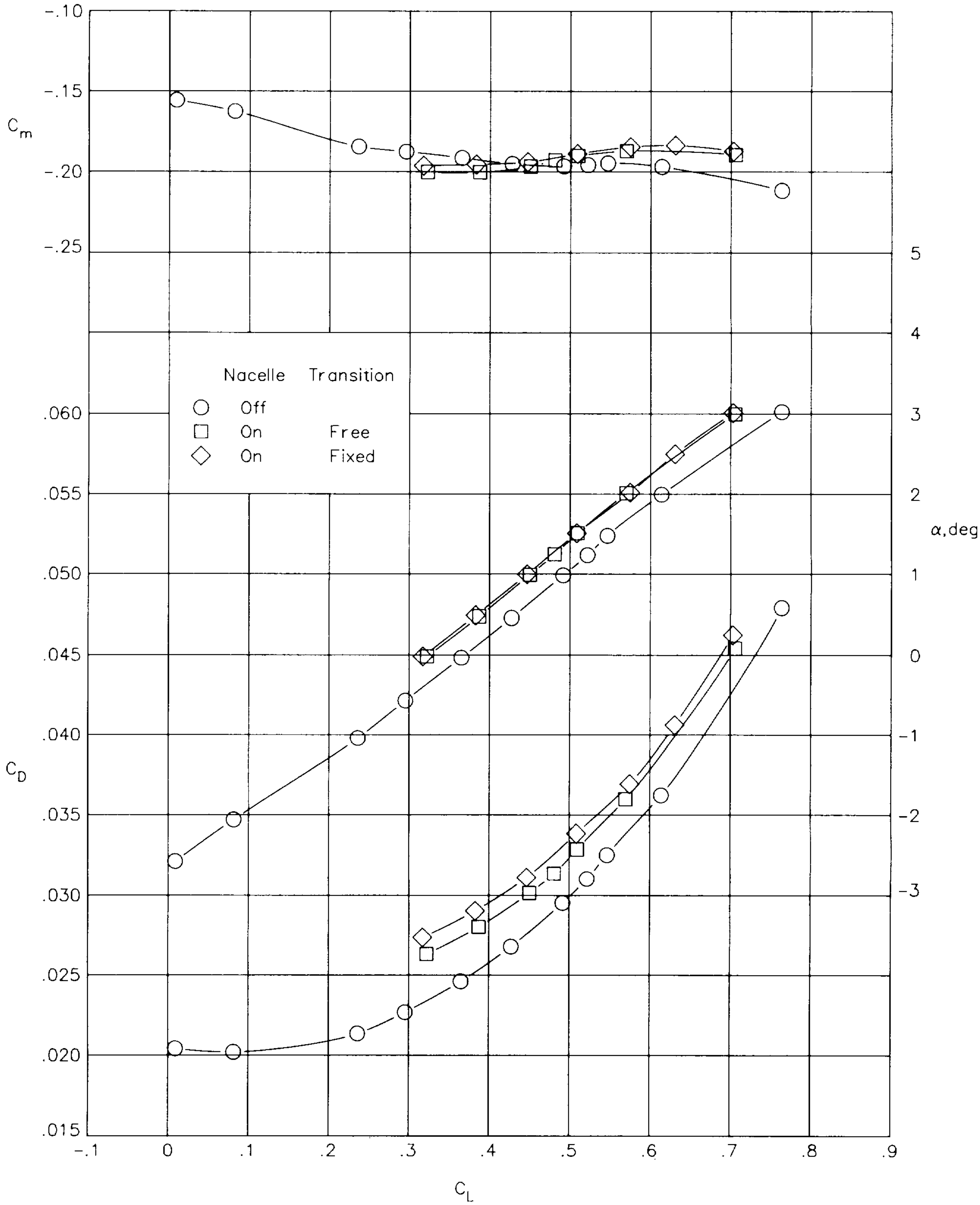

(c) $M = 0.78$.

Figure 5. Continued.

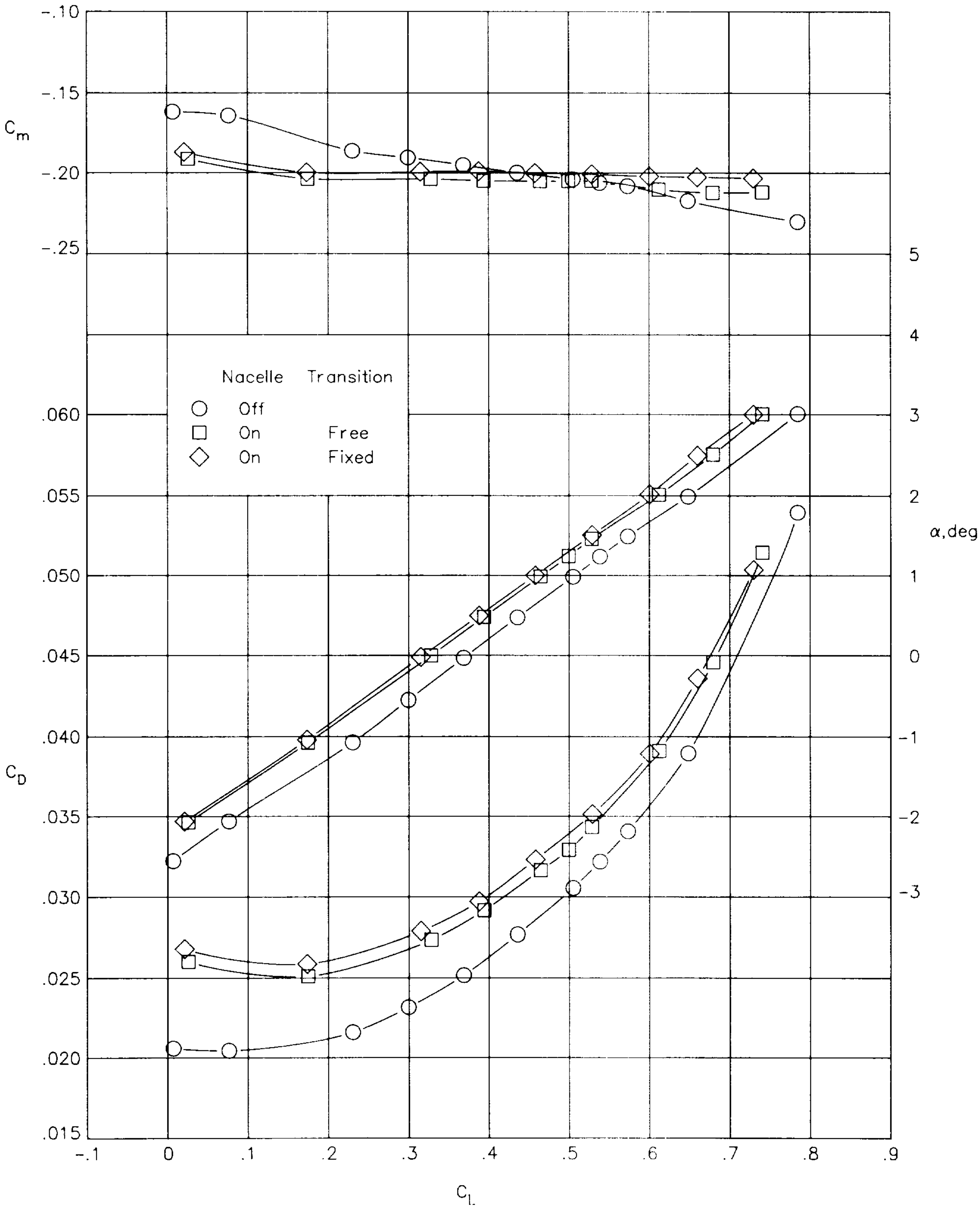

(d) $M = 0.80$.

Figure 5. Continued.

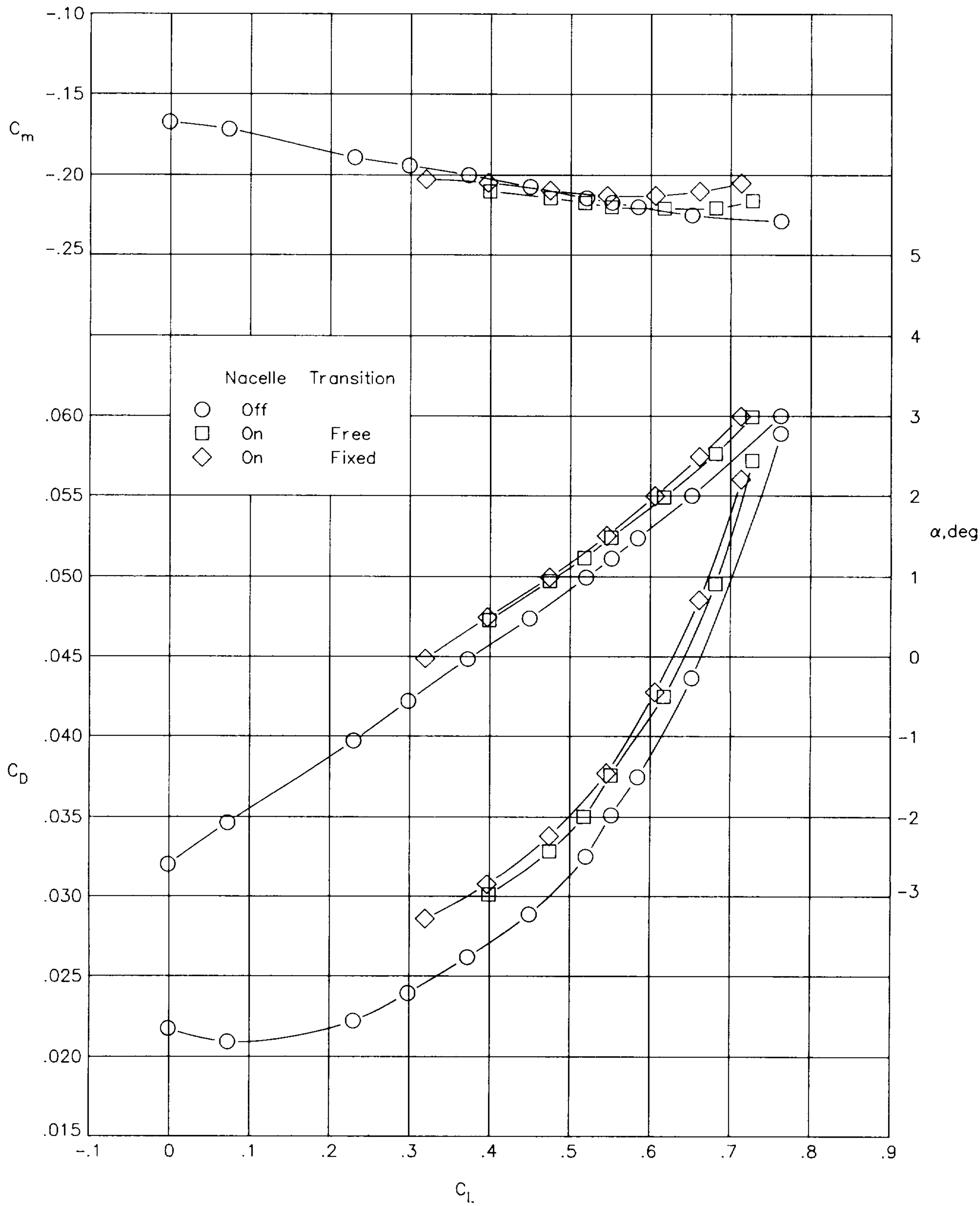

(e) $M = 0.82$.

Figure 5. Concluded.

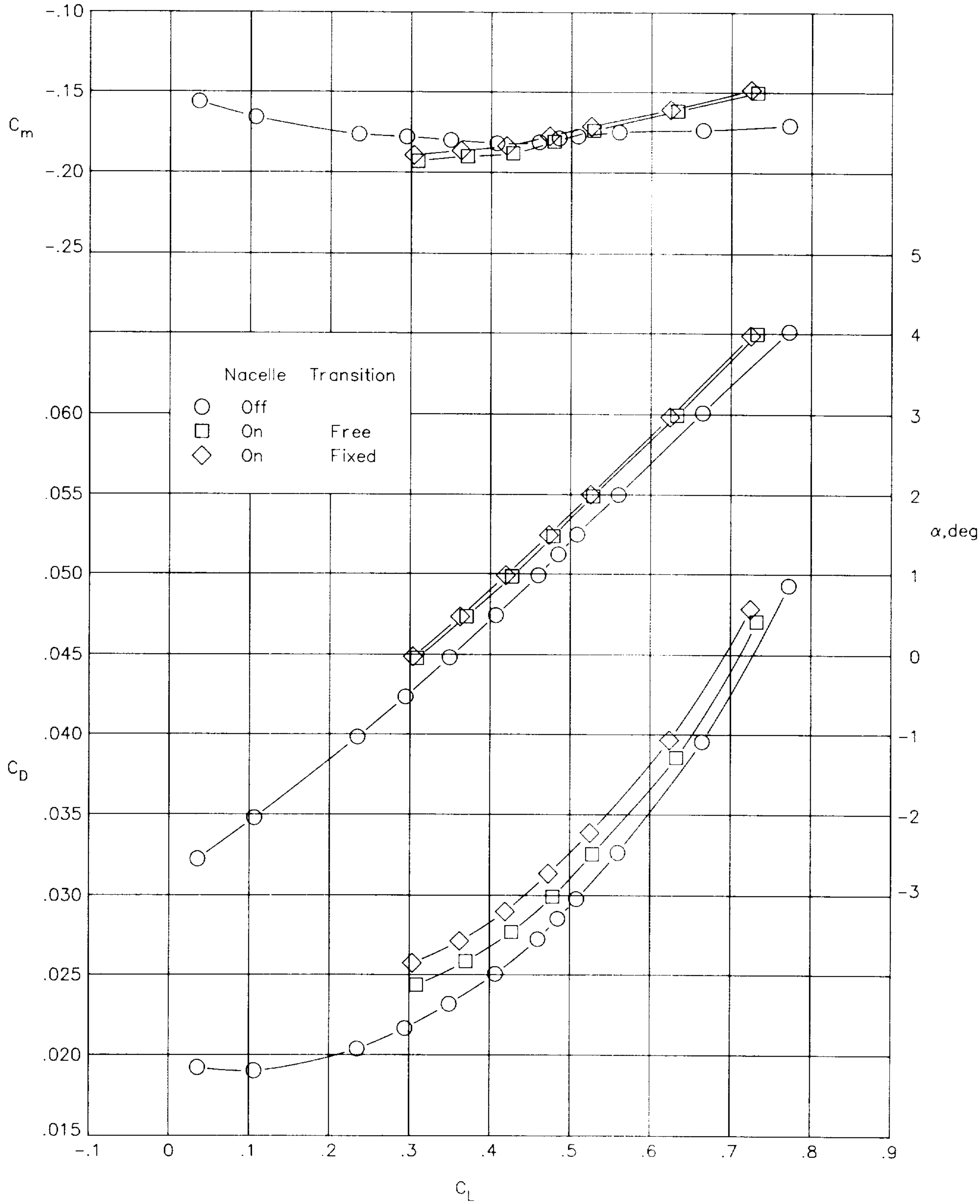

(a) $M = 0.70$.

Figure 6. Longitudinal aerodynamic characteristics with nacelles in forward position on contoured pylons.

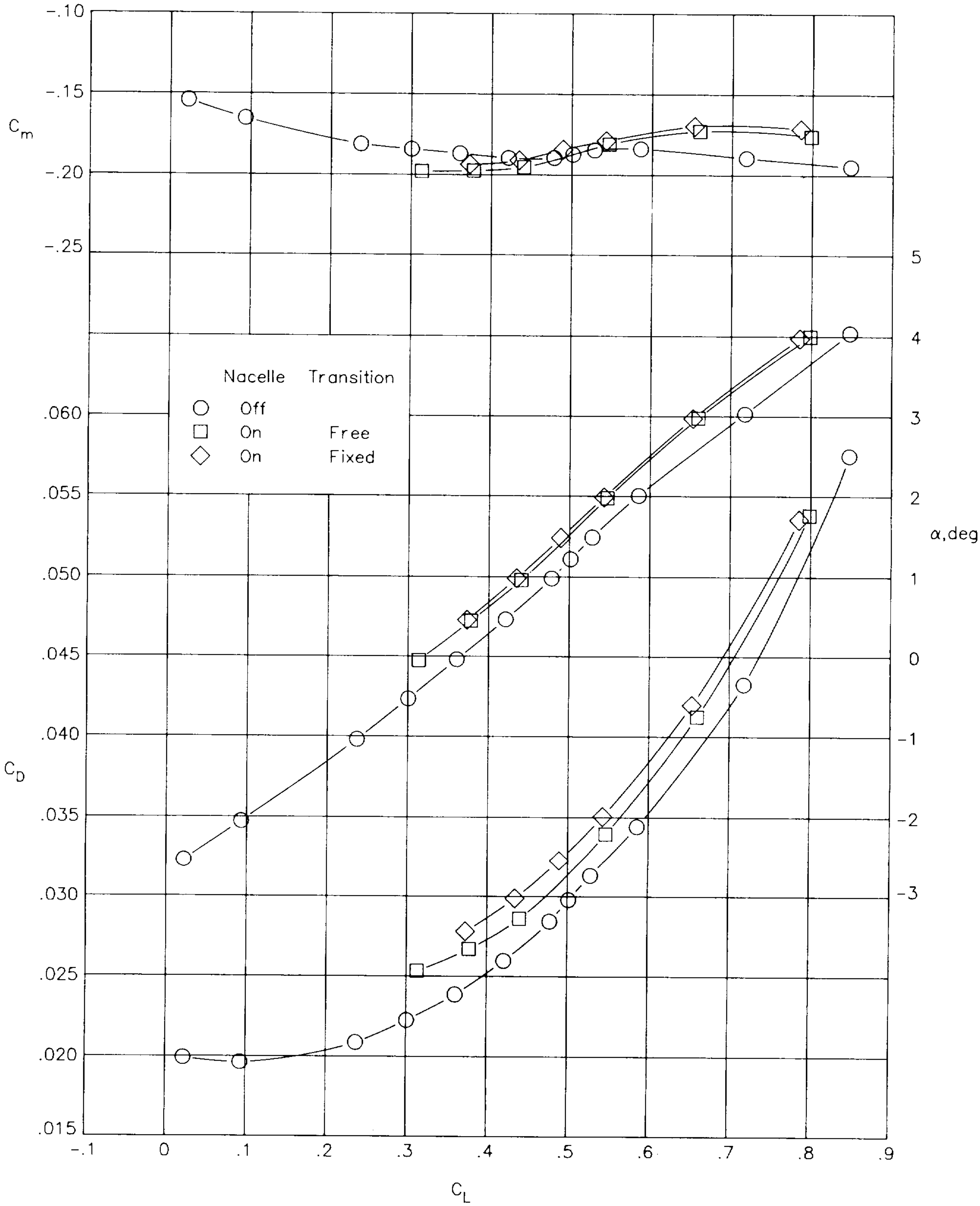

(b) $M = 0.75$.

Figure 6. Continued.

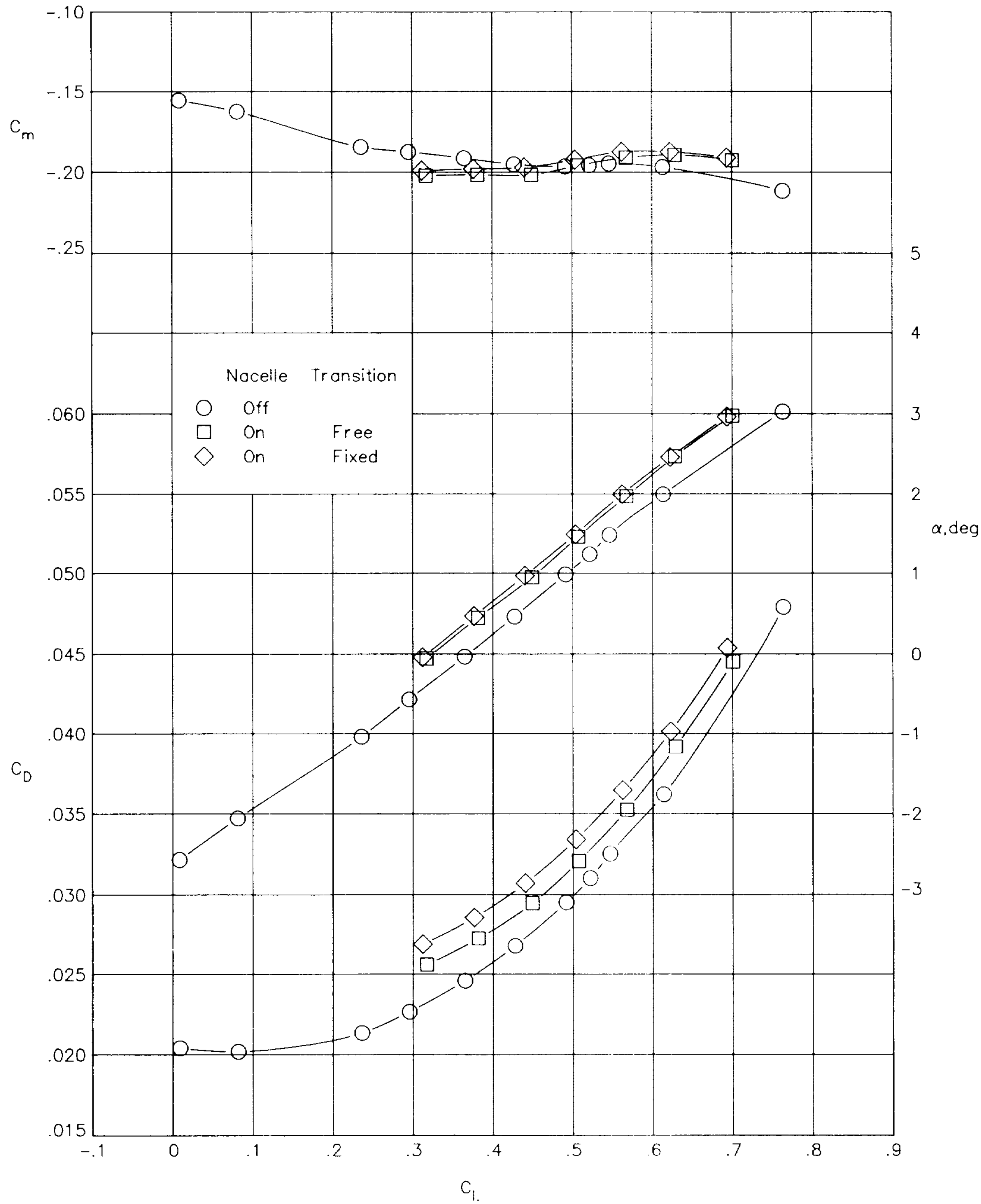

(c) $M = 0.78$.

Figure 6. Continued.

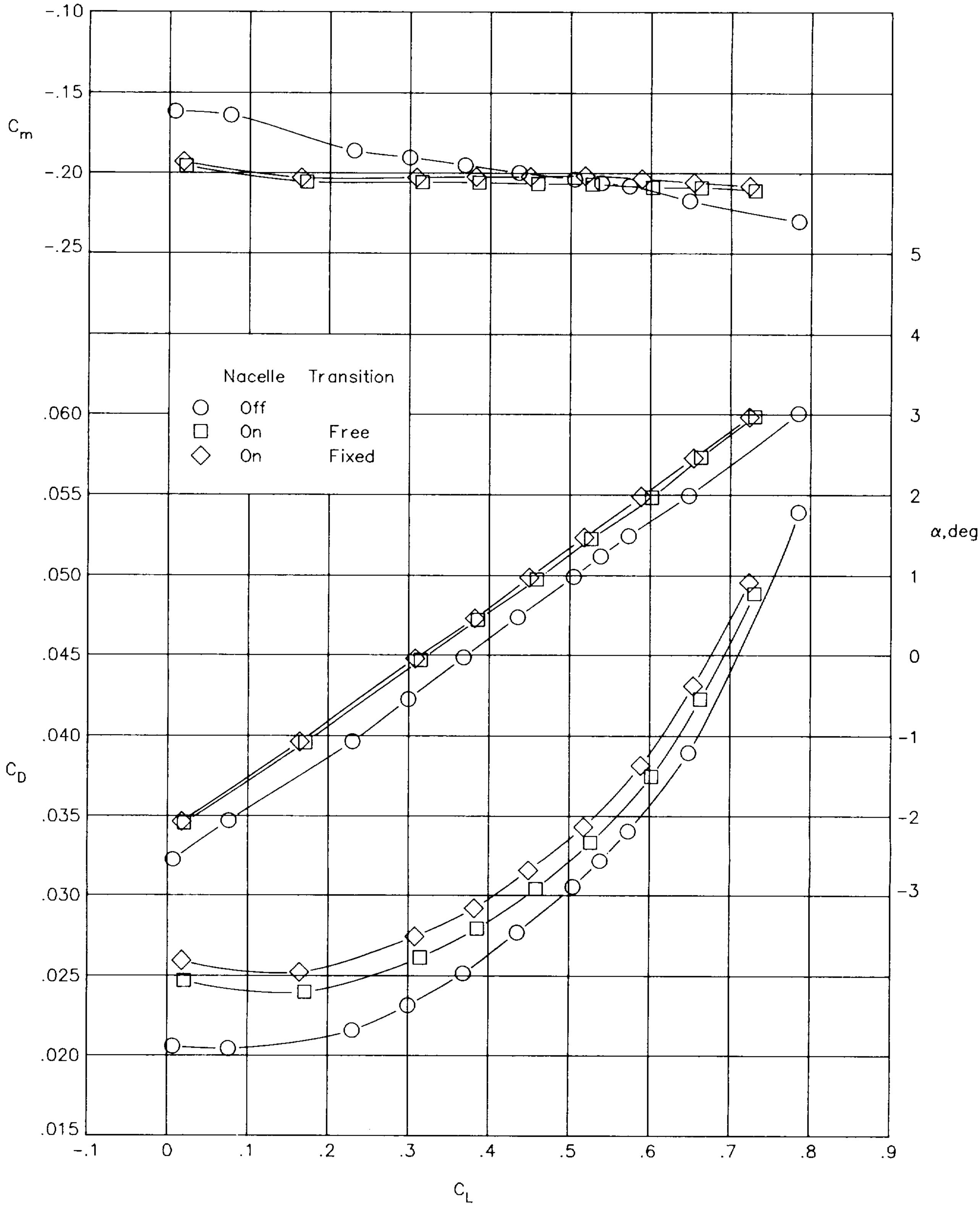

(d) $M = 0.80$.

Figure 6. Continued.

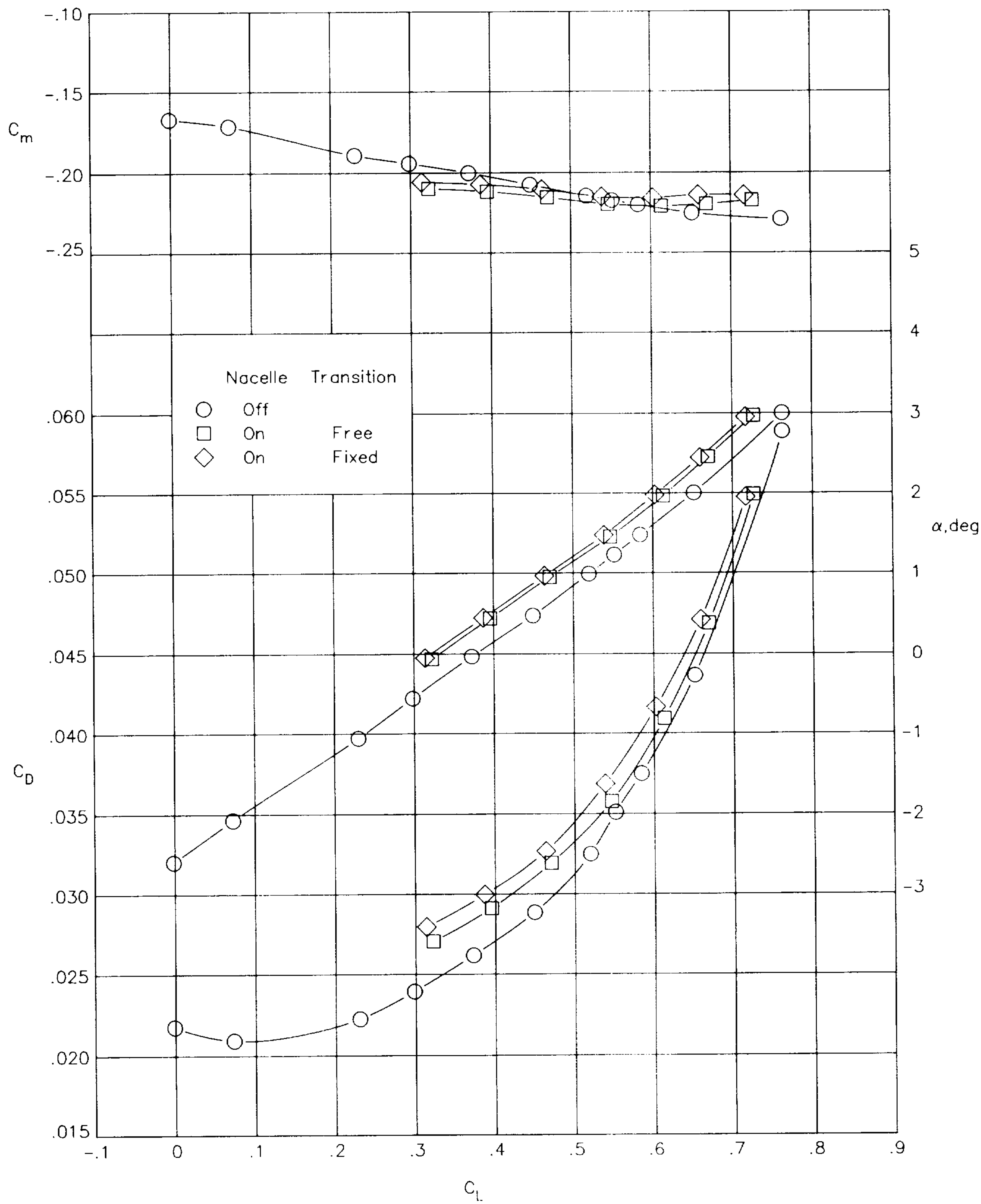

(e) $M = 0.82$.

Figure 6. Concluded.

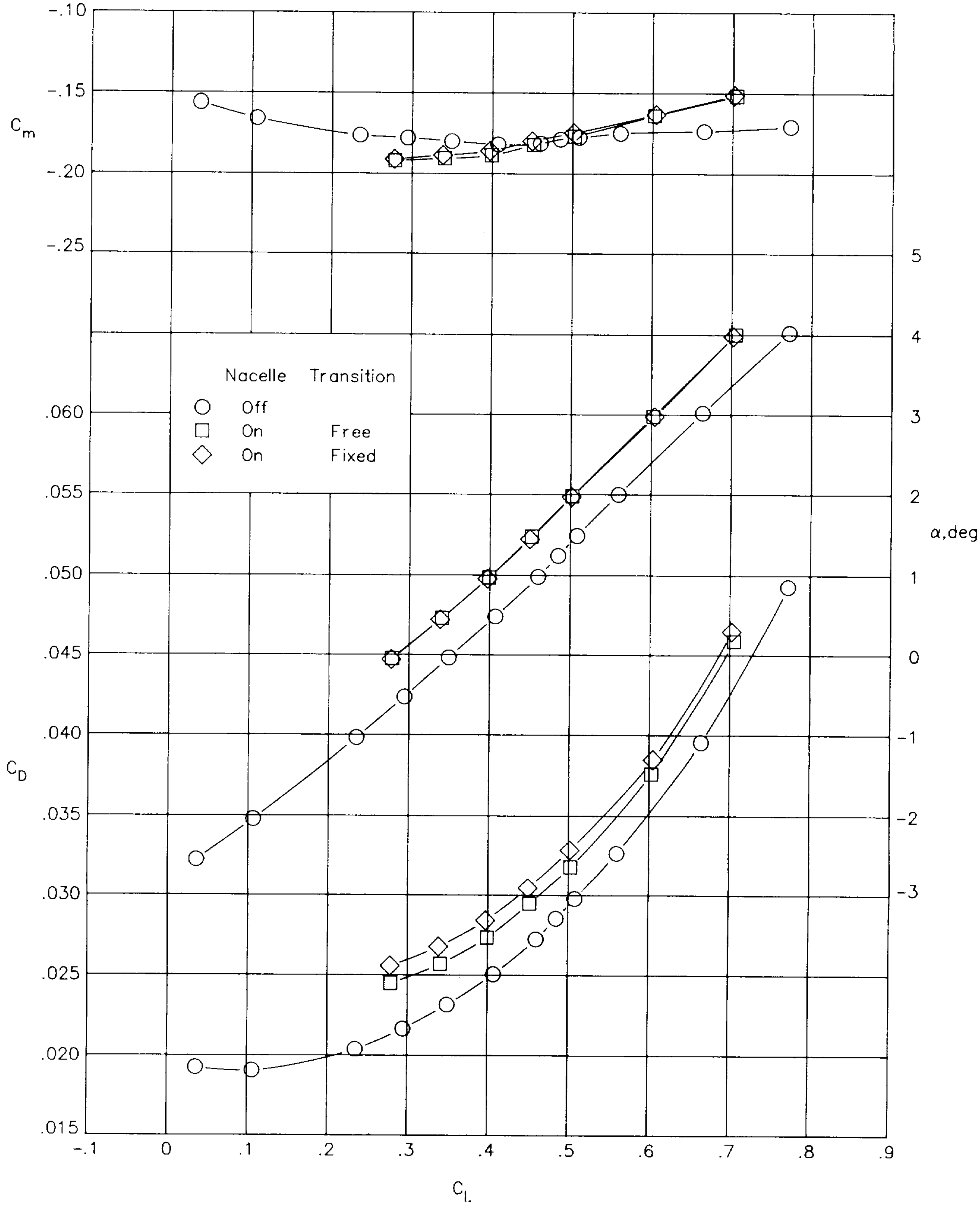

(a) $M = 0.70$.

Figure 7. Longitudinal aerodynamic characteristics with nacelles in rearward position on symmetrical pylons.

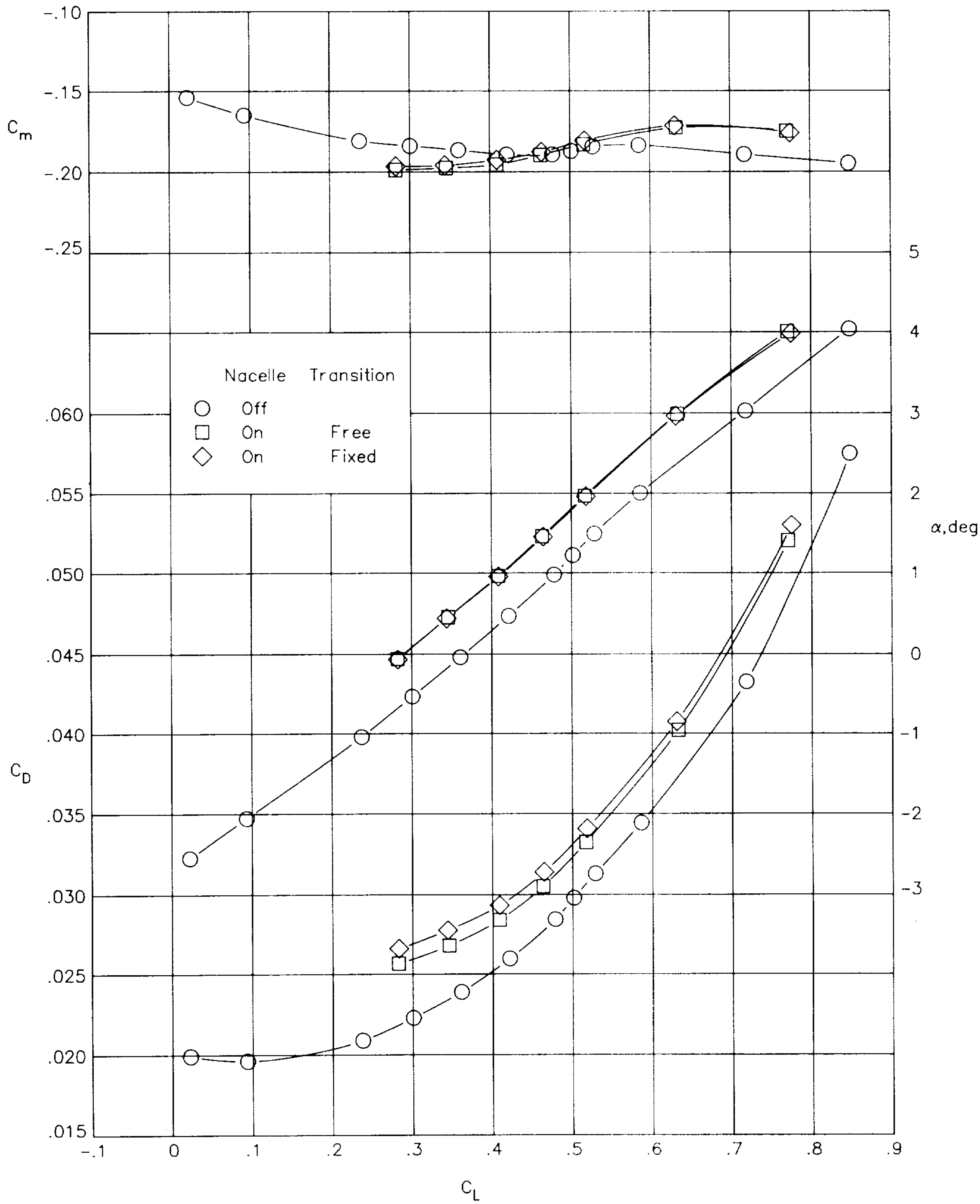

(b) $M = 0.75$.

Figure 7. Continued.

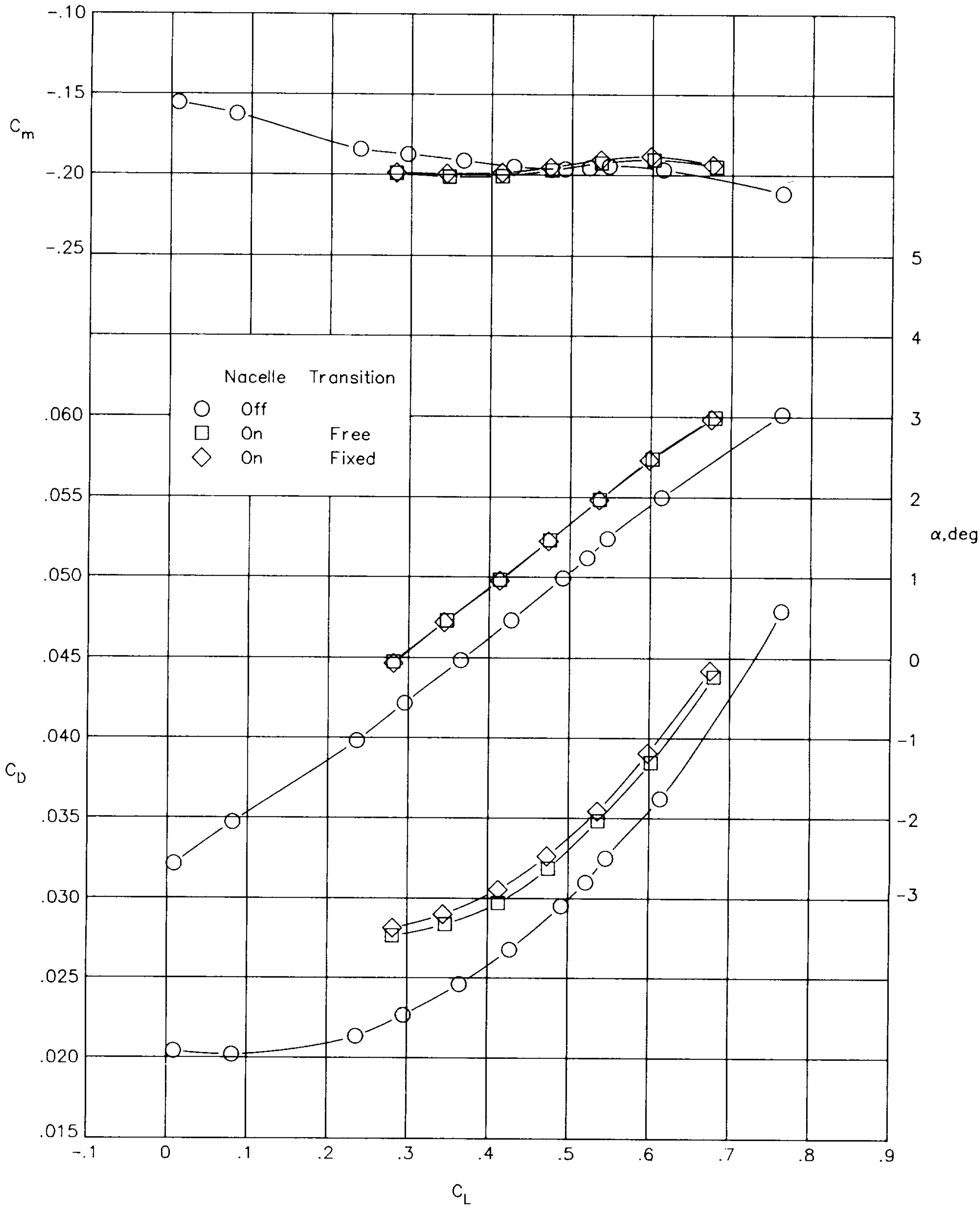

(c) $M = 0.78$.

Figure 7. Continued.

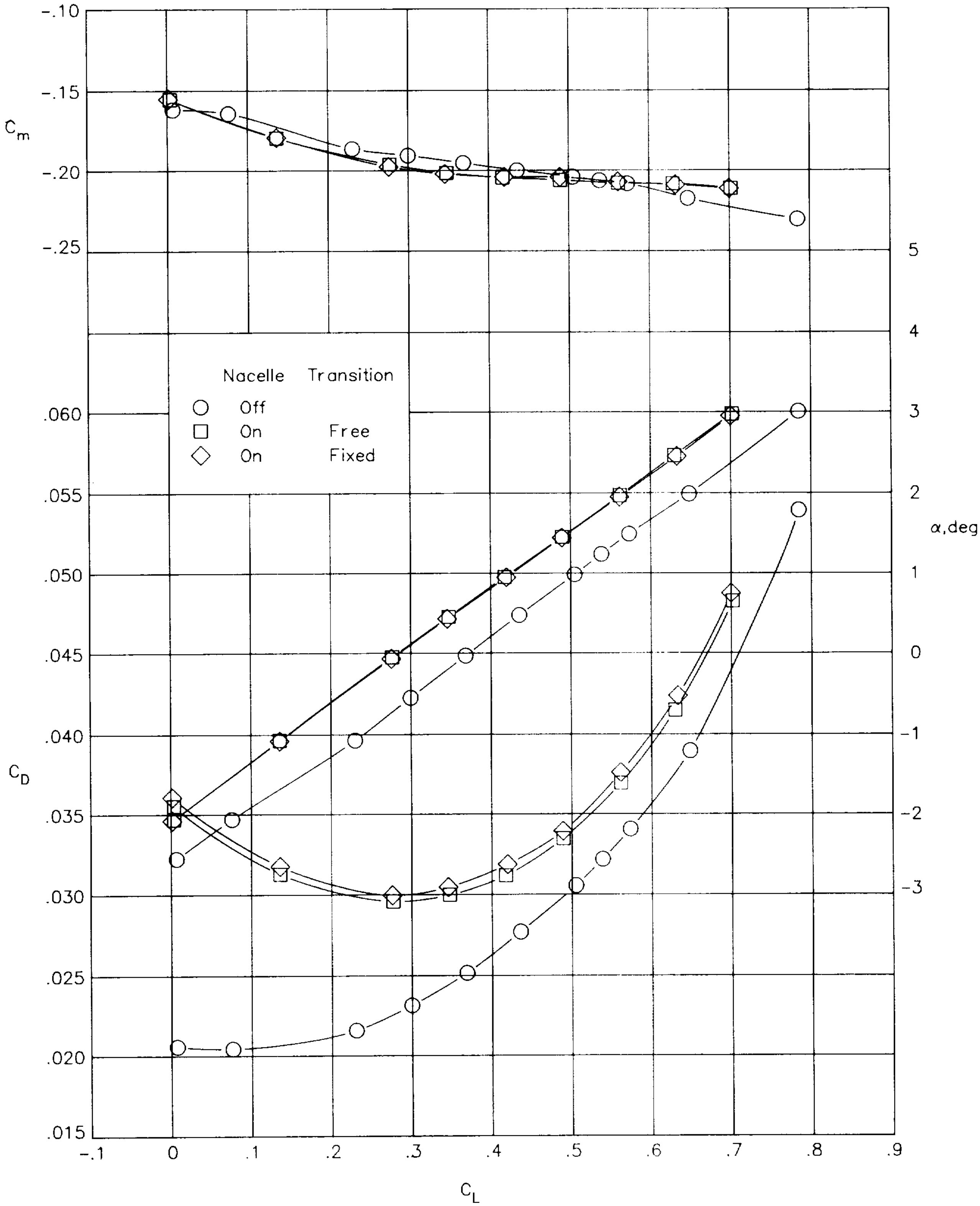

(d) $M = 0.80$.

Figure 7. Continued.

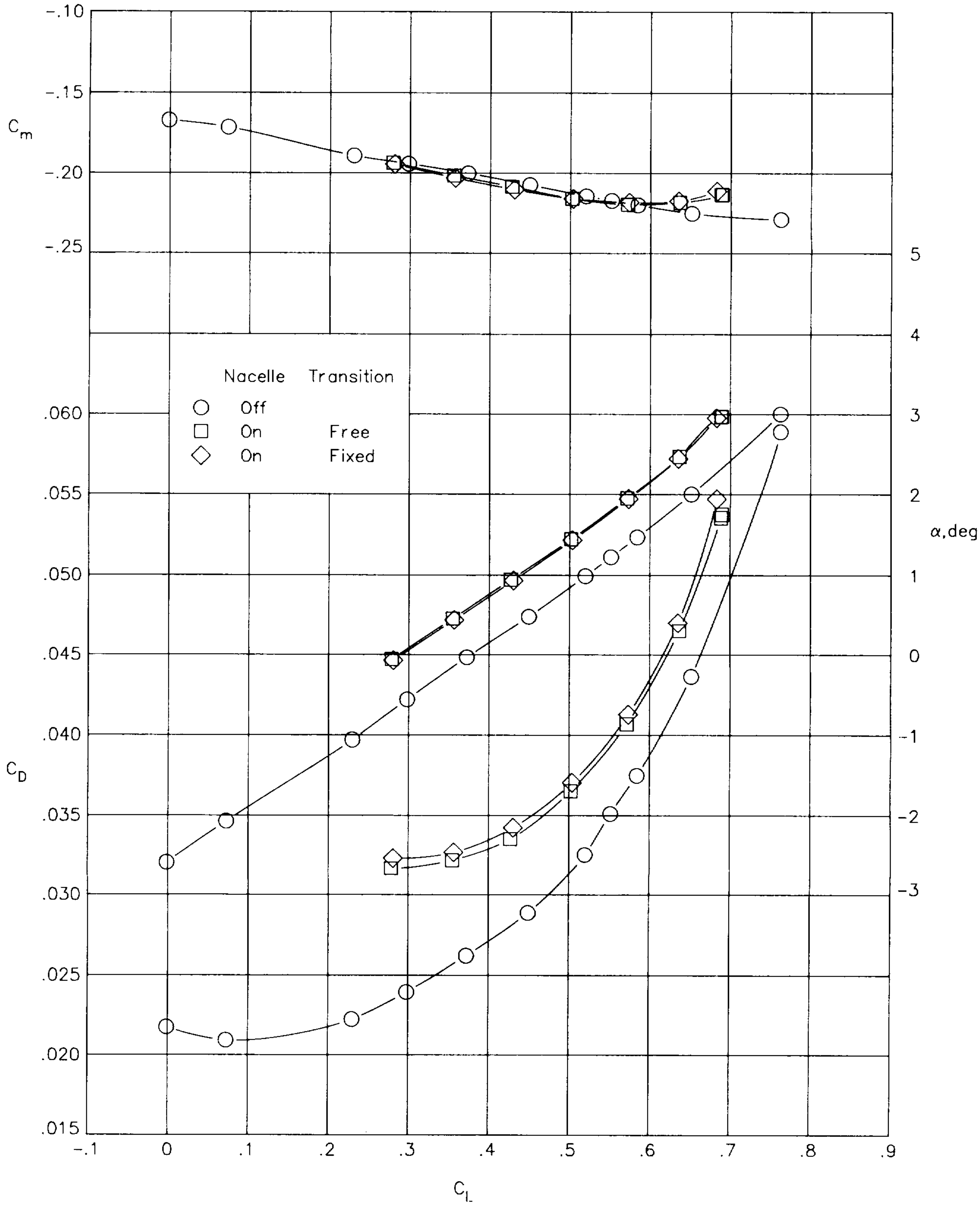

(e) $M = 0.82$.

Figure 7. Concluded.

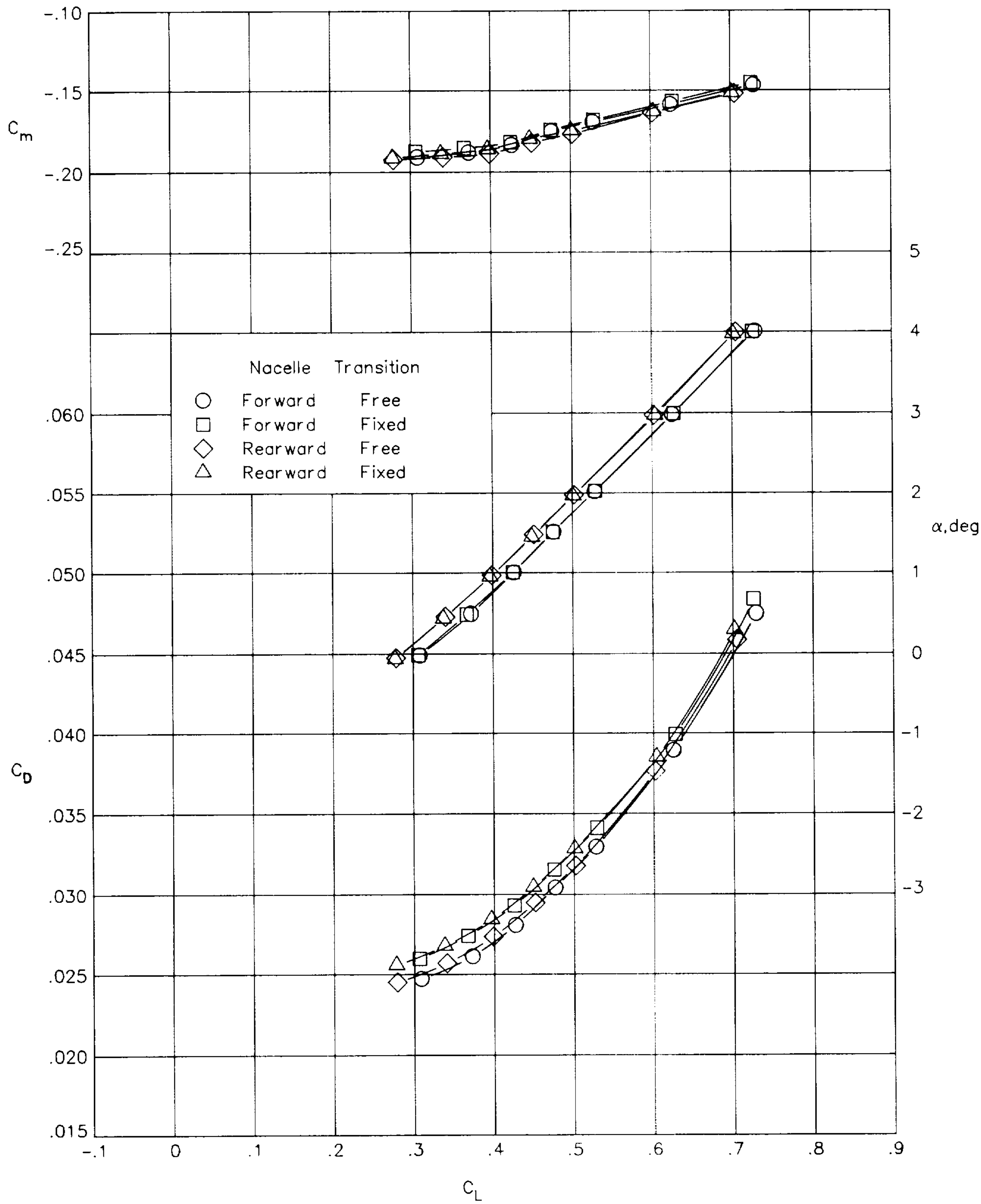

(a) $M = 0.70$.

Figure 8. Effect of longitudinal position of nacelles on aerodynamic characteristics with nacelles installed on symmetrical pylons.

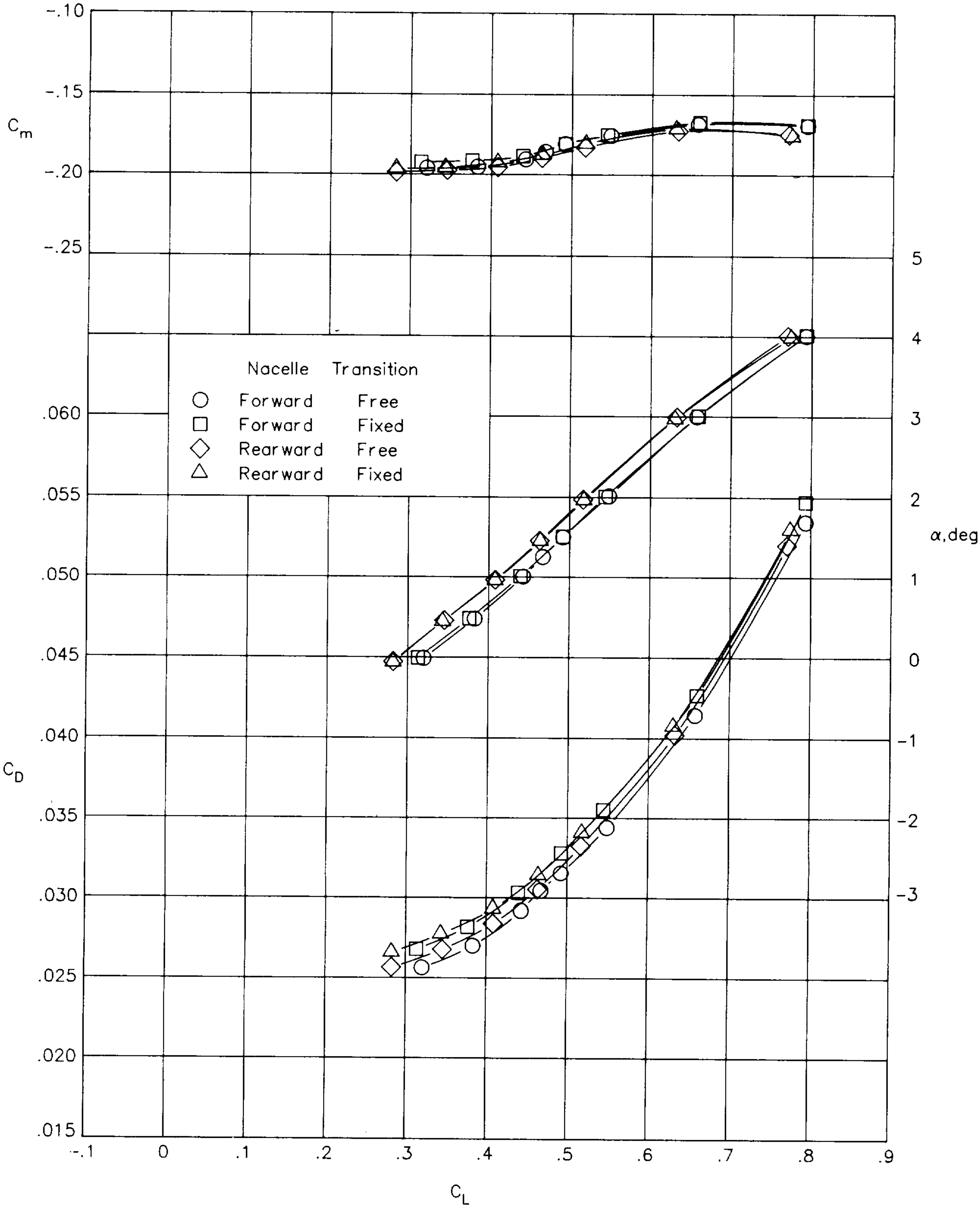

(b) $M = 0.75$.

Figure 8. Continued.

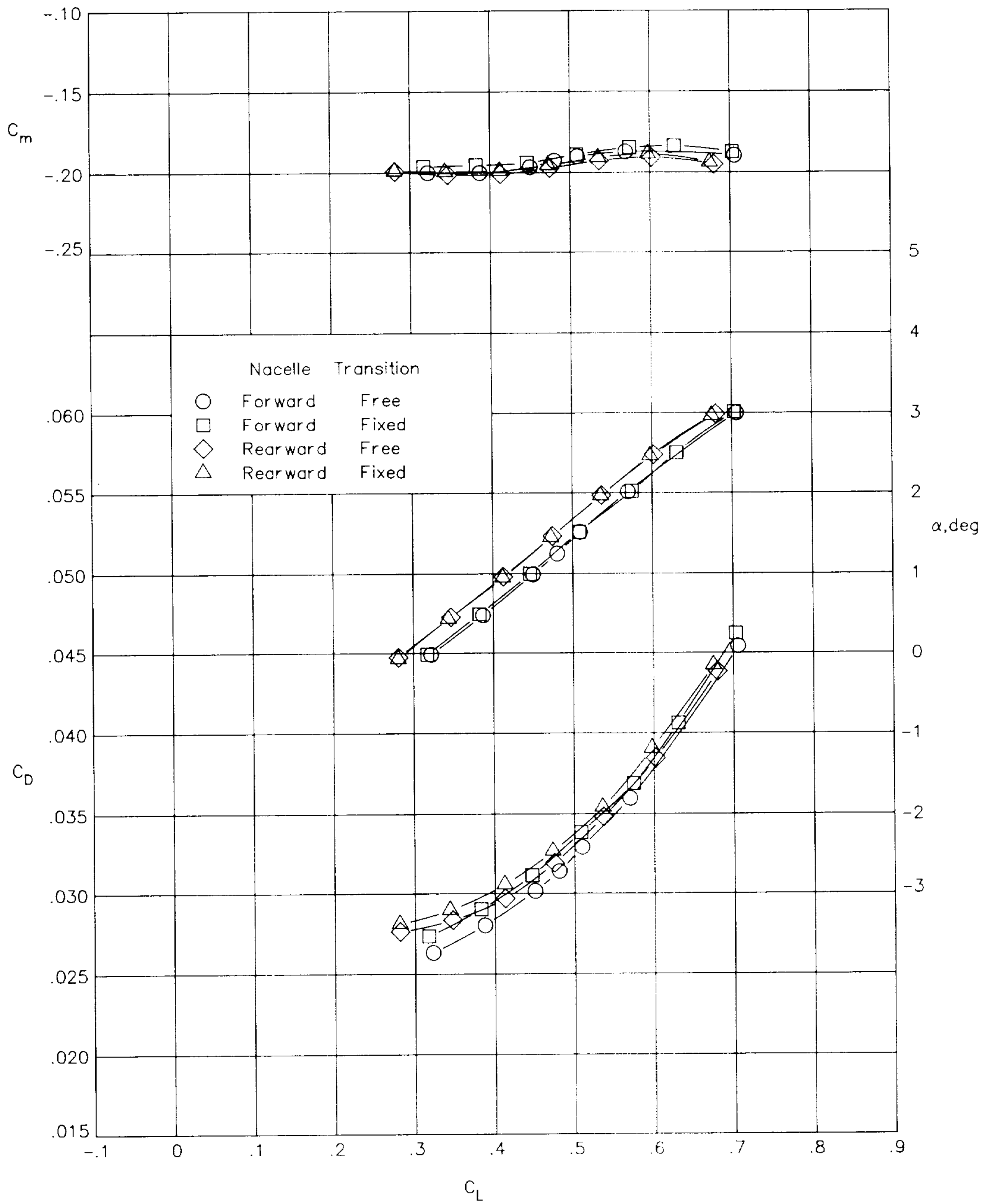

(c) $M = 0.78$.

Figure 8. Continued.

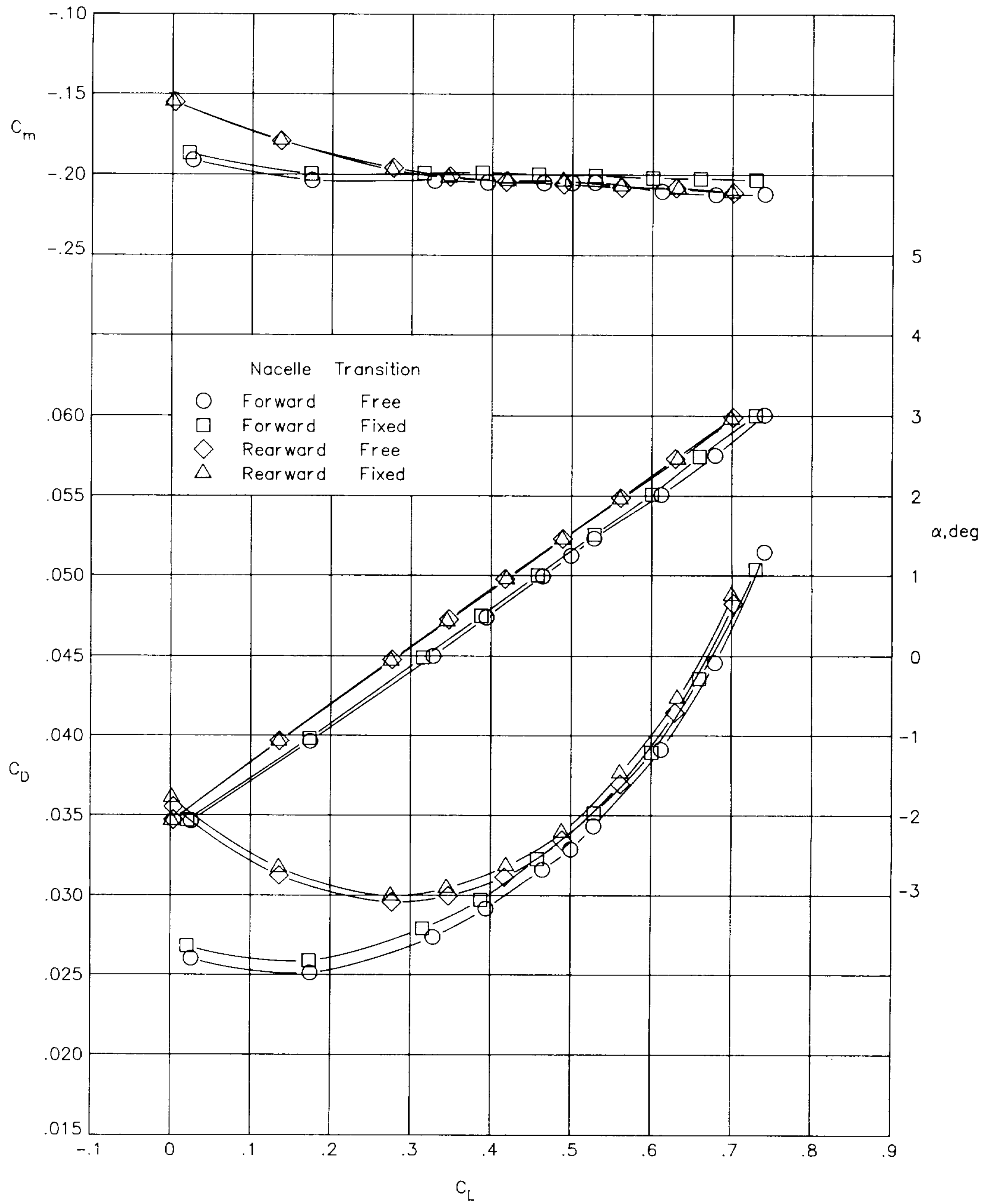

(d) $M = 0.80$.

Figure 8. Continued.

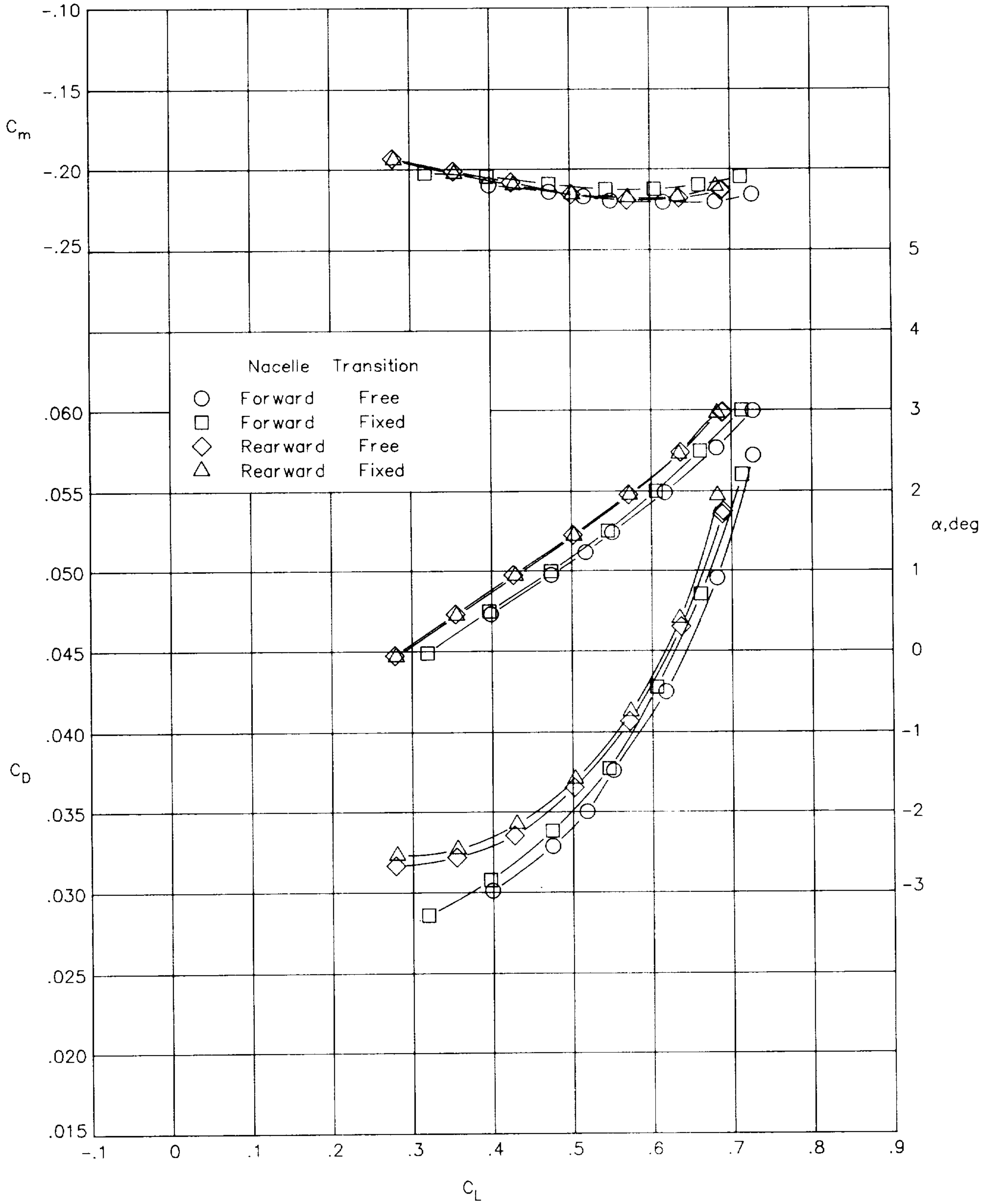

(e) $M = 0.82$.

Figure 8. Concluded.

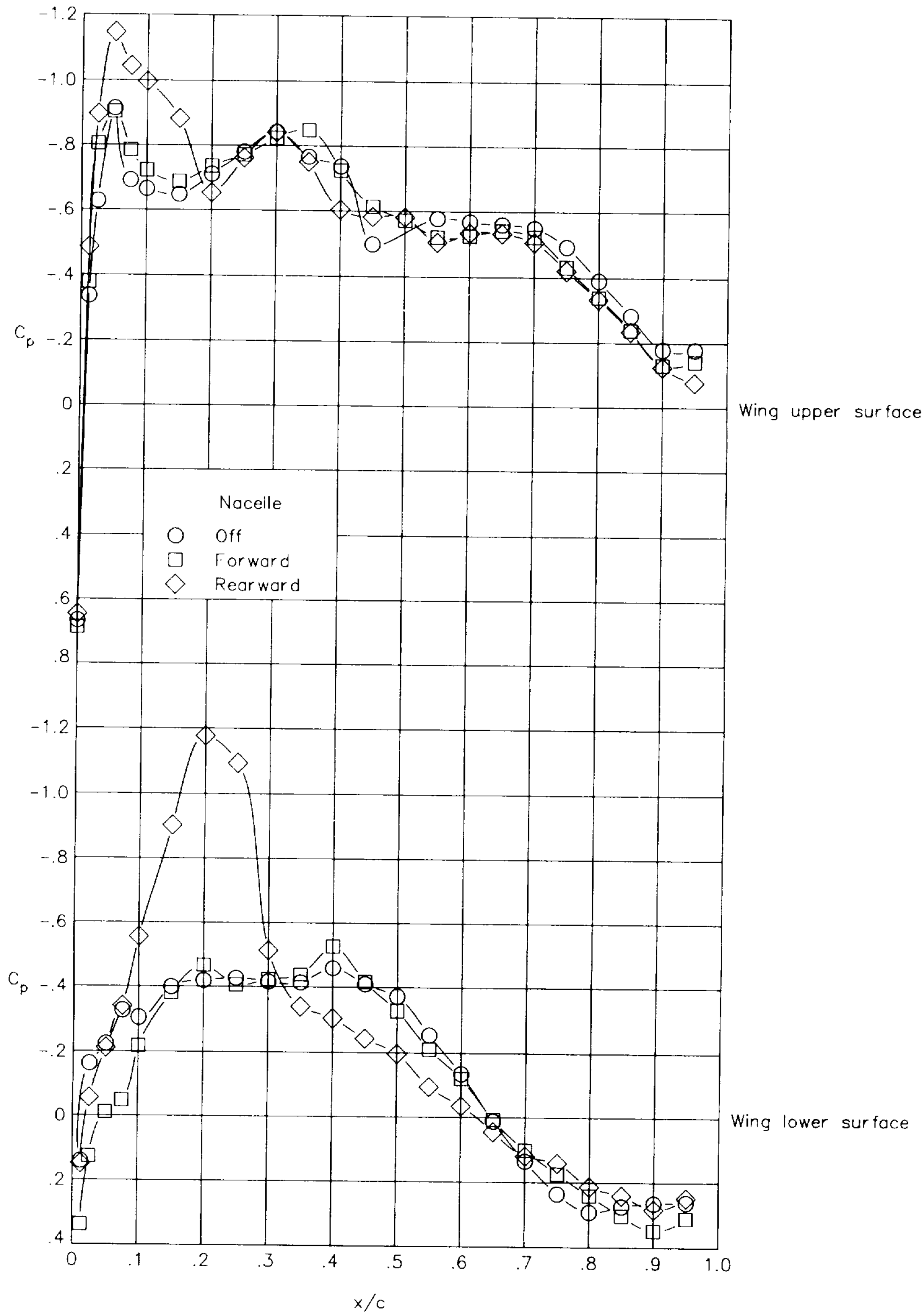

(a) Free transition.

Figure 9. Effect of nacelle position on wing chordwise pressure distributions inboard of pylon ($\eta = 0.328$). Nacelles on symmetrical pylons, $M = 0.80$, and $C_L \approx 0.45$.

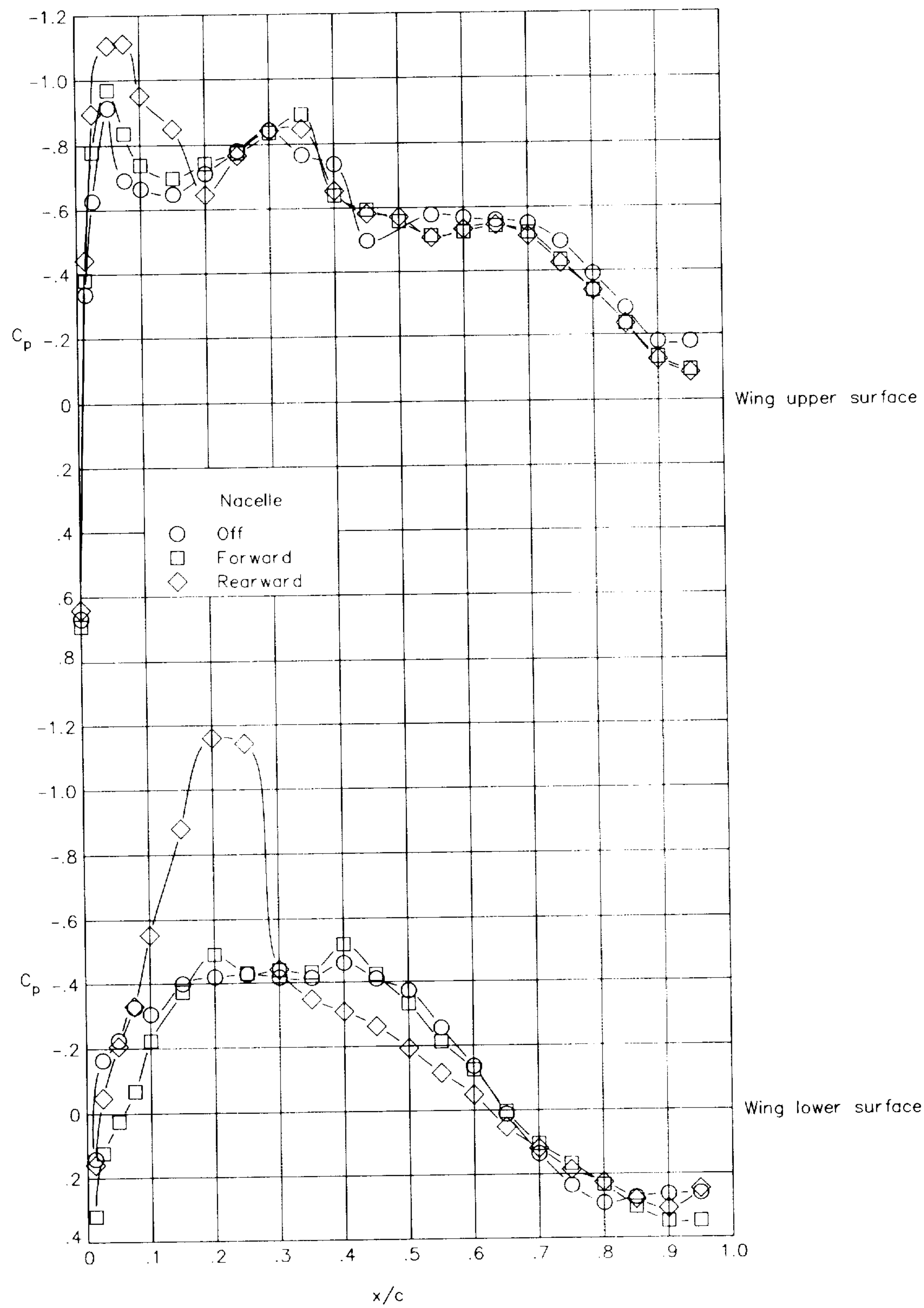

(b) Fixed transition.

Figure 9. Concluded.

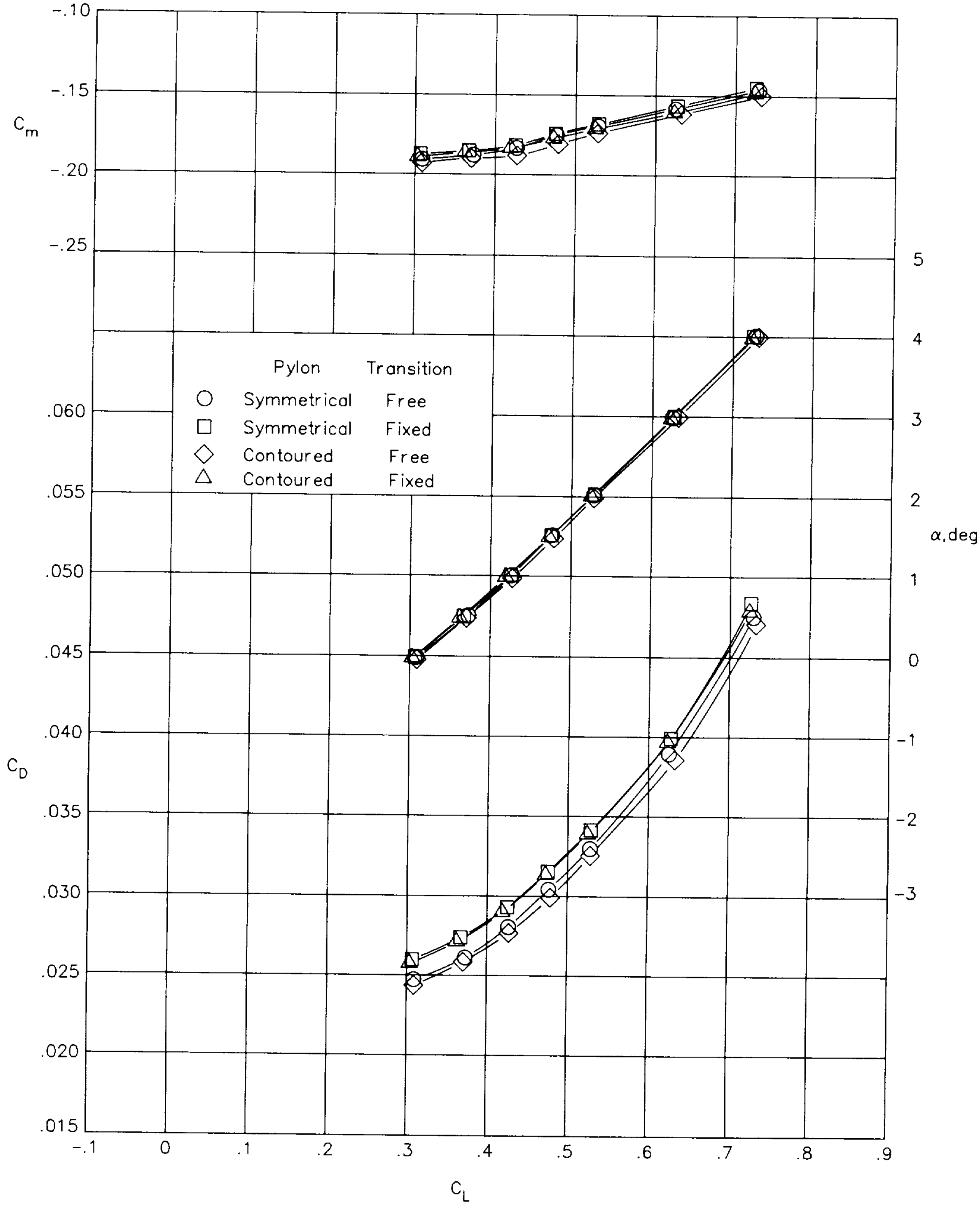

(a) $M = 0.70$.

Figure 10. Effect of pylon contouring on longitudinal aerodynamic characteristics with nacelles in forward position.

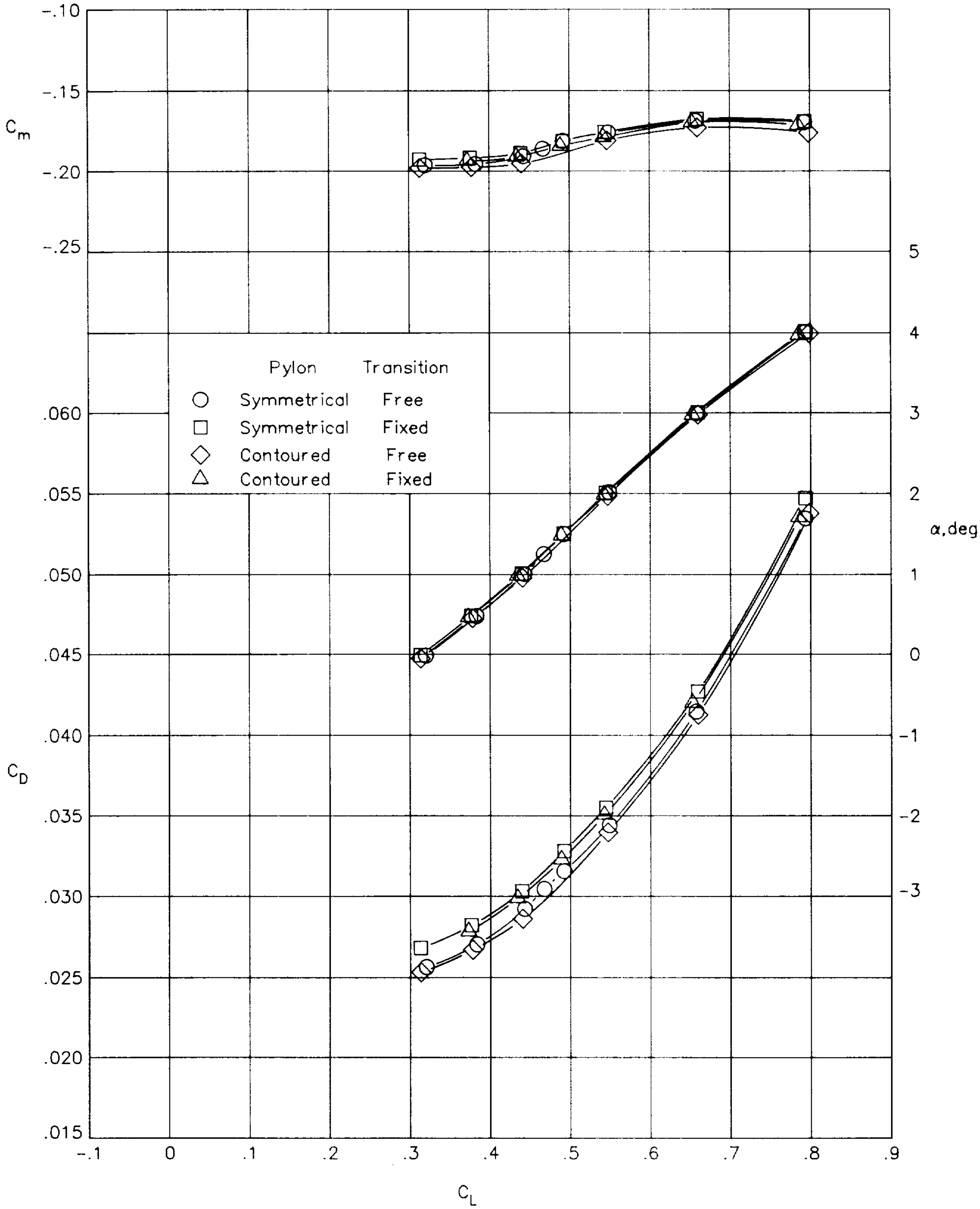

(b) $M = 0.75$.

Figure 10. Continued.

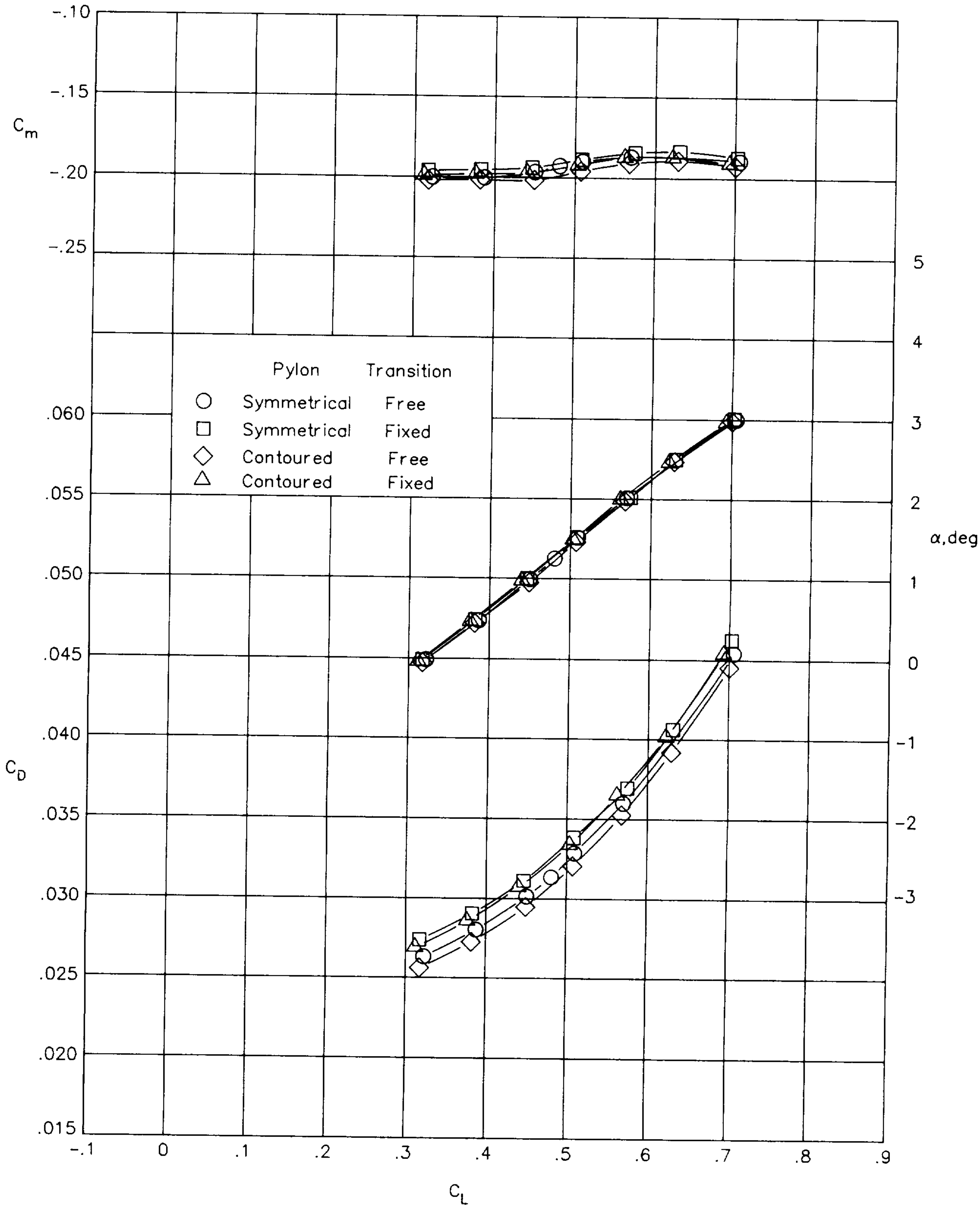

(c) $M = 0.78$.

Figure 10. Continued.

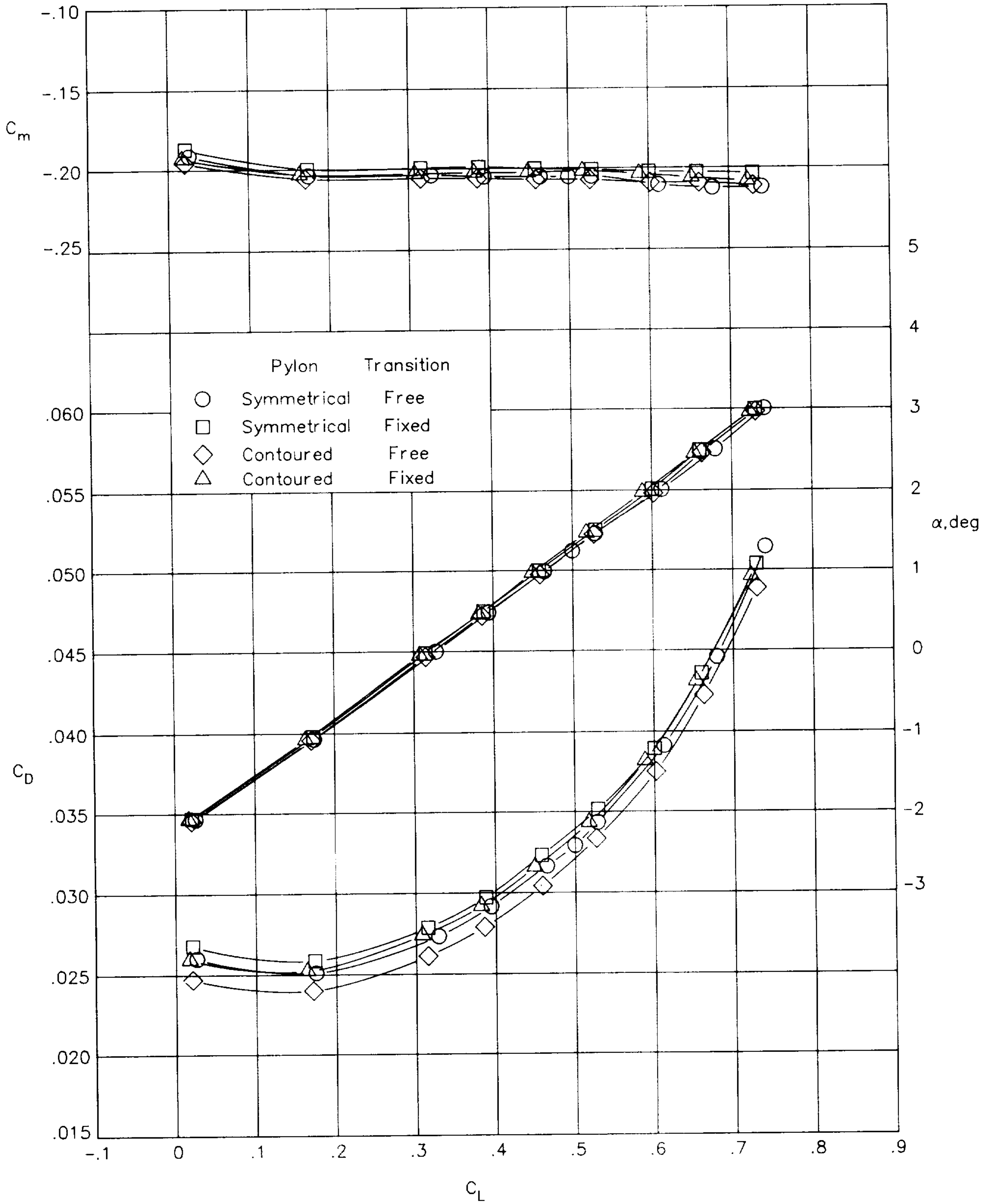

(d) $M = 0.80$.

Figure 10. Continued.

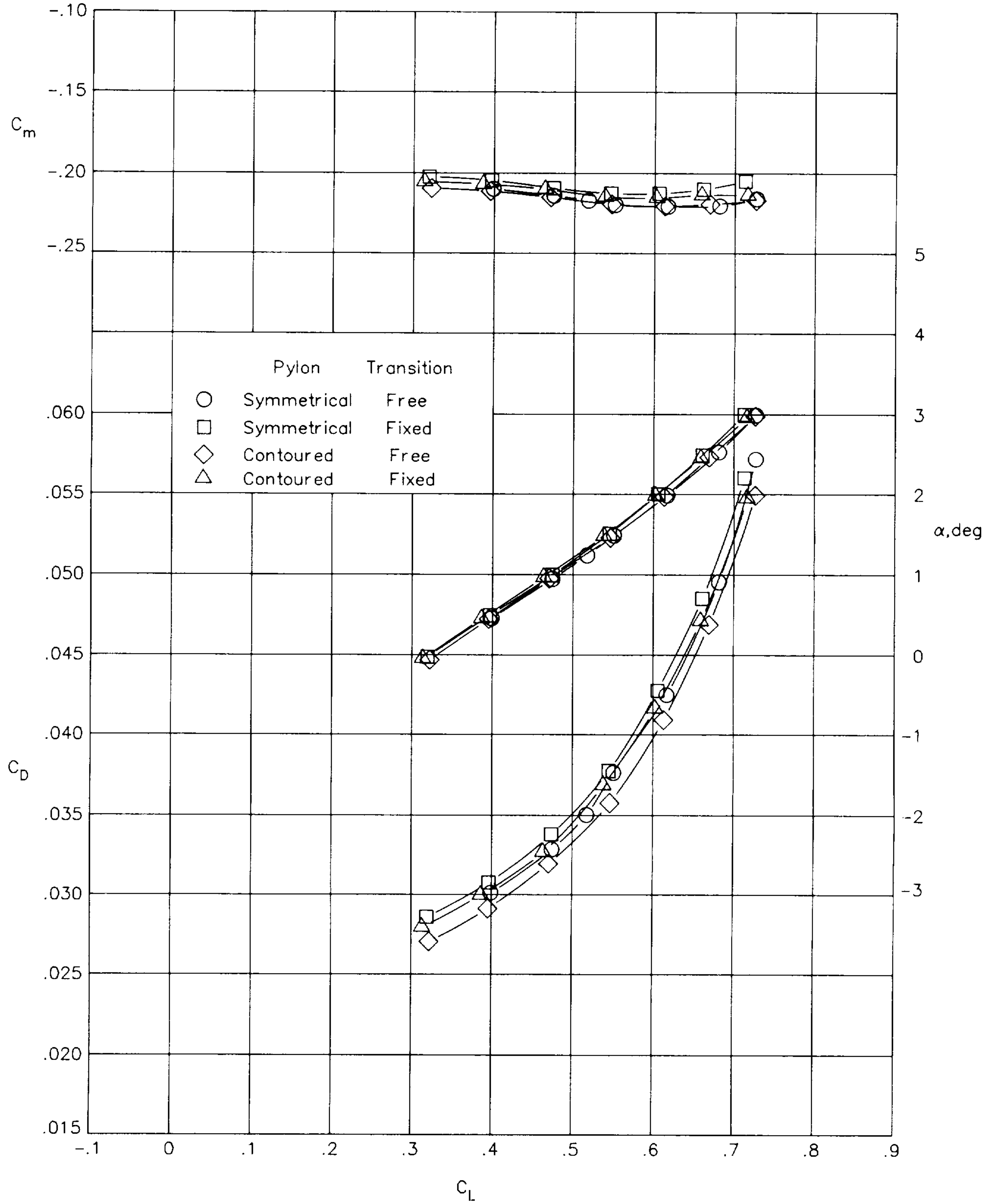

(e) $M = 0.82$.

Figure 10. Concluded.

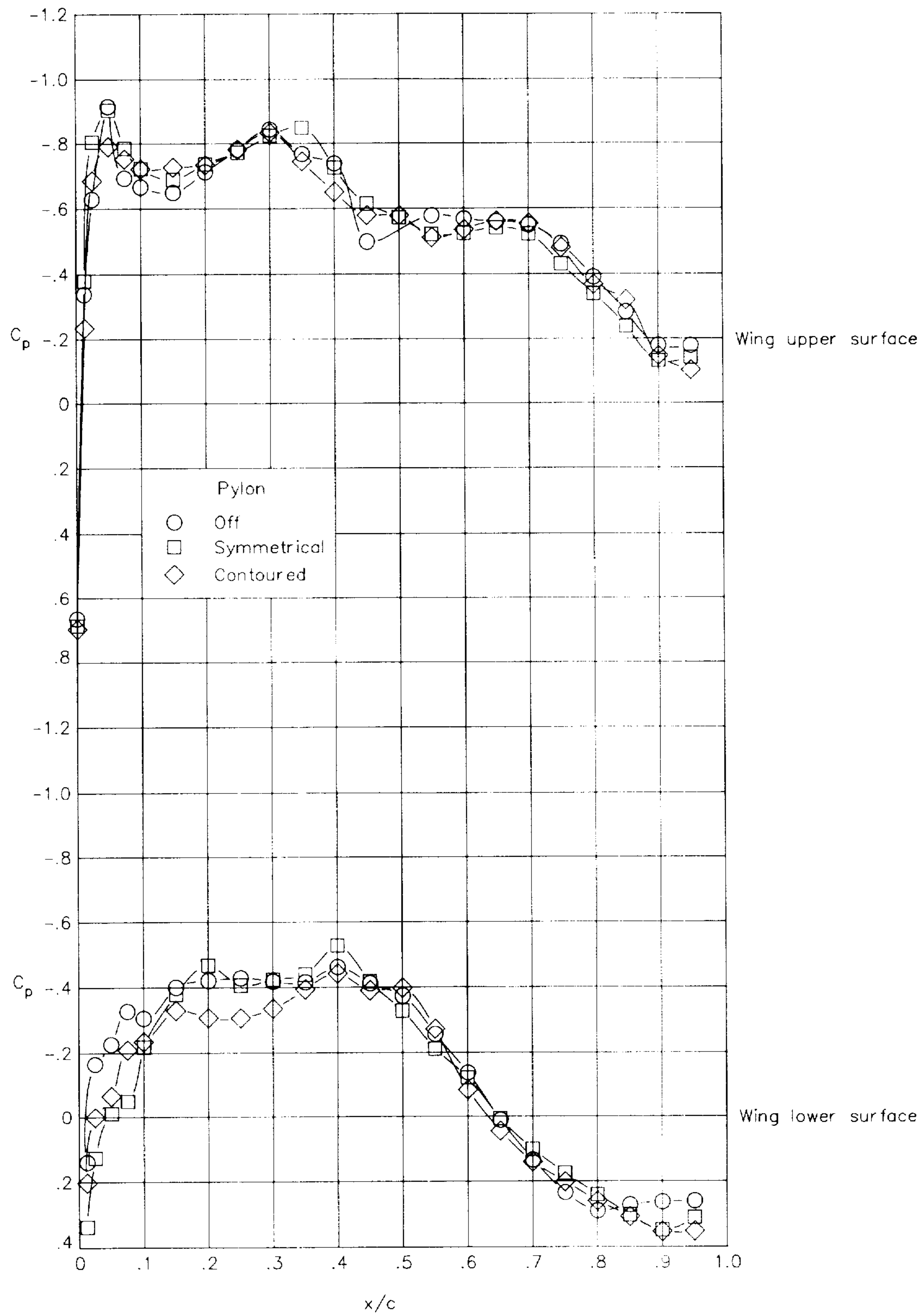

(a) Free transition.

Figure 11. Effect of pylon contouring on wing chordwise pressure distributions inboard of pylon ($\eta = 0.328$). Nacelles in forward position, $M = 0.80$, and $C_L \approx 0.45$.

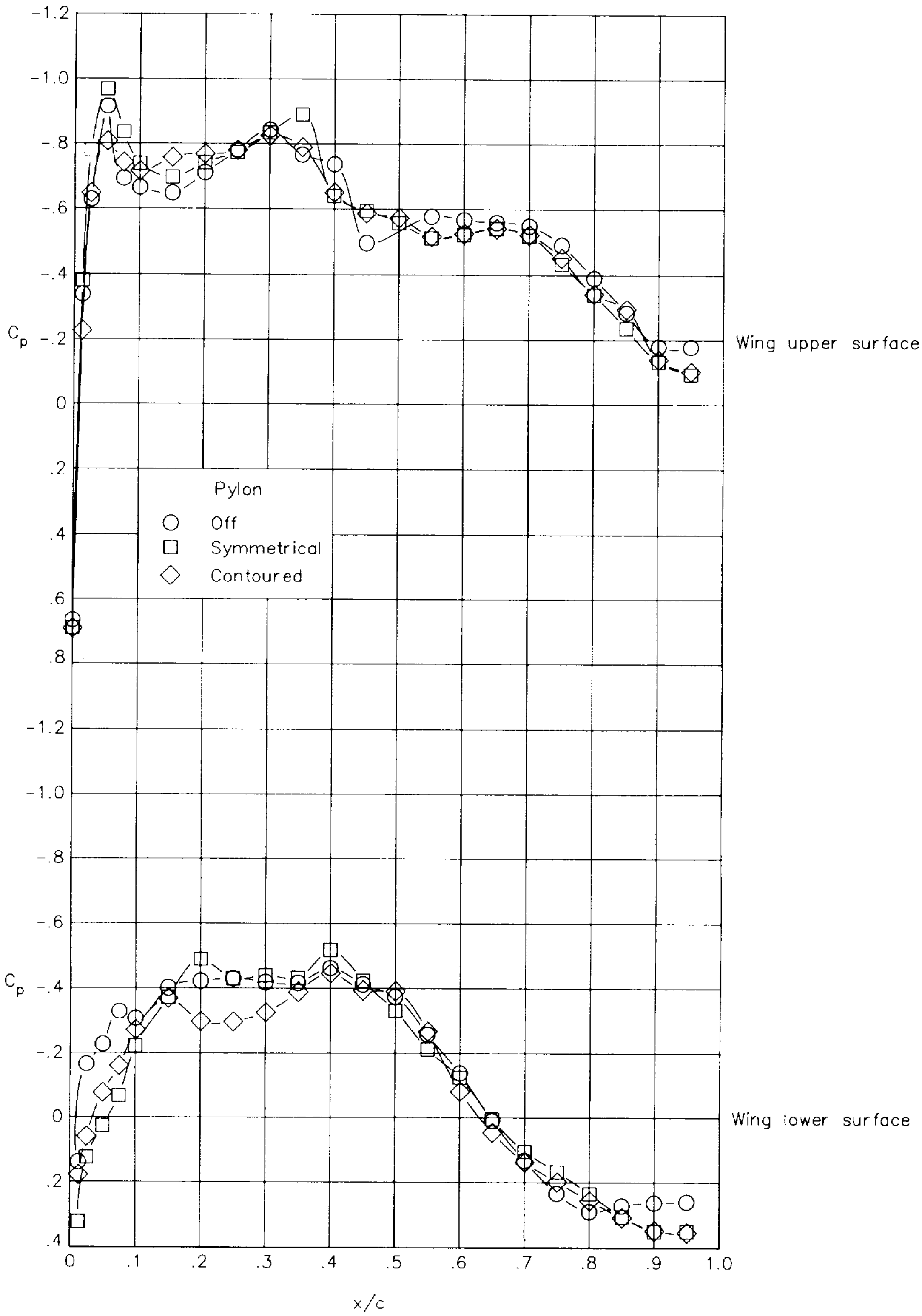

(b) Fixed transition.

Figure 11. Concluded.

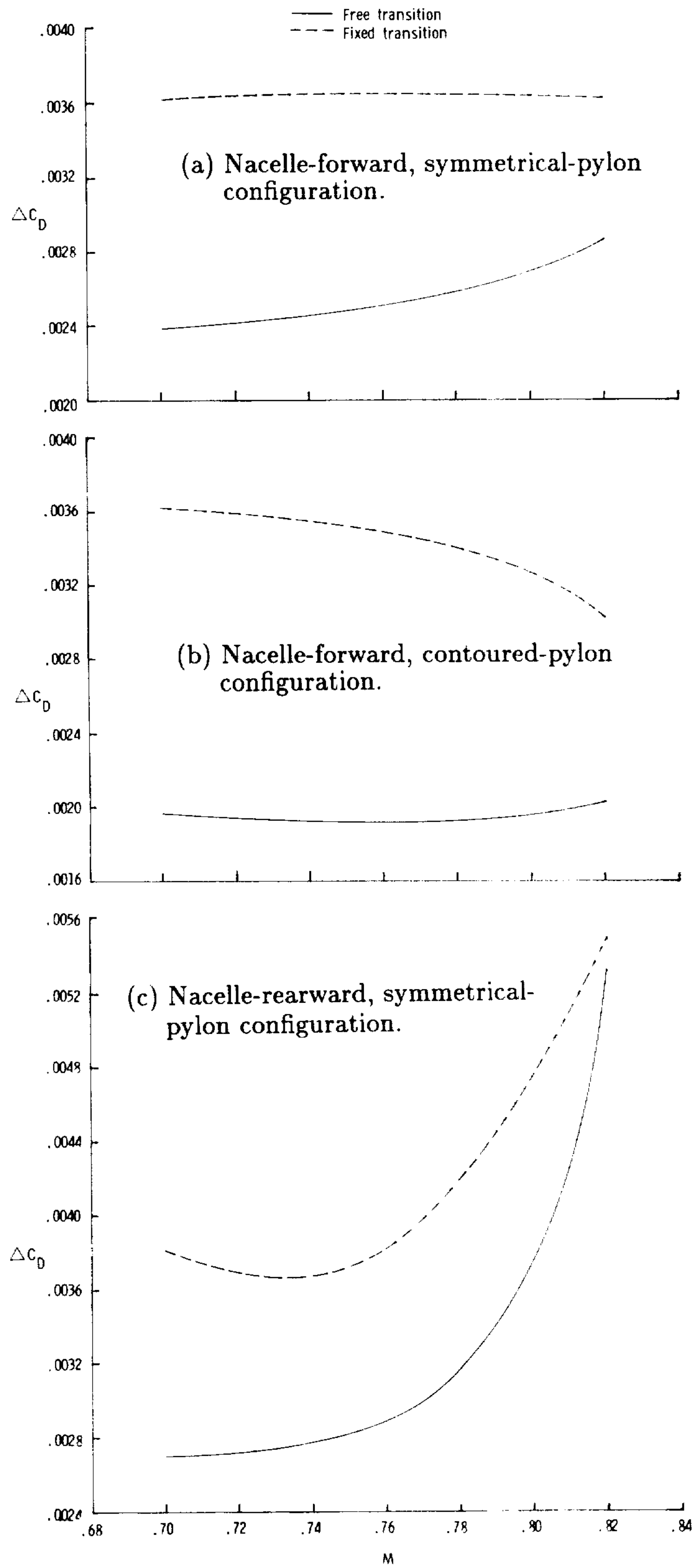

Figure 12. Variation of installed drag with Mach number for $C_L = 0.45$.

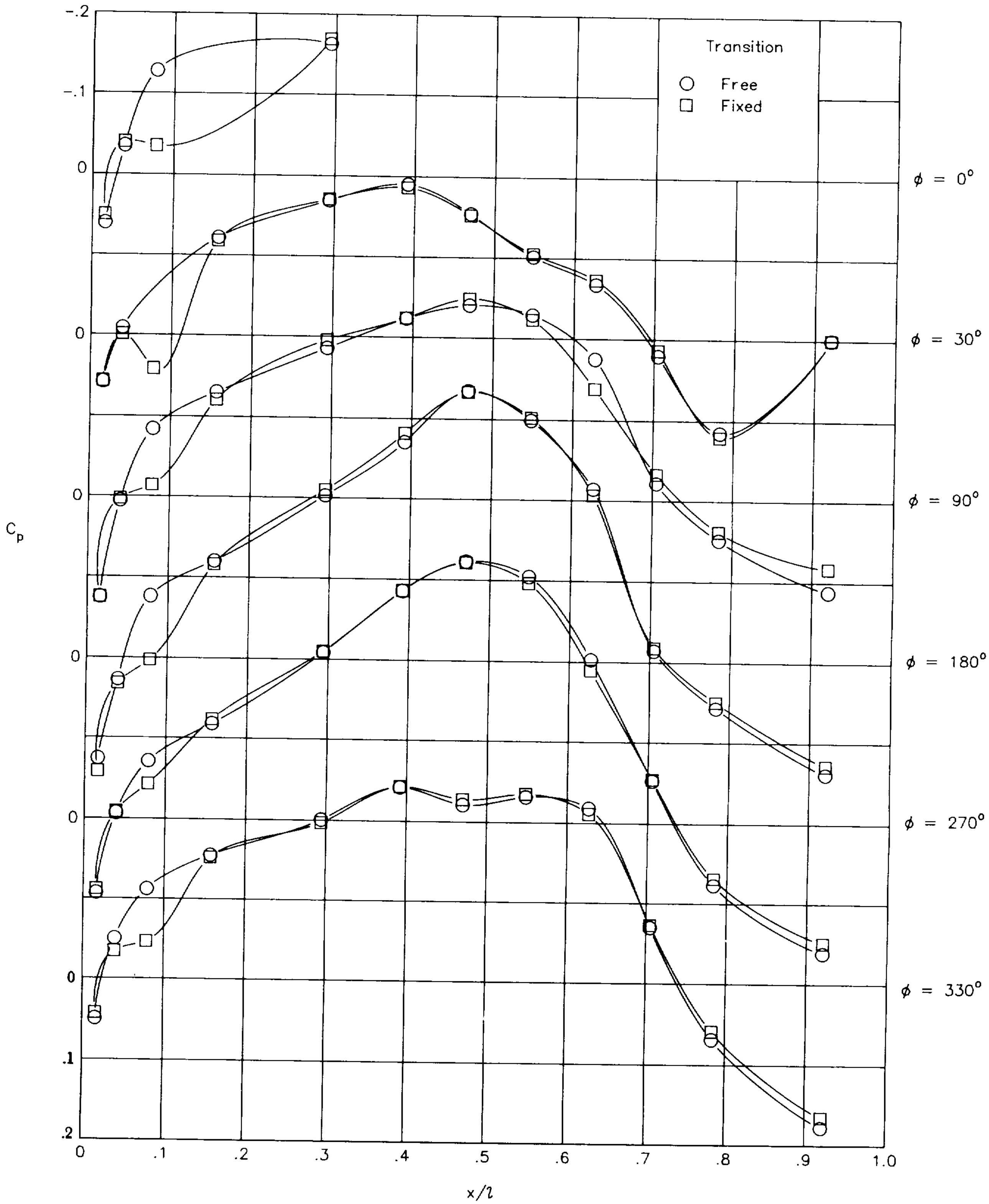

(a) $M = 0.70$.

Figure 13. Nacelle pressure-coefficient distribution at $C_L \approx 0.45$ of nacelles in forward position on symmetrical pylons.

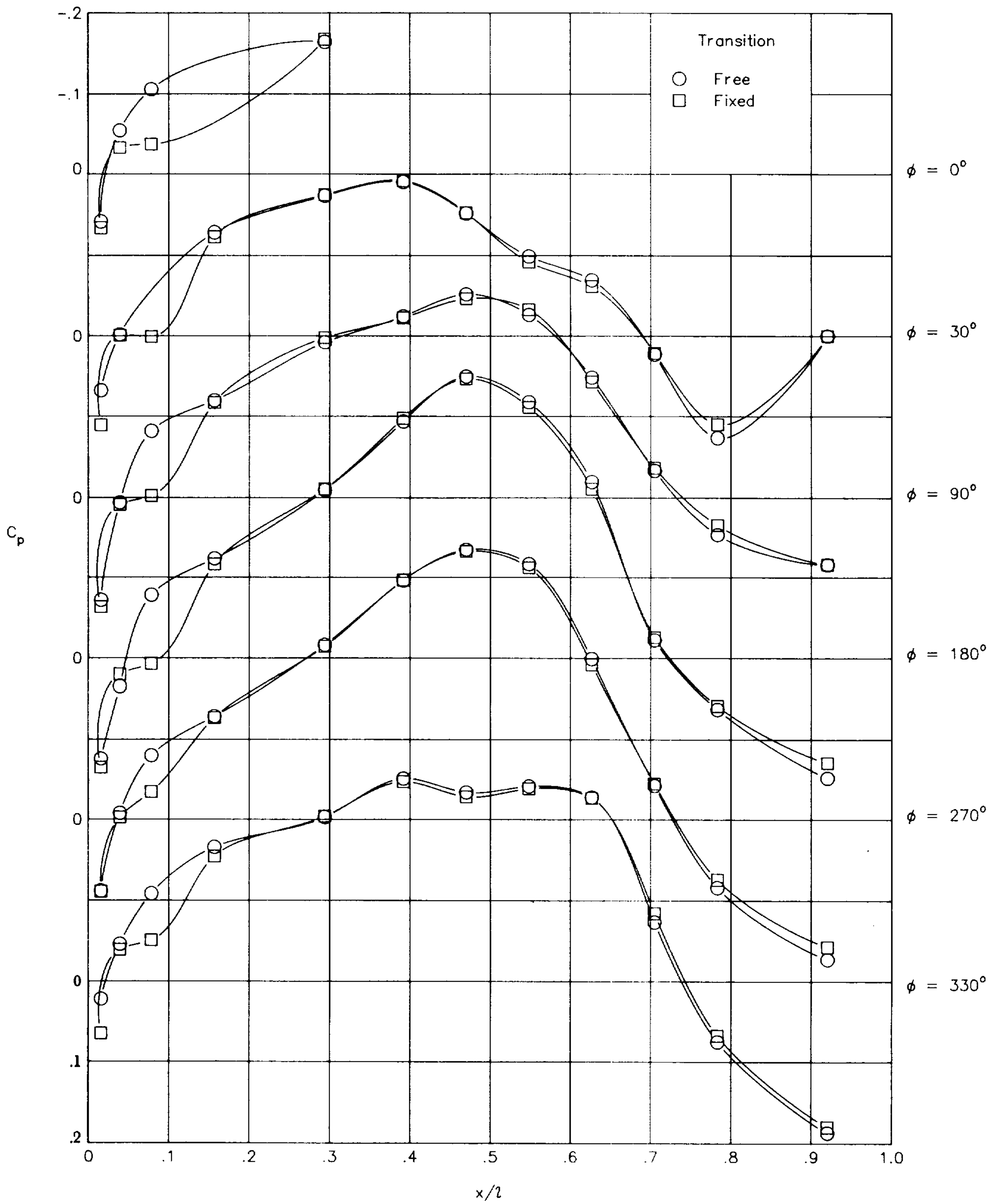

(b) $M = 0.75$.

Figure 13. Continued.

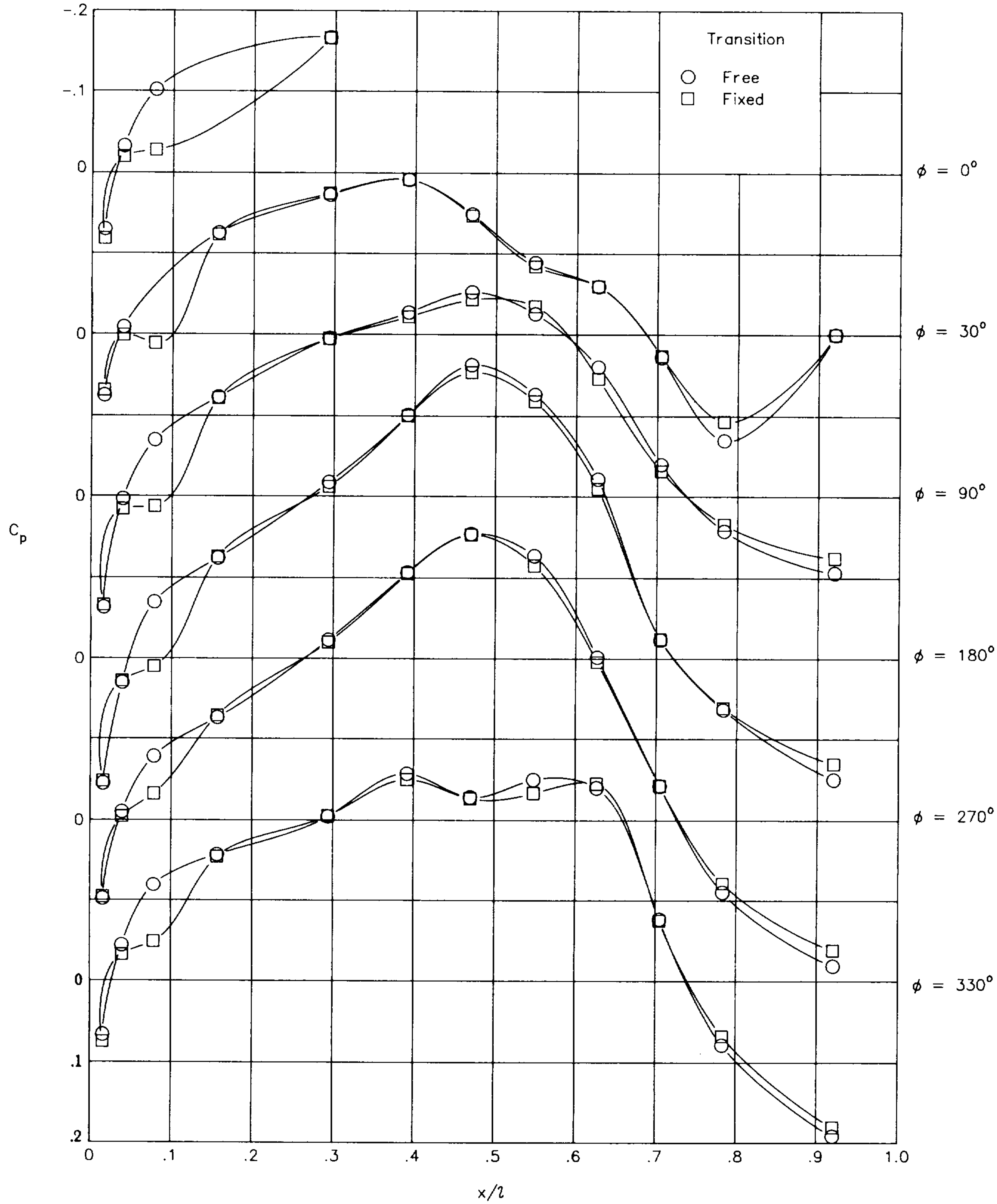

(c) $M = 0.78$.

Figure 13. Continued.

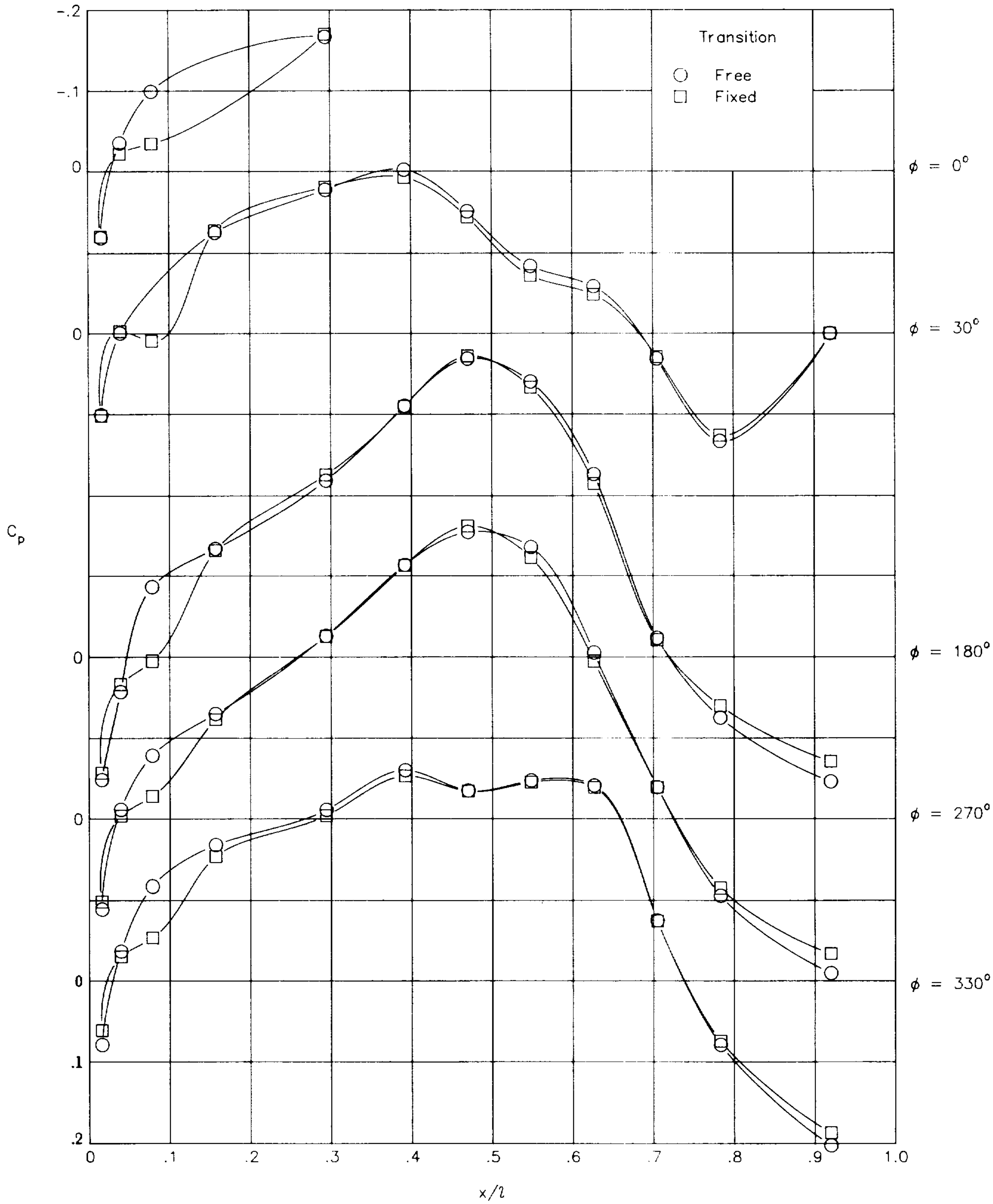

(d) $M = 0.80$.

Figure 13. Continued.

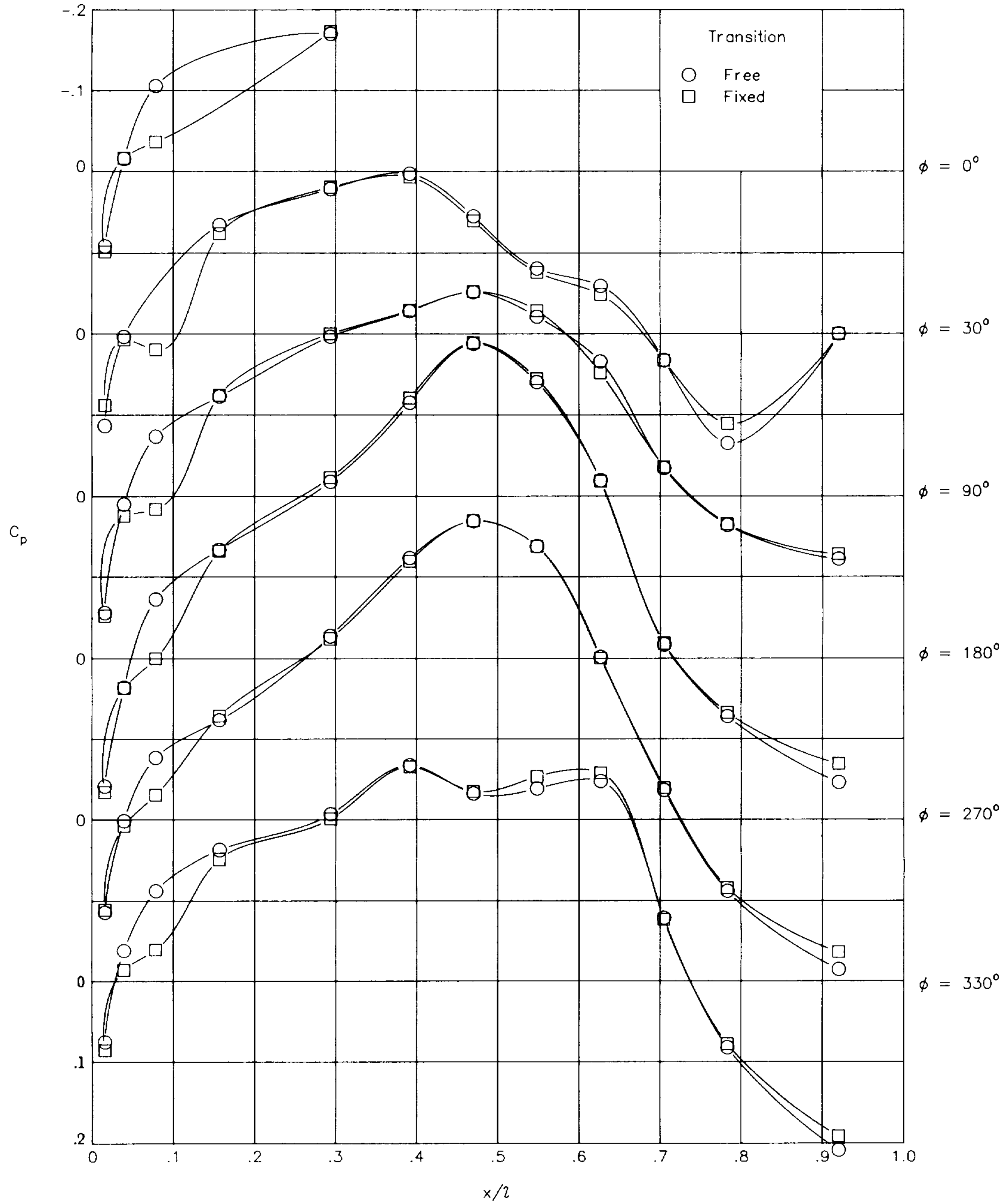

(e) $M = 0.82$.

Figure 13. Concluded.

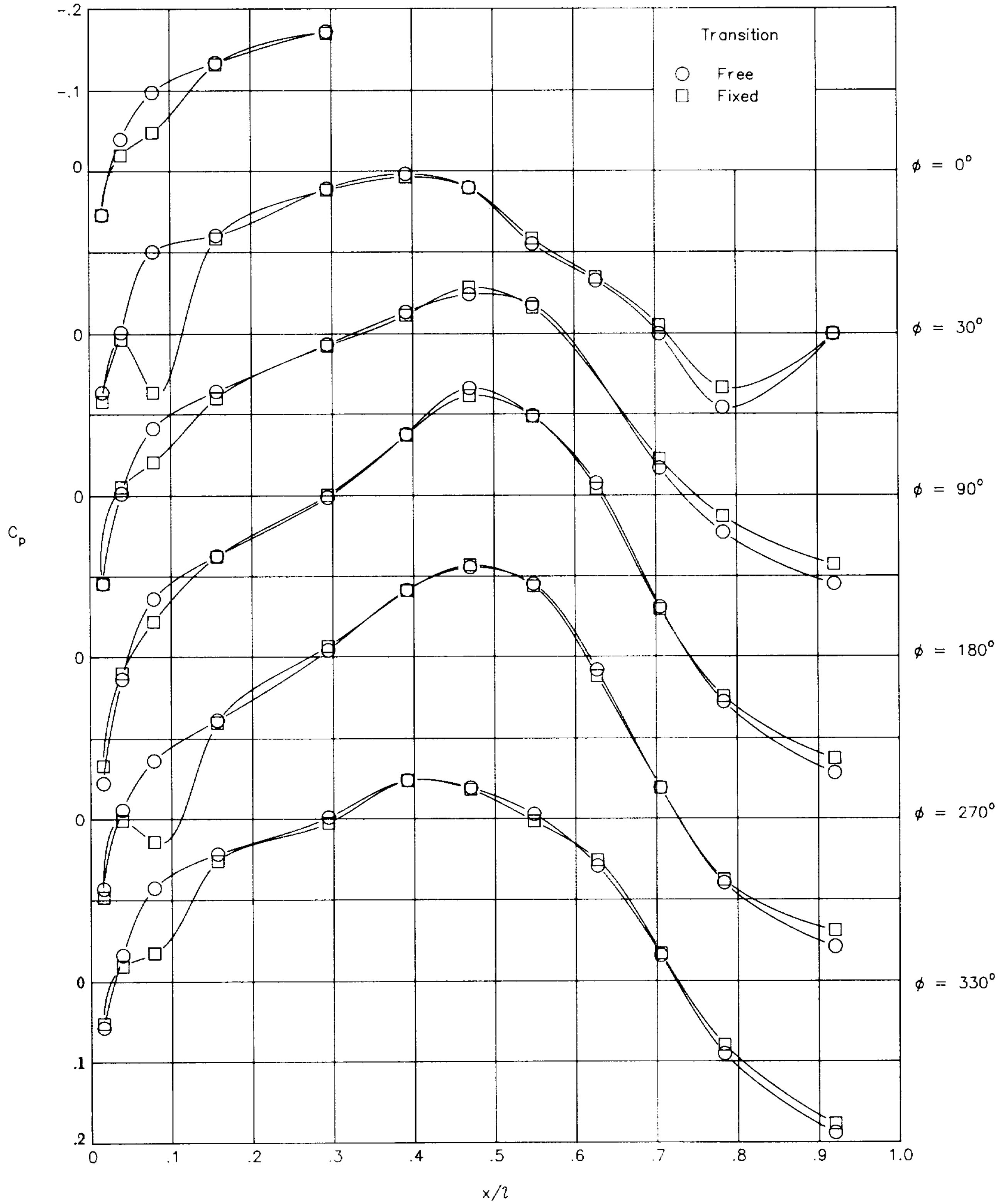

(a) $M = 0.70$.

Figure 14. Nacelle pressure-coefficient distribution at $C_L \approx 0.45$ of nacelles in forward position on contoured pylons.

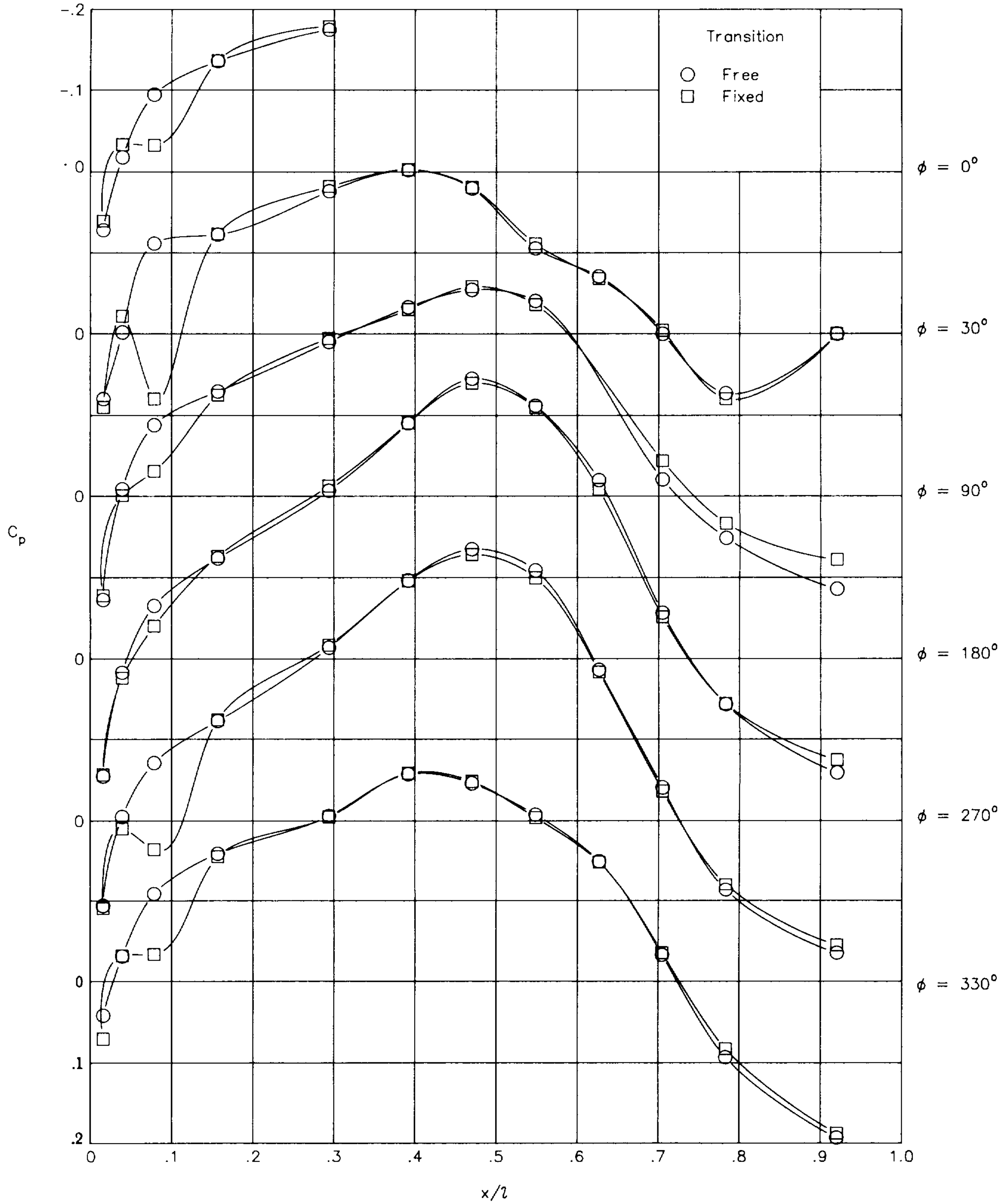

(b) $M = 0.75$.

Figure 14. Continued.

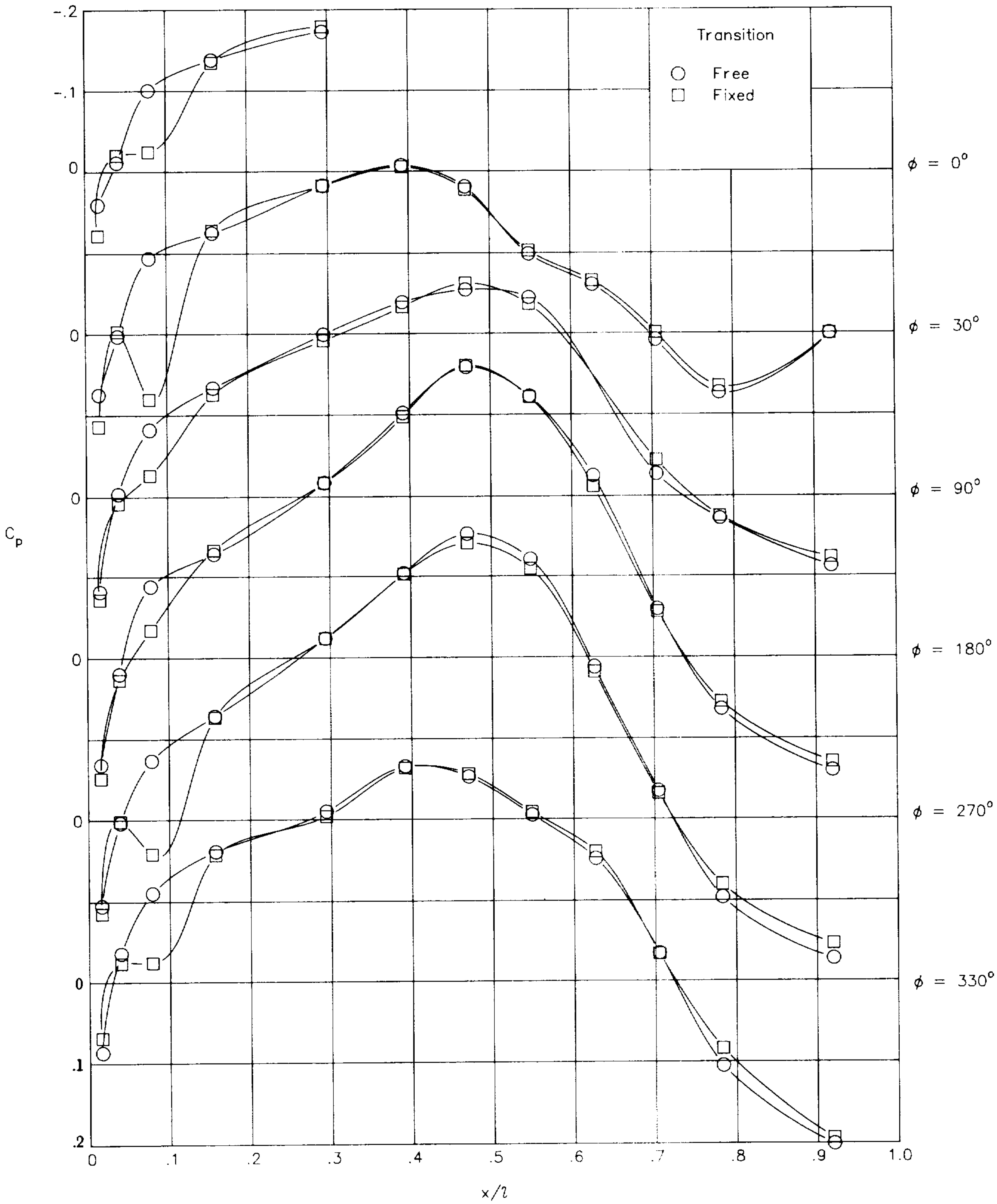

(c) $M = 0.78$.

Figure 14. Continued.

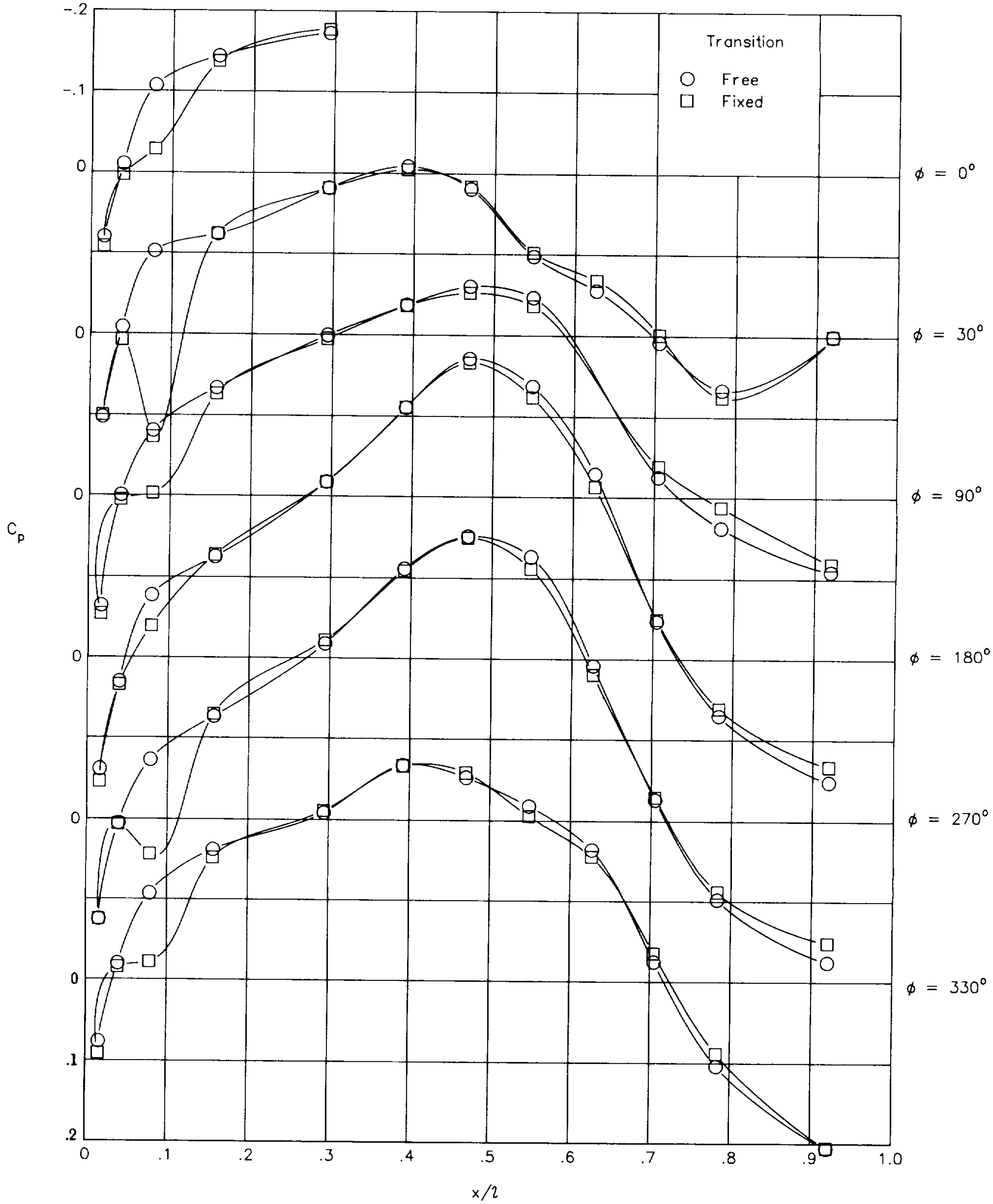

(d) $M = 0.80$.

Figure 14. Continued.

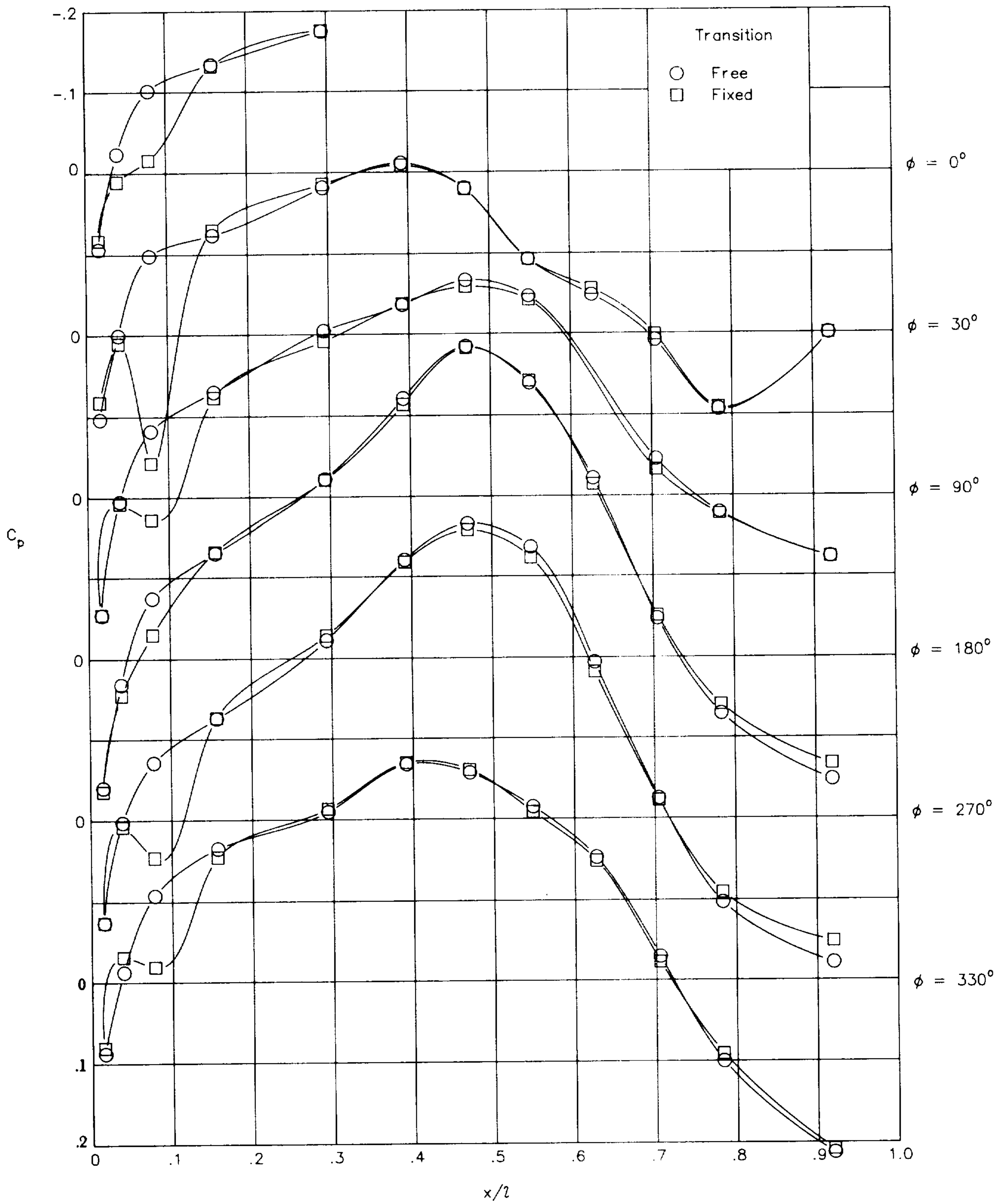

(e) $M = 0.82$.

Figure 14. Concluded.

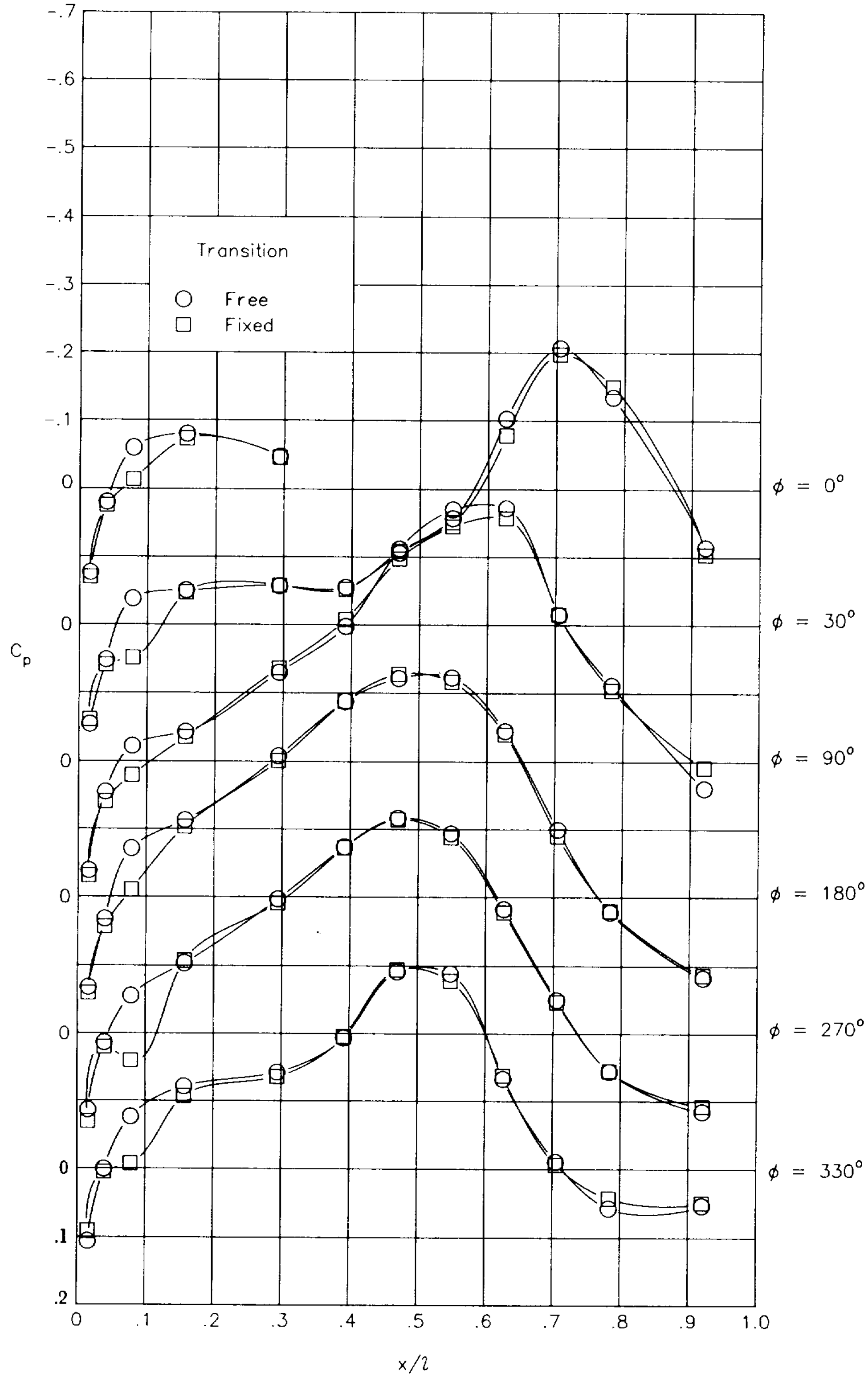

(a) $M = 0.70$.

Figure 15. Nacelle pressure-coefficient distribution at $C_L \approx 0.45$ of nacelles in rearward position on symmetrical pylons.

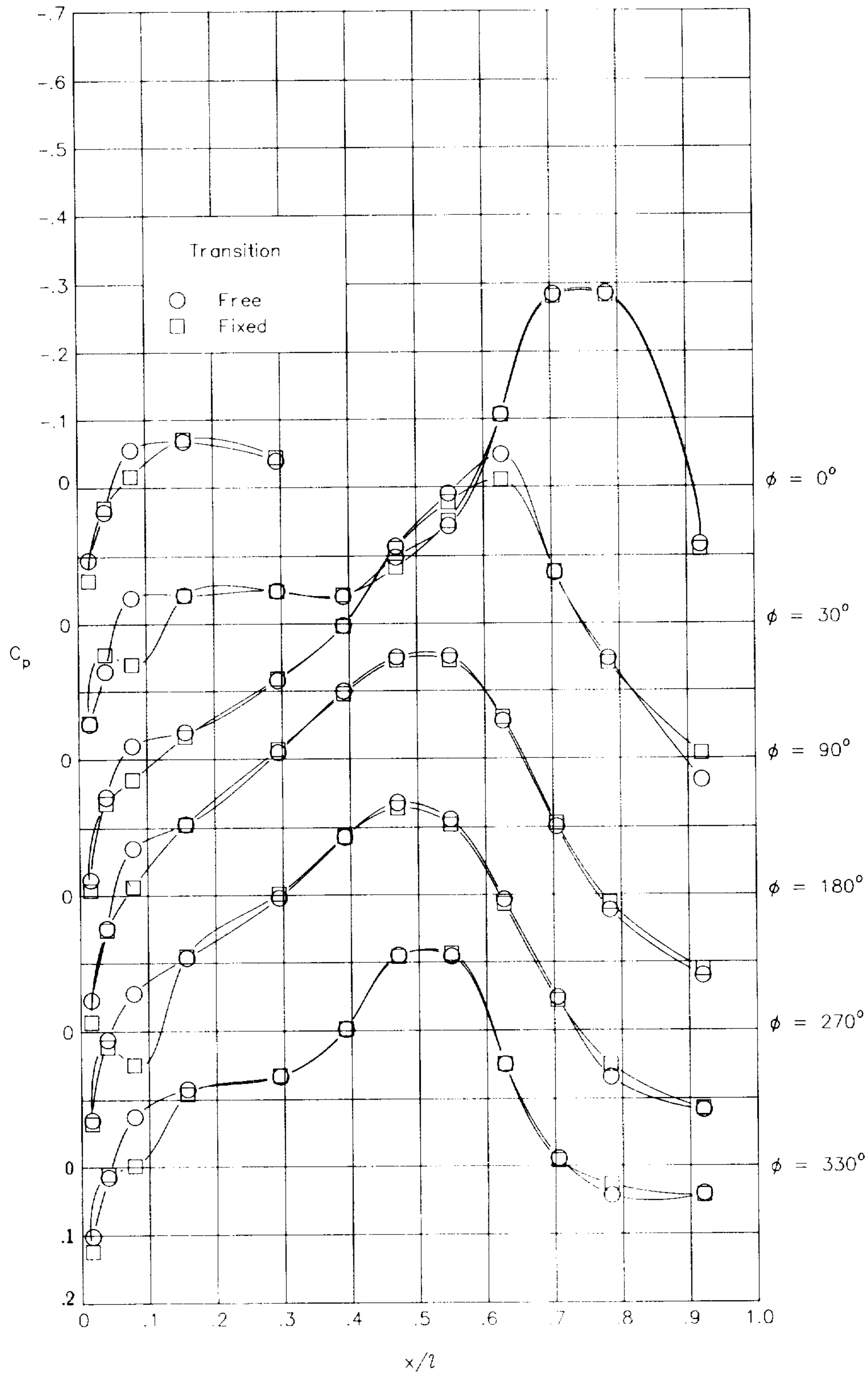

(b) $M = 0.75$.

Figure 15. Continued.

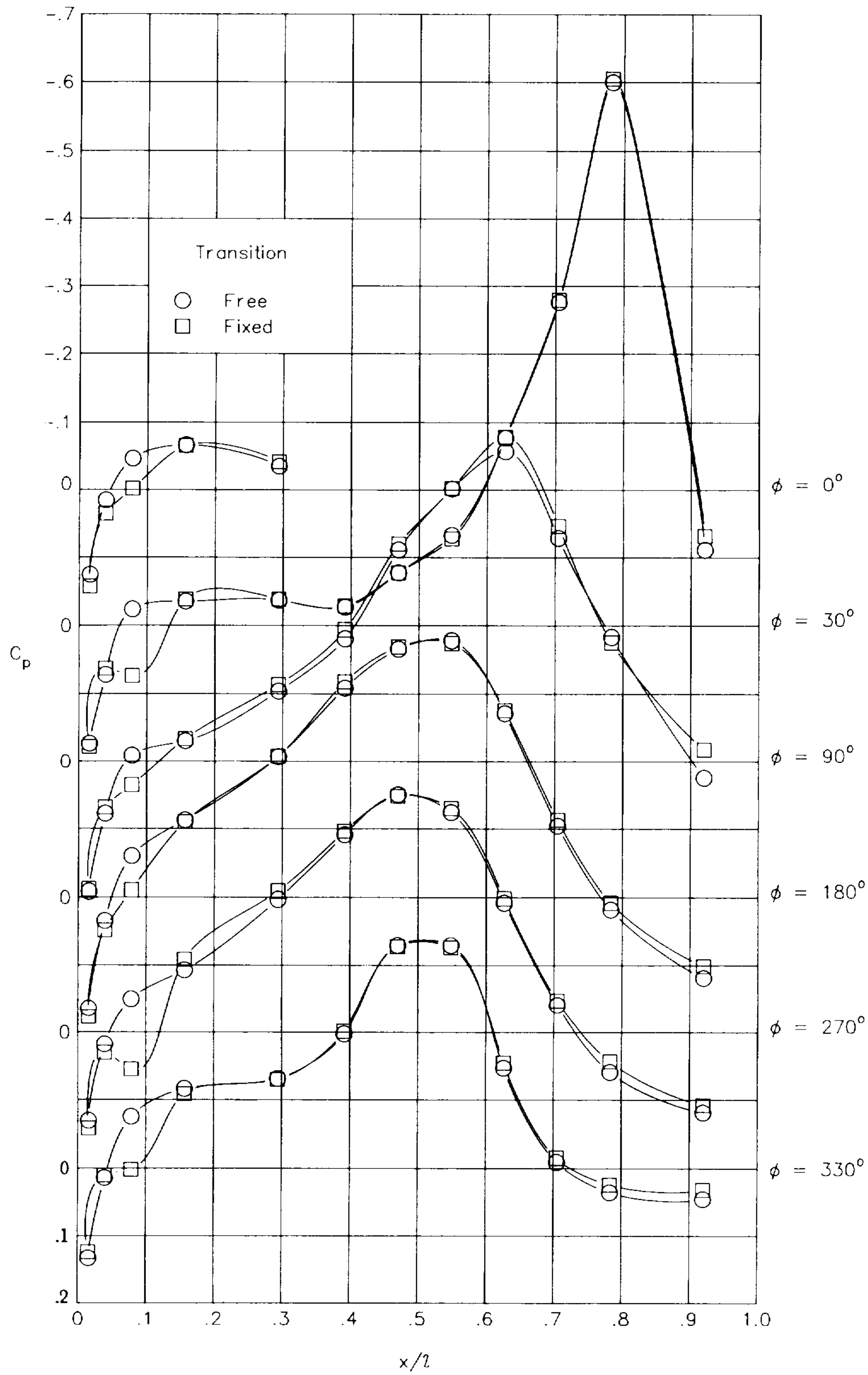

(c) $M = 0.78$.

Figure 15. Continued.

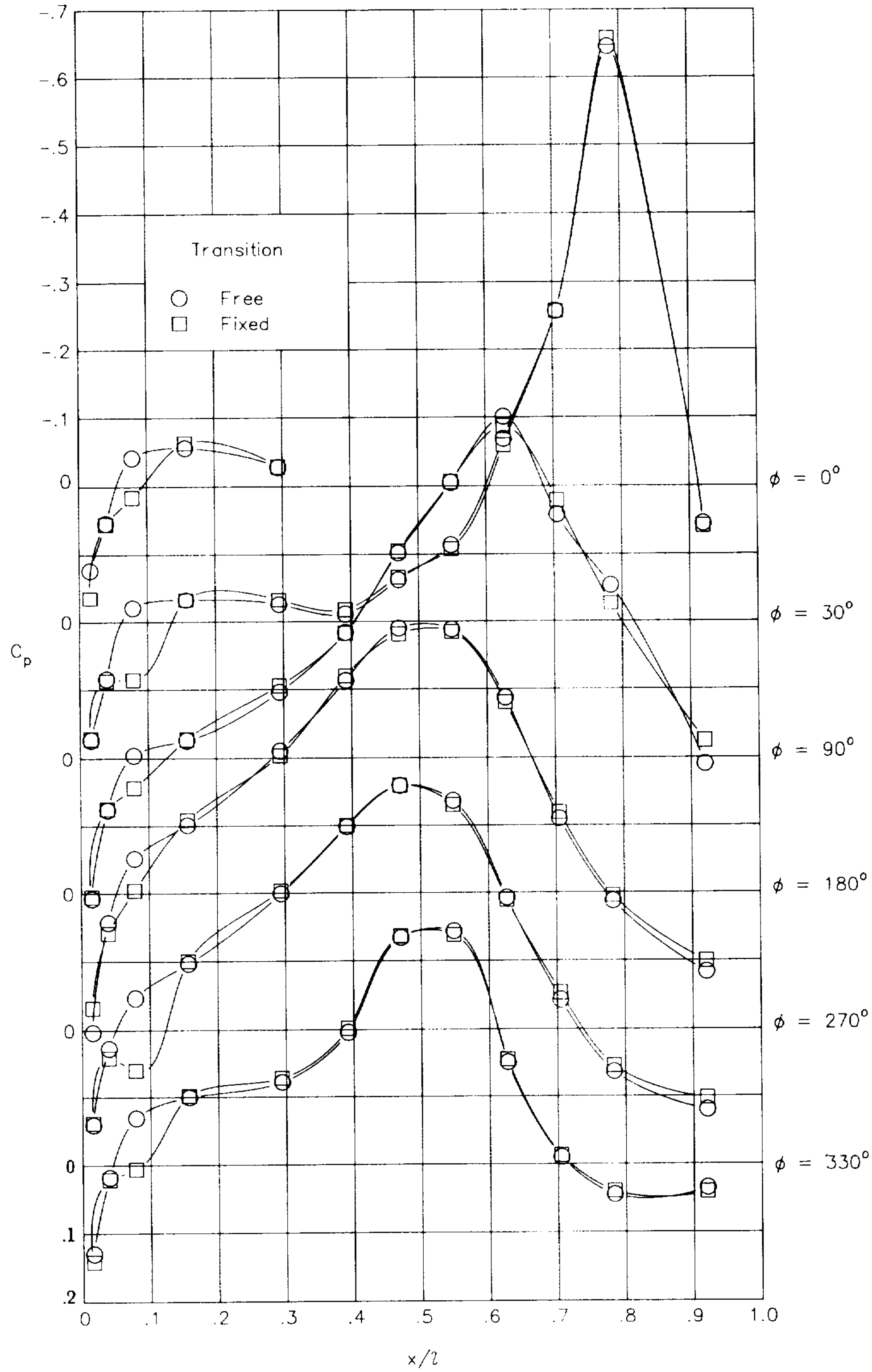

(d) $M = 0.80$.

Figure 15. Continued.

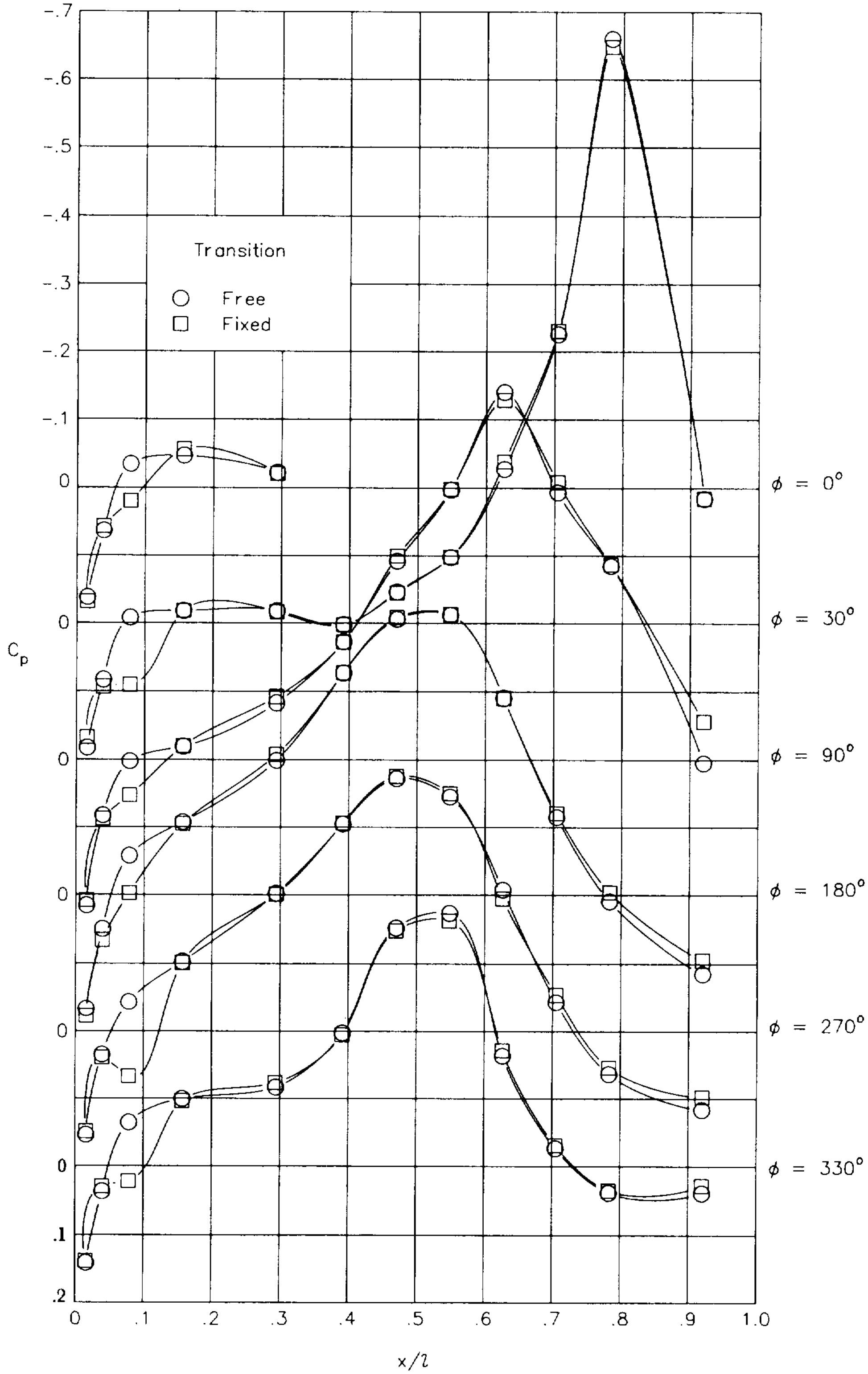

(e) $M = 0.82$.

Figure 15. Concluded.

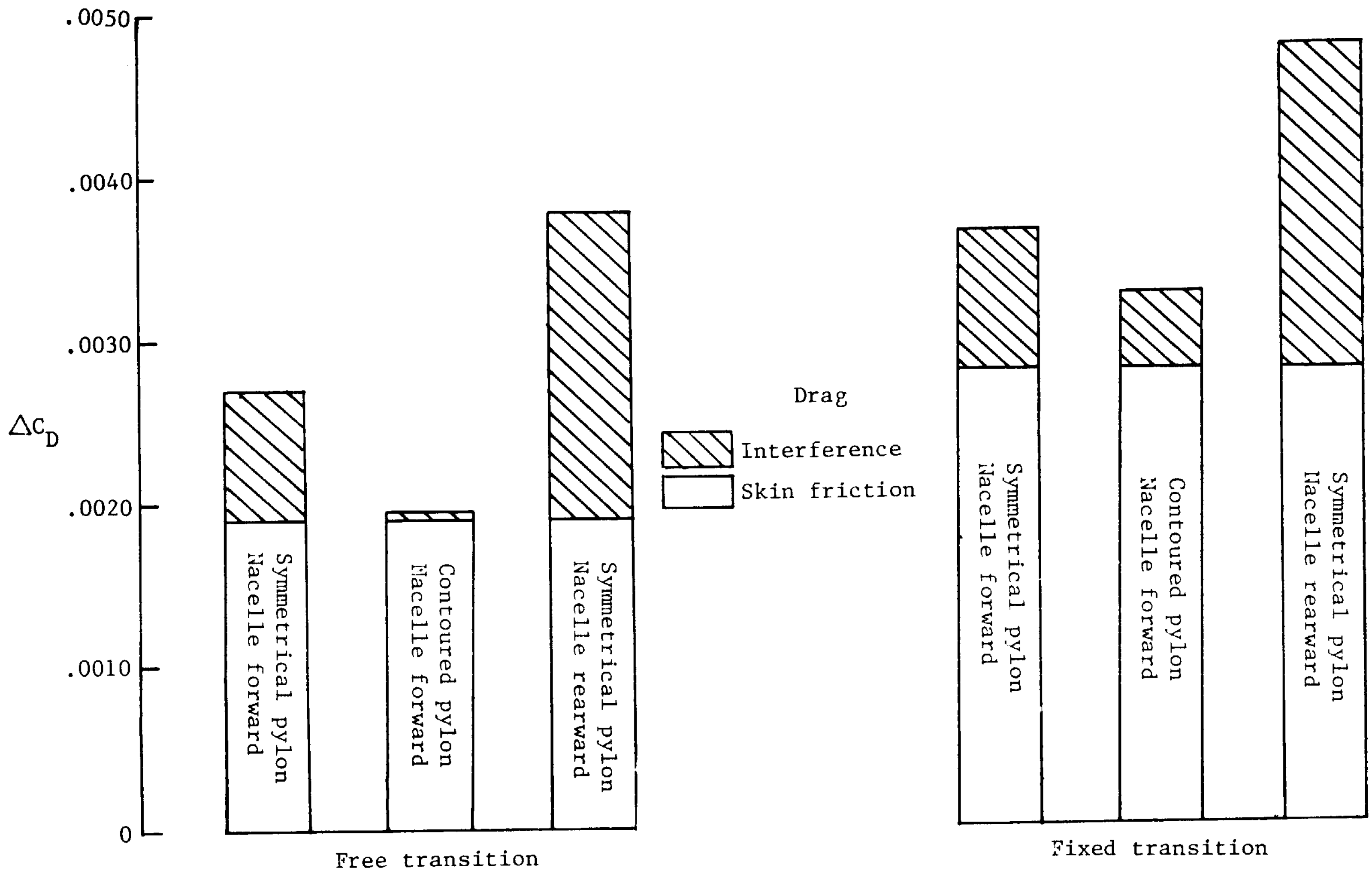

Figure 16. Comparison of installed drag coefficients at $M = 0.80$ and $C_L = 0.45$.

1. Report No. NASA TP-2439	2. Government Accession No.	3. Recipient's Catalog No.
4. Title and Subtitle Nacelle/Pylon/Wing Integration on a Transport Model With a Natural Laminar Flow Nacelle		5. Report Date July 1985
		6. Performing Organization Code 505-40-90-01
7. Author(s) Milton Lamb, William K. Abeyounis, and James C. Patterson, Jr.		8. Performing Organization Report No. L-15907
9. Performing Organization Name and Address NASA Langley Research Center Hampton, VA 23665		10. Work Unit No.
		11. Contract or Grant No.
12. Sponsoring Agency Name and Address National Aeronautics and Space Administration Washington, DC 20546		13. Type of Report and Period Covered Technical Paper
		14. Sponsoring Agency Code
15. Supplementary Notes		

16. Abstract

Tests were conducted in the Langley 16-Foot Transonic Tunnel at free-stream Mach numbers from 0.70 to 0.82 and angles of attack from -2.5° to 4.0° to determine if nacelle/pylon/wing integration affects the achievement of natural laminar flow on a long-duct flow-through nacelle for a high-wing transonic transport configuration. In order to fully assess the integration effect on a nacelle designed to achieve laminar flow, the effects of fixed and free nacelle transition as well as nacelle longitudinal position and pylon contouring were obtained. The results indicate that the ability to achieve laminar flow on the nacelle is not significantly altered by nacelle/pylon/wing integration. The increment in installed drag between free and fixed transition for the nacelles on symmetrical pylons is essentially the calculated differences between turbulent and laminar flow on the nacelles. The installed drag of the contoured pylon is less than that of the symmetrical pylon. The installed drag for the nacelles in a rearward position is greater than that for the nacelles in a forward position.

17. Key Words (Suggested by Authors(s))	18. Distribution Statement
Nacelle/pylon/wing integration Natural laminar flow nacelle Nacelle position Pylon contouring Transonic transport	Unclassified—Unlimited Subject Category 02

19. Security Classif.(of this report)	20. Security Classif.(of this page)	21. No. of Pages	22. Price
Unclassified	Unclassified	59	A04

For sale by the National Technical Information Service, Springfield, Virginia 22161

NASA-Langley, 1985